APPLICATION OF BASE ISOLATION SYSTEMS TO REINFORCED CONCRETE FRAME BUILDINGS

By

Mengyu Han

A thesis submitted to the University of Ottawa
in partial fulfillment of the requirements for
Masters of Applied Science in Civil Engineering

Department of Civil Engineering
Faculty of Engineering
University of Ottawa

Acknowledgements

I would have never been able to complete my thesis without the guidance of my supervisors Dr. Murat Saatcioglu. I would like to express my deepest appreciations to Dr. Murat Saatcioglu, for his excellent guidance, profound expertise and patience. Those meetings we had in the last one year would be my greatest and most valuable experience in my student career.

I would also like to thank my family for their support and encouragement throughout my whole life. Thanks also go to my fiancé Cheng Zeng who helped review my thesis paper and kept me company on all these nights as I was working on the project.

In addition, I want to thank my cat, Marshmallow, for her cuteness that pleased me greatly at times of frustration when I got stuck with my research work.

Abstract

Seismic isolation systems are widely used to protect reinforced concrete (RC) structures against the effects of strong ground motions. After a magnitude 6.6 earthquake, the outpatient building of Lushan People's hospital in China remained in good condition due to the seismic isolation technology, while the non-isolated older outpatient building nearby experienced major damage. The building provides a good opportunity to study and assess the contribution of isolation systems to seismic performance of RC structures. In the current research project, the isolated outpatient building was modelled and analyzed using computer software SAP2000. The post-yield behaviour of the structure was modelled by assigning multi-linear plastic links to frame objects. The rubber isolators were represented by rubber isolator link elements, assigned as a single joint element between the ground and the superstructure. The isolated structure was subjected to four earthquake records with increasing intensity. The performances of the isolated structure were compared with those of the fixed-base structures in terms of lateral inter-storey drifts, peak absolute floor accelerations, and residual drifts. The laminated rubber bearings, the high damping isolation devices, composed of rubber bearings and viscous dampers, and the hybrid isolation system of rubber bearings and friction pendulum bearings were analysed. The effectiveness of the three base isolation systems considered in enhancing structural performance was investigated. The results show the level of improvement attained in seismic response by each system. They also illustrate that the rubber bearings coupled with friction pendulum bearings produce best drift control without causing excessive horizontal displacements at the base level and without adversely affecting floor accelerations.

Table of Contents

List of Tables

List of Figures

Chapter 1

Introduction

1.1 General

Strong earthquakes in the past have resulted in significant property damage and loss of lives. Earthquake damage is mainly associated with damage to seismically deficient buildings, often designed prior to the enactment of modern building codes. Therefore, researchers have focused their efforts to developing new and effective seismic risk mitigation strategies for such buildings. Conventional seismic protection methods, such as enlarging structural elements or adding new strengthening and stiffening elements (i.e. bracing systems) focus on improving the capacity of buildings to meet likely demands. However, stiffening buildings results in shorter vibration periods and higher floor accelerations, resulting in higher structural damage. Therefore, a preferred approach for seismic retrofitting buildings may be to decrease demands rather than to increase capacities. This can be achieved by introducing flexible devices to buildings at their ground levels to isolate them from the transfer of seismic energy.

The seismic isolation is used extensively for strategically important post-disaster buildings, such as hospitals, schools and critical facilities to protect them against the effects of strong ground motions. The isolation systems consist of isolators and auxiliary devices [1]. The isolators, having low horizontal stiffness or low friction, provide lateral flexibility at the base and separate the main structure from ground motions. By increasing the flexibility of the isolated building, the isolators shift the fundamental period of the structure beyond the range where the maximum effect of ground motions occurs. Hence, they limit the seismic energy transfer to the superstructure so that inter-storey drifts and floor accelerations are reduced significantly [2]. Also, the auxiliary devices dissipate the

residual seismic energy in damping, controlling lateral deformations of isolators. Additionally, the devices can provide horizontal resistance against non-seismic loads like service loads and lateral wind loads [1].

Various seismic isolation systems can be implemented for structural retrofits. They include rubber bearing systems, sliding bearing systems, the combination of different isolation systems, and a system of hybrid devices composed of isolators and external dampers. The laminated rubber bearings (LRB), consisting of elastomeric rubber layers and steel plates, are one of the most commonly adopted isolation systems. The rubber layers provide lateral flexibility to the isolator while the steel plates are responsible for vertical and horizontal stability [2]. However, LRB systems have poor energy dissipation capacity associated with low damping characteristics of the rubber material, which may not be effective for strong earthquakes [3]. One way to improve isolator damping is to insert lead cores into the center of rubber layers, resulting in a lead-rubber bearing (LLRB) system. The LLRB dissipates larger quantity of seismic energy as the lead plugs experience large hysteresis deformation after their yield [4]. In addition, the lead plug has a much higher lateral stiffness compared to rubber layers prior to yielding. This means that the incorporation of lead plugs can contribute towards lateral resistance to non-seismic loads, thereby controlling base displacements during strong earthquakes. On the other hand, heat caused by plastic deformations of the lead core can degrade its strength, changing the hysteretic behaviour of the LLRB system [5].

The sliding isolation systems are widely used in recent years due to the physical stability of bearings. Similar to the rubber isolator, the sliding bearing integrates the functions of supporting the building weight and decoupling the superstructure from the ground in one device. One of the highly developed sliding bearing systems is the fiction pendulum bearing (FPB). The FPB is a friction-type sliding isolation system that consists of an articulated slider and a low-friction spherical sliding surface [2]. This system can produce a high energy dissipation capacity by dissipating residual seismic energy through overheating of contact surfaces, and the uplift of the superstructure [6]. Better than the rubber bearing, the FPB system has a larger horizontal displacement allowance. It also possesses self-centring capacity to limit residual displacements owing to the restoring

force provided by gravity [7]. Moreover, The FPB system can mitigate the torsional response of the building, because the lateral stiffness of the FPB is proportional to the weight of the main structure, and the centre of stiffness of the isolation system coincides with the centre of mass. Remarkably, the period of the FPB system is irrelevant to the mass of the superstructure, only controlled by the radius of sliding surface [8].

In practise, external damping device can be installed in combination with either rubber bearings or sliding bearings to create an additional source of viscous damping. [9]. In the case of near-fault ground motions, which are characterized by long periods and large intensities, lateral displacements of conventional isolators could be high, leading to system instability. Thus, the isolators require a large dimension to keep the stability of the structure, which may not to be practical. Moreover, the large size of bearing can be costly, which defeats the purpose of selecting seismic isolation system as a retrofit method. In this situation, viscous dampers with appropriate damping levels can be implemented to restrain the isolator displacements. These external viscous dampers, placed in parallel with conventional isolators, can work as supplementary energy dissipation devices as they develop compression, tension and shear deformations of the viscoelastic material [10,11]. During strong ground motions, the combination of isolators and viscous dampers works effectively to reduce dynamic responses of the isolated structure, as well as to ensure an acceptable lateral displacement at the isolator level.

In the current investigation, the effectiveness of rubber bearings (LRBs and LLRBs), friction pendulum bearings and supplemental viscous dampers was investigated through a case study, using the outpatient building of Lushan People's Hospital in China. The new wing (outpatient building) of this hospital was equipped with base isolation devices and was subjected to the magnitude 6.6 earthquake of 2013. The outpatient building remained in good condition because of the seismic isolation technology, while the non-isolated older wing nearby experienced significant damage. This building was modeled in SAP2000 software, and was studied as a typical reinforced concrete frame building that benefitted from a base isolation system to assess the applicability and performance of different types of base isolation system. Nonlinear behaviour of the superstructure and the isolators was modelled using appropriate link/support elements. Dynamic analyses of the

building were conducted with and without the isolation systems. Four input motions were applied in the horizontal Y-direction with the same frequency content but with increasing levels of intensity. The record selected was the EI Centro earthquake excitation (La11-005), and the record was scaled to four different levels. The effects of isolator properties on seismic behaviour of buildings were studied through a parametric investigation. The parameters considered pertained to the analytical building model, ground motion intensity and types of isolators having different characteristics. In addition, the building behaviour was assessed without any isolation system, and comparisons are made with the performance of buildings with different isolation systems. Results are compared in terms of lateral drift, peak absolute acceleration and residual drift, providing information for the effectiveness of the three isolation systems considered both under near-field and far-field earthquakes.

1.2 Objectives

The objective of the current investigation is to assess the performance of different types of base isolation systems for seismic protection of reinforced concrete frame buildings, through dynamic inelastic response history analysis of a selected prototype building. The isolation systems considered include, i) rubber isolators (LRBs &LLRBs), ii) rubber isolators with energy dissipation systems, and iii) rubber isolators coupled with friction pendulum isolators.

1.3 Scope

The following forms the scope of the research project:

- Literature review and overview of existing base isolation systems available in the construction industry.
- Selection of a prototype building (The outpatient building of Lushan City People's Hospital in China) for investigation.
- Structural and hysteretic modelling of the prototype building for dynamic inelastic analysis.
- Dynamic inelastic response history analyses of the selected building without base isolation, with and without infill masonry walls.

- Dynamic inelastic response history analyses of the selected building with three types of base isolation systems, each having varying characteristics.
- Comparisons of building performance and the three types of base isolation systems considered.
- Discussion and presentation of results.

1.4 Literature Review on Seismic Isolation System

Several research programs were conducted in the past to assess the effectiveness of base isolation systems for seismic protection. Yi and Bijan [12] studied the effectiveness of a rubber isolation system under different earthquake excitations. In their research, a five-storey steel frame was analysed under four ground motions of variable intensity and frequency content through numerical analysis and shake table tests. Results confirmed the efficiency of rubber bearing system for seismic retrofitting, but the benefits gained from this type of bearing system were highly dependent on the type and nature of the ground motion. It was noted that the lateral displacements in the isolators were dependent on the intensity and frequency contents of the seismic records, while the floor accelerations were significantly reduced regardless of the ground motion.

Bong and Yang [13] investigated the effects of damping on seismic performance of laminated rubber bearings and lead rubber bearings. The LLRBs studied in this research project had different diameter of lead plugs, and thus had variable damping levels. In spite of the significant reduction in seismic response of the isolated model structure, the lateral displacements were found to be excessive, exceeding the deformation capacity of the LLRB isolator especially under near-field ground motions. The diameter of the lead plugs was enlarged for the purpose of generating increased level of damping. This enlargement increased the stiffness of the isolation system and consequently intensified the floor acceleration response, causing more damage to the secondary systems and the internal components attached to the primary structures. Results showed a slight amplification in floor acceleration response spectra as the isolation damping reached 8%, and it became considerably large when the damping in the isolators exceeded 24%, resulting in adverse effects on non-structural elements.

A series of shake table tests were conducted by Mauro and Donatello [1] to investigate the beneficial effects of four isolation systems on seismic response, including the rubber bearing system. The implementation of the rubber isolation system provided outstanding structural enhancement in terms of reducing inter-storey drifts, floor accelerations and shear forces even under strong earthquakes. Results of their study showed that the rubber isolation system produced the smallest floor acceleration in comparison with other systems, but at the expense of base displacement and base shear coefficient. Moreover, the seismic performance of base isolated structures with and without the masonry infill walls were compared. The results showed that the installation of infills had significant influence on base shear, base displacement and inter-storey drifts of the superstructure due to the stiffening provided by the masonry walls. The results also showed that the presence of infills affected the effectiveness of rubber bearing system minimally, as compared with the effects on other systems, especially when the structure was subjected to strong earthquakes.

Briseghella and Zordan [14] confirmed the contribution of FPB isolation system to seismic retrofit through a case study. An existing building that was heavily damaged in the 2009 L'Aquila earthquake was retrofitted by an FPB system, and its performance was studied through response spectrum analysis, the linear dynamic analysis and nonlinear dynamic analysis. The FPB system was shown to be effective in restraining the storey shear and inter-storey drifts of the building model. It also presented a significant energy dissipation capacity attributed to the strong non-linear behaviour of FPBs.

The influence of isolator properties (i.e. friction coefficient) and the earthquake characteristics on seismic reliability of building isolation with FPBs were analysed by Castaldo and Palazzo [15]. The factors affecting structural response were considered as random variables; and the monovariate and multivariate probability density and cumulative distribution functions were computed. Also, assuming limit state thresholds and domains (performance objectives), the monovariate and bivariate exceeding probabilities (structural performances) were evaluated. The structural performance (SP) curves were compared with the performance objectives (PO) curves. The researchers showed that, employing FPBs with lower friction coefficients could improve seismic

structural performances. Additionally, the SP curves of the isolation level or the proposed equations could be used to calculate the plane dimension of the isolators in terms of reliability levels.

Shih and Nicos [16] studied the behaviour of hybrid isolation system that composed of either LLRBs or FPBs supplemented with fluid viscous dampers. An extensive programme of shake table tests was conducted to investigate the effectiveness of the hybrid system with different damping levels that was provided by bearings and dampers. Results showed that viscous dampers were effective in restraining base displacements. However, redundant viscous damping may cause unexpected large inter-storey drifts. When viscous damping was synchronized with friction damping, the latter became more efficient than the former in controlling spectral displacements, which would be amplified as the isolation periods increased. For long-isolation periods (like prototype isolation period, T=3 sec), neither the installation of viscous damping nor the increase of friction damping could largely change the acceleration and displacement response. When the isolation period exceeded 3 sec, further lengthening the period had minor effects on the acceleration, displacement, and velocity spectra; meaning that it was needless to pursue extremely large isolation periods to realize the benefits of seismic isolation. As to the lead rubber bearings, the energy dissipation capacity of LLRBs that were evaluated by the plastic performance of lead plugs was found to be over-estimated, leading to the under-estimation of spectra displacements.

Providakis [17] examined seismic performance of LLRBs with external damping devices, as they affected base and superstructure drift when subjected to near-field and far field ground excitations. It was found that the supplemental viscous damping could remarkably reduce large isolator displacements excited by near field excitations with large velocity pulses. However, this high level of additional damping that was required for near-field ground motions might become superfluous if the structure experienced ground motions coming from the far fault sites. As a result, it might restrain the movements of isolators and thus, impair the efficiency of the seismic isolation. Besides, the provision of supplemental damping limited the base drift and enhanced the stiffness of the isolated building by creating higher-mode effects, and thereby increasing superstructure drifts,

especially in the case of far-field excitations. Also, in another paper of Providakis [18], the author accounted for the effects of supplemental damping on floor accelerations of the isolated buildings (supported on LLRB and FPS systems). This additional consideration proved that viscous damping sufficient to control the absolute floor acceleration for both the LLRB and FPB systems under near-field ground motions, but generated adverse effects for the acceleration response when subjected to far-field excitations.

Dolce and Cardone [19] demonstrated advantages and disadvantages of base isolation systems through their research when the isolators were used for seismic protection of light, secondary systems. The effectiveness of seismic isolation on protecting internal contents and equipment was also evaluated by the researchers based on the acceleration response spectra of modeled buildings from shake table tests. It was reported that, seismic isolation systems could significantly reduce dynamic response on the secondary systems. However different isolation systems could perform differently due to the differences in their hysteretic behaviour. For instance, the isolation system that has strong nonlinear behaviour (such as the SMA system) tends to produce high frequency vibrations in the superstructure, bringing out a high acceleration on components whose frequencies were close to the 2^{nd} and 3^{rd} mode frequency of the isolated structure, causing severe damages on those components. On the contrary, the quasi-elastic isolation system, such as the rubber bearing isolation system, concentrates a significant amount of energy in a narrow low-frequency range, which may include the natural frequencies of some internal contents. This may result in tuning effects on these components. The authors emphasized that the design of isolation system should account for the protection of light secondary systems. This is especially true for the period of quasi-linear isolation systems and the threshold force levels of strongly non-linear systems, which could largely influence the performances of secondary systems.

Yu and Goodarz [20] studied the wind load sensitivity of base-isolated structures with rubber bearings and sliding bearings. The structure was considered as a rigid block and the variation of wind velocity along the structure height was neglected. Both the mean and random conditions of wind loads were accounted for in the research program. A stationary random model for wind velocity was selected, and the displacement response

of the modeled structure was studied through the equivalent linearization method. The researchers concluded that the isolated structure was insensitive to wind excitations subjected to common storms for both the rubber bearings and sliding bearings. However, with regard to extreme wind conditions, like hurricanes, the isolated structure installed with rubber bearings experienced a few centimeters base displacement. The sliding bearing isolation system showed better performance to resisting wind loads. The experiments showed that the base displacement of sliding bearing isolation system was relatively small under hurricanes. Also, it showed that the increase in isolation damping could help restrain displacements in the isolator, and thus, detuning the sensitivity to wind effects.

Chapter 2

Prototype Building

2.1 General

The outpatient building of Lushan People's hospital in China was selected as the prototype building in the current research project, and used to investigate the contribution of base isolation systems to seismic response of reinforced concrete frame buildings. The outpatient building is a reinforced concrete moment resisting frame, located in Lushan County of Ya'an City in the Sichuan Province of southwest China. According to the latest Chinese design code (GB 50011-2001, 2010 edition), Lushan County is categorized as an area with VII fortification intensity (the required construction standard for individual structures), on the basis of the soil type and topographic conditions of the site. The design spectral acceleration for Lushan county is equal to 0.15g regarding VII fortification intensity [21]. Surprisingly, the outpatient building of Lushan People's hospital, seismically isolation, remained in good conditions and only experienced slight damage to non-structural elements even though it was subjected to a magnitude 6.6 earthquake (Lushan Earthquake). On the contrary, the adjacent non-isolated building suffered major damage to both structural and non-structural elements. Due to its excellent structural performance during the earthquake, the isolated outpatient building was selected as a good example to study the effectiveness of different base isolation systems on reinforced concrete frame buildings.

2.2 Structural Layout and Member Properties

The outpatient building of the Lushan City People's Hospital in China was selected as the prototype building. The building is a seven-story reinforced concrete frame structure with a total seismic mass of 9137 tons. It has an average inter-storey height of 4.2m, resulting in a total building height of 23.4 m above the ground level. Figure 2.1 provides a typical plan view of the building. Each storey of the building has a floor area of approximately 1256 m^2 with plan dimensions of 67.4 m by 19.5 m. The structural frame system comprises of 600 mm square columns and main beams having cross-sectional dimensions of 300 mm x 500 mm and 300 mm x 700 mm in the long direction (X direction), and 300 mm x 600 mm in the short direction (Y direction). The secondary beams are attached to the main beams, with cross sectional dimensions of 200 mm x 500 mm or 200 mm x 600 mm. The building also features flexible slabs with 120 mm thickness at each floor and the roof. The structural components of this building were built with C30 (30 MPa) concrete. The external frames had infill masonry walls. The walls around the elevator shaft and staircases were grouted. This resulted in somewhat higher stiffness as compared to other walls. The external infill walls had large window openings, whereas some of the walls in the short direction had small openings.

Seismic isolation layer was placed between the foundation and the first storey of the building. A total of 79 isolation devices were installed at individual isolated footings. The isolators consisted of 47 laminated rubber bearings (LRBs) and 32 lead laminated rubber bearings (LLRBs). The design properties of the isolators used in the structural system are listed in Table 2.1. The diameter of the bearings was determined as 500 mm and 600 mm depending on vertical load, wind loading, and the required isolator displacement control. Figure 2.2 shows the layout of the isolation system. The LLRBs were placed under the external columns to help resist wind loading and the LRBs were placed beneath the other columns. Also, an extra isolator was installed under the columns subjected to high vertical loads (shown as 2LRB500) to support the structural weight. A separation gap was set around the building to allow movements of the isolation system during earthquake. The structural plan is symmetric in the "y" direction, as showed in Figure 2.1, while the placement of the infill walls and seismic isolators could generate an eccentricity between

the centre of mass and the centre of stiffness, causing torsional response of the isolated building during earthquakes.

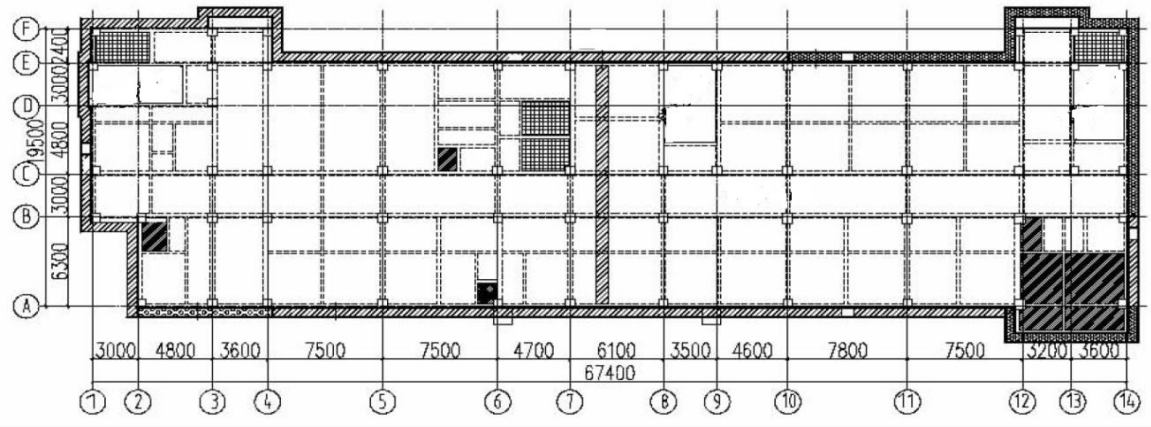

Figure 2.1: Building Plan of the Outpatient Building of Lushan People's Hospital

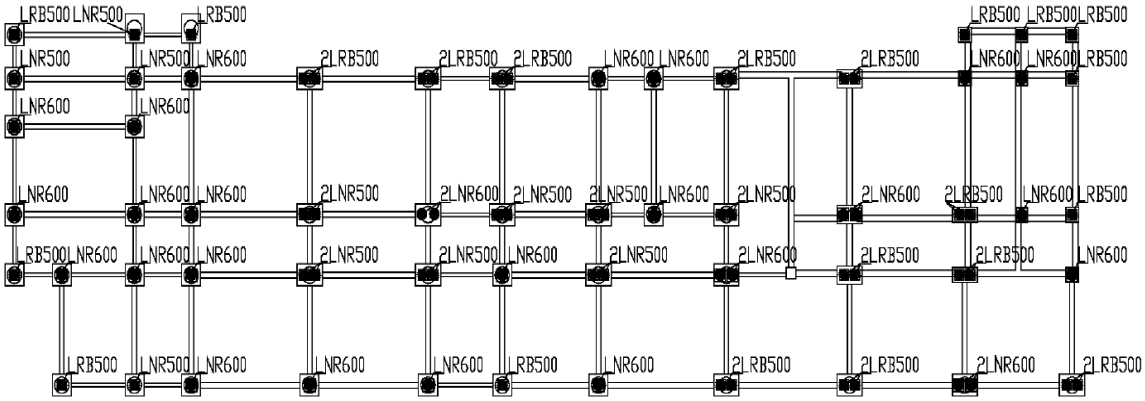

Figure 2.2: Locations of the Seismic Isolation System

Table 2.1: Design Parameters of the Isolators

Design Properties	LLRB	LRB#1	LRB#2
Thickness of the Rubber Layer (mm)	86.4	86.4	100
Diameter of the Isolator (mm)	500	500	600
Area (cm^2)	1963	1963	2827
Vertical Load Capacity (kN)	2466	2356	3392
Vertical Stiffness (kN/mm)	2044	1694	2517
Elastic Stiffness (kN/mm)	7.591	0.876	1.091
Post-yield Stiffness (kN/mm)	1.354	None	None
Yield Strength (kN)	40.1	None	None

2.3 Performance of the Prototype Building during the 2013 Lushan Earthquake

A strong earthquake occurred near Lushan County, Ya'an City, Sichuan Province on April 20, 2013. The earthquake's epicenter was located at $30^{o}17'02''$N and $102^{o}57'22''$ E. The focal depth was 12.3 km. The magnitude of was determined as M7.0 by the China Earthquake Networks Center (CENC). The United States Geological Survey (USGS) determined the magnitude to be M6.6 [22]. The PGA of 0.4g to 0.5g recorded (according to CENC) during the earthquake caused thousands of buildings to be damaged and partially or fully collapsed, while the outpatient building of the Lushan People's Hospital, which is located within a 10-kilometer radius from the epicenter, remained intact during and after the earthquake. This was attributed to the installation of an isolation system whose protection made the outpatient building more resilient to the Lushan Earthquake. The structural members of the building stayed unharmed without any visible cracks, as depicted in Fig. 2.3. The non-structural elements such as infill walls, ceiling tiles and light fixtures, experienced minor damage. Moreover, there was little impact on the internal contents and equipment attached to the main structure, enabling the hospital to be fully functional, providing medical services during and after the earthquake.

In spite of the excellent seismic performance of this isolated building, the isolation system experienced large horizontal deformations that damaged the cover on some of the isolators; and a residual lateral displacement of 30 to 50 mm was observed at the isolation level. Also, the connected bolts of the isolators were corroded, indicating that the isolators were inadequately protected. This poor condition may influence the efficiency of the isolation system. Moreover, insufficient space was left between the superstructure and the surrounding ground for the movement of the isolation system during the earthquake. In the short direction of the structure, the smallest width of the separation gap was only 50 mm and no separation gap was left at the main entrance and at the back of the building. This consequently caused damage to the surrounding concrete floor and the staircase at the first storey level due to the impact from the superstructure. Furthermore, the plumping system was damaged because of lack of flexible connections at the isolation interface, which hampered the normal operation of the building. The damage associated with the above is illustrated in Fig. 2.4.

(a) Outside of the Building

(b) Inside of the Building

(c) Ceilings

(d) Infill Walls

Figure 2.3: Isolated Outpatient Building of the Lushan People's Hospital after the 2013 earthquake

Another building of the Lushan People's Hospital that was not seismically isolated, was located nearby, connected to the isolated outpatient building by staircases, as shown in Figure 2.5. The non-isolated building (left wing) was built in 2004 before the 2008 Wenchuan Earthquake, while the base isolated building (right wing) was built after the Earthquake. In contrast with the superior performance of the new outpatient building, the old building became highly vulnerable to the strong ground motion. Although no serious damage was detected in structural elements, non-structural elements were severely damaged and mostly destroyed during the earthquake. Figure 2.6 illustrates damage to suspended ceilings, which fell on the floor. Some infill walls experienced significant diagonal tension cracking, while others experienced partial failures. Damage during the earthquake paralyzed the normal operation of the hospital. The falling debris destroyed the hospital equipment, putting them out of commission. Due to the significant damage,

the old building was evacuated after the earthquake and emergency operations were forced to be conduct in temporary tents to maintain medical services.

(a) Isolators

(b) Separation Gap around the Superstructure

(c) Damage on the Staircase at First Floor

(d) Pipeline at the Isolation Interface

Figure 2.4: Isolated Outpatient Building of Lushan People's Hospital after the 2013 Earthquake

Figure 2.5: The Non-isolated Outpatient Building and the New Isolated Outpatient Building

(a) Outside of the Building

(b) Inside of the Building

(c) Ceilings

(d) Infill Walls

Figure 2.6: Non-isolated Outpatient Building of Lushan People's Hospital after the 2013 Earthquake

The difference in performance of these two adjacent buildings of the Lushan Earthquake was mainly attributed to two reasons. First, the new outpatient building was designed according to the updated design regulations that increased the seismic design force requirements after the 2008 Wenchuan Earthquake. Second, the installation of seismic isolation system mitigated the transfer of seismic energy to the superstructure, thereby significantly reducing its dynamic response. Consequently, the floor accelerations and inter-storey drifts of the superstructure were well controlled, and little damage was incurred on structural and non-structural elements. The difference in seismic response of the two buildings highlight the importance of implementing seismic isolation systems both in new buildings, as well as in existing buildings as a seismic retrofit strategy.

Chapter 3

Structural Modelling and Computer Software

3.1 General

Computer software SAP2000 was used to conduct dynamic inelastic response history analysis of the selected prototype building. The program incorporates features for nonlinear modelling of structural components, as well as base isolators, making it a suitable choice of software for the project. The beams and columns of the prototype building (outpatient wing of the Lushan City Hospital) was modeled by frame elements with non-linear material properties for concrete and reinforcement. Multi-linear plastic links were assigned to the ends of the frame members to simulate post-yield behaviour. The isolation systems, such as the rubber bearing system and the friction pendulum bearing system, were simulated by the rubber isolator links and the friction isolator links, respectively, with appropriate design properties. Also, the external viscous dampers that were attached to the isolators were modeled by the damper link element.

The outpatient building was modelled both as a fixed structure, and as a base-isolated structure to investigate the effectiveness of the seismic isolation system. Four input ground motions with the same frequency content but with different levels of intensity were applied in the short direction of the structure. Gravity (dead and live) loads and wind loads were determined based on the Chinese building code. The analytical models of the building represented the actual building structure as closely as possible, and hence are believed to give accurate results for the linear and non-linear dynamic response of the building under seismic loading.

3.2 SAP2000 Software

The software SAP2000 was developed by Computers and Structures, Inc. It is a general purpose finite element program that has been widely used in recent years. The program is ideal for design and analysis of structures, such as buildings, bridges, and industrial plants. 2D and 3D structural models with simple to complex geometry can be easily modeled and analysed through a relatively simple engineering process, owing to its practical and intuitive object-based modeling environment. Additionally, SAP2000 handles a wide variety of structural analysis procedures, including static and dynamic analysis, linear and nonlinear analysis, pushover analysis, seismic analysis under ground excitations, response spectra analysis, as well as others types of dynamic analyses under time varying forcing functions. Three different levels of sophistication are available for structural analysis, namely the SAP2000 Basic, the SAP2000 PLUS and the SAP2000 Advanced. The SAP2000 Advance option employed in the current project extends the basic capacities by introducing nonlinear hinge elements and the multi-linear plastic link elements that make it possible to capture inelastic response of frame elements. All options of the SAP2000 programs support various design codes, including ACI, CSA and AISC building codes.

The SAP2000 elements that were used in this research program are listed below.

Frame Element:

Frame elements are used to model beams, columns, braces, and truss members in both 2D and 3D systems. The geometry and the reinforcement details of concrete elements are determined in Frame Section Properties (database tables). Elements that have nonstandard or composite sections of arbitrary geometry can be modeled in Section Designer that allows for custom-defined cross sections. The frame behaviour is characterized based on a three-dimensional beam-column formulation (Bathe and Wilson, 1976) that accounts for the coupled effects of biaxial bending, torsion, axial deformation and biaxial shear deformation. The nonlinear material properties of the frame are incorporated by assigning nonlinear hinge and link elements.

Link/Support Element:

The link element is used for connecting two joints, and the support element is used for connecting a joint to the ground. Various behaviours, specified as linear, nonlinear and frequency-dependent, can be assigned to different degrees of freedom (DOF), consisting of axial, shear, torsion and bending components in a single link/support element. For all six DOF, regardless of the properties assigned, linear effective stiffness and damping are required for the purpose of calculating the natural period of vibration for the structure. If a DOF is defined as nonlinear, the nonlinear force-deformation relationship must be specified. Various types of nonlinear properties are available for the link/support element, including the multi-linear plastic property, hysteretic (rubber) isolator property, friction-pendulum isolator property and damper property. When the multi-linear plastic link is used to simulate the material nonlinear behaviour, the direct-integration time-history analysis should be selected instead of the fast nonlinear analysis (FNA) which will be applicable only if the nonlinearity is limited to the nonlinear links.

Hinge Element:

Uncoupled moment, torsion, axial force and shear hinges, and coupled P-M2-M3 hinges are available in SAP2000. A hinge element with a specific length can be assigned to the frame or the tendon member to simulate yielding and post-yielding behaviour. The plastic behaviour only occurs within the hinges and the elastic behaviour occurs over the member length. A series of hinges can be assigned at discrete locations along the member length to capture distributed plasticity. Also, more than one type of hinge can be placed at the same location to simulate different nonlinear behaviour for each DOF. The hinge element could affect structural performance in nonlinear static and nonlinear time-history analysis, but it wouldn't be active in the FNA analysis.

3.3 Modeling of the Superstructure

3.3.1 Modeling of Frames

A 3D model of the selected building was created using SAP2000 as shown in Figure 3.1. The same model was used for both fixed base buildings (without base isolation) and base-

isolated buildings having different base isolation systems. The superstructure elements of the building model were modelled using the frame elements in SAP2000, and the sections of beams and columns were defined in the Section Designer (SD) as shown in Figure 3.2. These sections were then assigned to frame objects. The unconfined concrete used was of C30 based on the Chinese practice with 2400 kg/m^3 mass density and 30 MPa compressive strength. Confined concrete was used for the core and unconfined concrete was used for the cover concrete for both beams and columns. The reinforcement for the beams and columns was determined by SAP2000 through Concrete Frame Design option. The reinforcing steel used was of HRB 335 type.

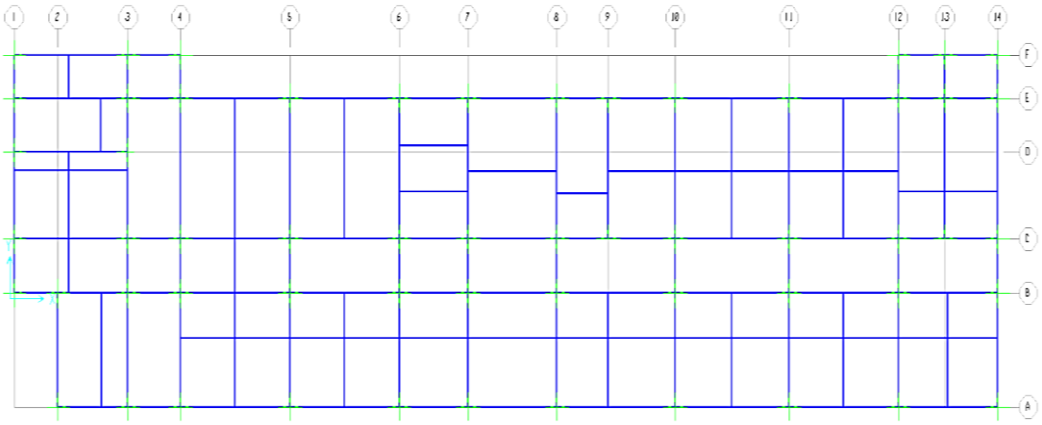

(a) Plan

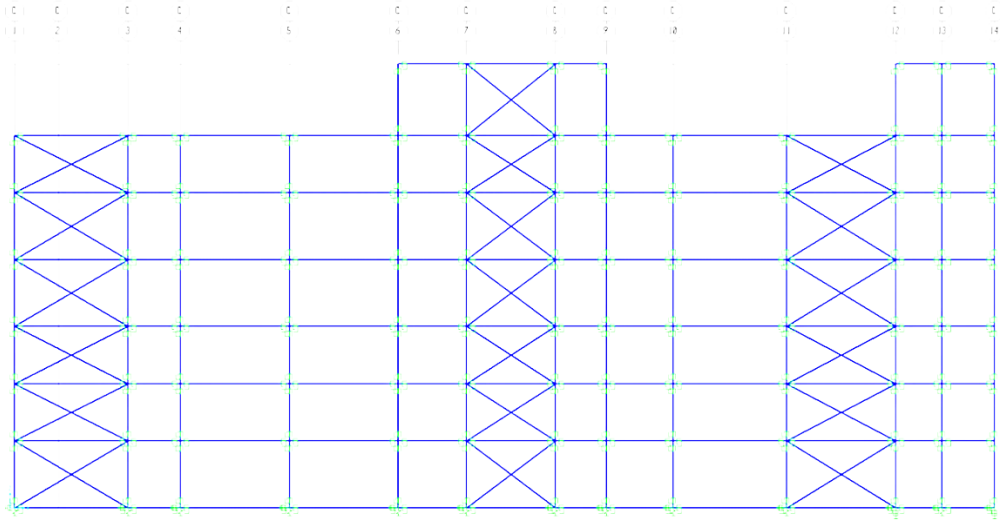

(b) Elevation

Figure 3.1: Modeling of the Superstructure in SAP2000

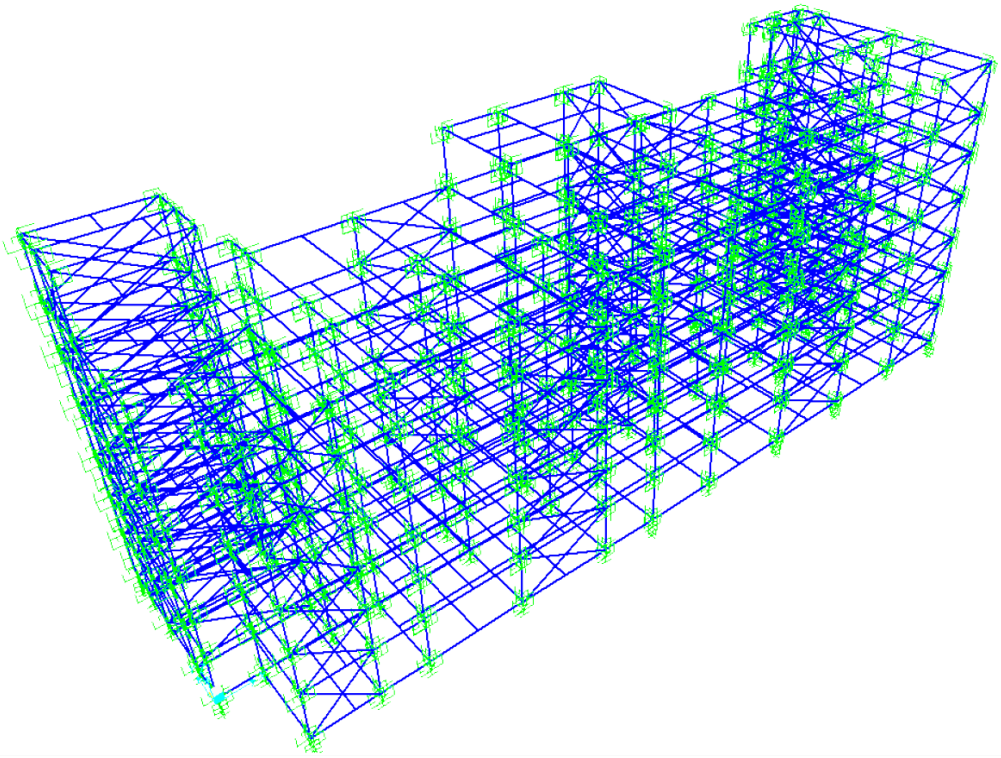

(c) 3D View

Figure 3.1: Modeling of the Superstructure in SAP2000

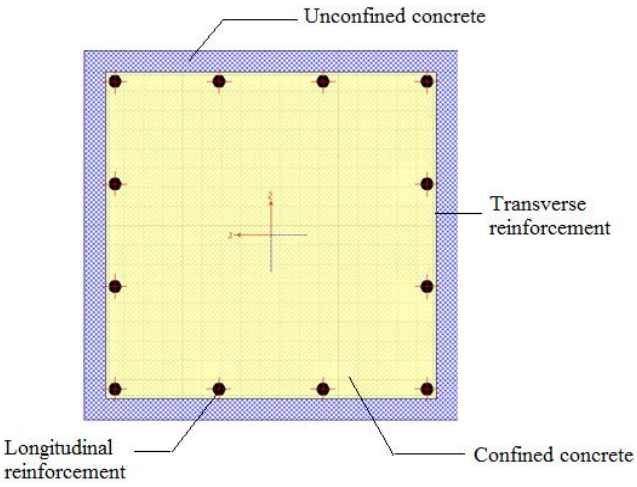

Figure 3.2: SD Section of a Square Column

The actual design details for the building were not available. Therefore, the National Building Code of Canada (NBCC-2010) seismic provisions were used to design the buildings. The building was assumed to be a conventional reinforced concrete frame building, without the special seismic detailing for ductile or nominally ductile buildings.

Equivalent static force approach was used for seismic design based on first mode response. The design base shear was computed as described below.

$$V = \frac{S(T_a)M_V I_E W}{R_d R_o} \tag{3.1}$$

Where R_d and R_o are the ductility related force modification factor and overstrength raleted force modification factor for the moment-resisting frames, selected as 1.5 and 1.3 respectively. T_a in the base shear equation is the empirical fundamental period for the concrete moment frames, given by $T_a = 0.075(h_n)^{3/4} = 0.72s$; I_E is the building importance factor for the hospital and is equal to 1.5; M_V is the higher mode factor, specified as 1 for the moment-resisting frames for $T_a \le 1.0$ and $S_a(0.2)/S_a(2.0) \ge 8.0$; W is the structural weight contributing to inertia forces, computed using the following load combination.

$$W = D + 0.25L + 0.6L_s = 223712.5kN \tag{3.2}$$

The design spectral acceleration $S_a(T)$ is related to the building fundamental period T_a and the peak acceleration $\alpha_{\max}$. According to the Chinese design code, the design spectral acceleration was computed by Eq. 3.3.

$$\alpha = \left(T_g / T_a\right)^{\gamma} \eta_2 \alpha_{\max} \tag{3.3}$$

where $\alpha_{\max}$ is specified as 0.12g for Lushan county, T_g is the characteristic site period, specified as 0.35s; η_2 is the damping adjustment coefficient, determined as 1; and γ is equal to 0.9. Thus, $S_a(T)$ is calculated as 0.063g and the equivalent static force is obtained as 10789.22 kN.

Inverted triangular distribution of lateral seismic forces was used. The seismic force at each floor level (shown in Table 3.1) was calculated according to:

$$F_i = \frac{W_i h_i (V - F_t)}{\sum W_i h_i} \tag{3.4}$$

Where V is the seismic base shear, F_i is seismic force distribution factor at i floor, W_i is the structural weight at the i floor, h_i is the height from the base to the i floor.

Table 3.1: Seismic Force at Each Floor Level

No. of Floor	$h_i(m)$	$W_i(kN)$	$W_i h_i(kN.m)$	$F_i(kN)$
1st	27.9	9746.17	271918.2	803.73
2nd	23.4	35743.81	836405.1	2472.24
3rd	19.8	35743.81	707727.4	2091.89
4th	15.6	35743.81	557603.4	1648.16
5th	11.4	35743.81	407479.4	1204.42
6th	7.8	35743.81	278801.7	824.08
7th	4.2	35743.81	150124	443.73

The above seismic forces were applied to the model structure for static lateral load analysis, from which the frame members were designed. The reinforcement details of the frame elements are presented in Table 3.2.

Table 3.2: Reinforcement Details of the Frames

No. of Floor	Column(600*600)	Beam1 (300*500)	Beam2 (300*700)	Beam4 (300*600)
1st	1.04% (12#20d)	1.25% (6#20d)	1.05% (7#20d)	0.82% (6#25d)
2nd	1.04% (12#20d)	1.25% (6#20d)	1.05% (7#20d)	0.82% (6#25d)
3rd	1.04% (12#20d)	1.25% (6#20d)	1.05% (7#20d)	0.82% (6#25d)
4th	1.04% (12#20d)	1.25% (6#20d)	0.9% (6#20d)	0.82% (6#25d)
5th	1.04% (12#20d)	0.67% (5#16d)	0.57% (6#20d)	0.82% (6#25d)
6th	1.04% (12#20d)	0.67% (5#16d)	0.57% (6#20d)	0.68% (5#20d)
7th	1.04% (12#20d)	0.67% (5#16d)	0.57% (6#20d)	0.68% (5#20d)

3.3.2 Modeling of Post-yield Behaviour of Frame Elements

Under sufficiently high lateral forces the frame members yield when they reach their yield moments. When the yield moment is reached, plastic hinge starts forming near the ends of frame members, developing large rotations. To capture inelastic behaviour of frame members, nonlinear material stress-strain relationships shown in Figure 3.3 are assigned to concrete and reinforcing steel. The plastic behaviour in SAP 2000 is simulated by assigning concentrated plastic hinges or the multilinear plastic links to the frame objects. When the frame member deformation exceeds the elastic limit, the expected plastic behaviour occurs entirely within the plastic hinge or link, while the elastic behaviour taking place over the member length.

In this project, the nonlinearity of the frame system was modeled by using the multilinear plastic link rather than the concentrated hinge because the hysteretic behaviour could be specified for multiple DOF within a single link, which is not possible for concentrated hinges. The multilinear plastic links with selected lengths were inserted at both ends of beams and columns as shown in Figure 3.4. The link length was specified as being equal to the equivalent plastic hinge length (l_p), calculated as $l_p = 0.5d + 0.05z$ (Mattock method), where z is the shear span of the frame objects and d is the effective depth. The beam-column joints (the overlap of beams and columns, depicted as shadow areas in Figure 3.4) were made rigid to eliminate the rotation of the connection. Moreover, the behaviour of plastic link was defined as nonlinear in two horizontal directions (R_2 and R_3 directions) and linear in the other four directions. The effective stiffness of the multilinear plastic link in the six principal directions was calculated using the formulae given in Table 3.3, where L is the link length and A is the area of the frame member. Also, the weight of plastic links was calculated as the weight per unit length of reinforced concrete times the link length. Figure 3.5 shows nonlinear force-deformation characteristics of plastic links. The multilinear force-deformation data were obtained from the moment-curvature relationship of RC frame members though sectional analysis. The hysteresis model proposed by Takeda et al. (1972) was adopted to describe the hysteretic behaviour of plastic links. In this degrading hysteretic model, the reloading stiffness is lower than the initial loading stiffness because of stiffness degradation associated with cracking of concrete and yielding of reinforcing steel.

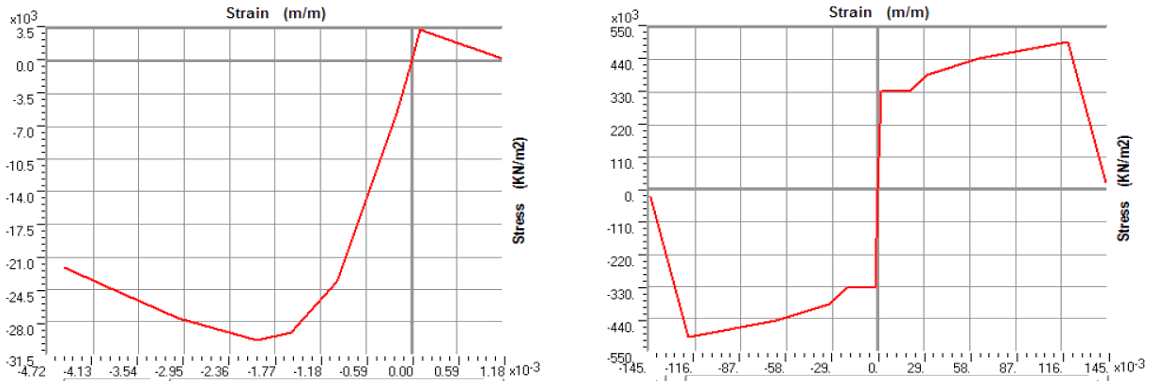

(a) Unconfined C30 Reinforced Concrete (b) HRB335 Steel

Figure 3.3: Stress-strain Relationships of Unconfined C30 Concrete and HRB335 Steel

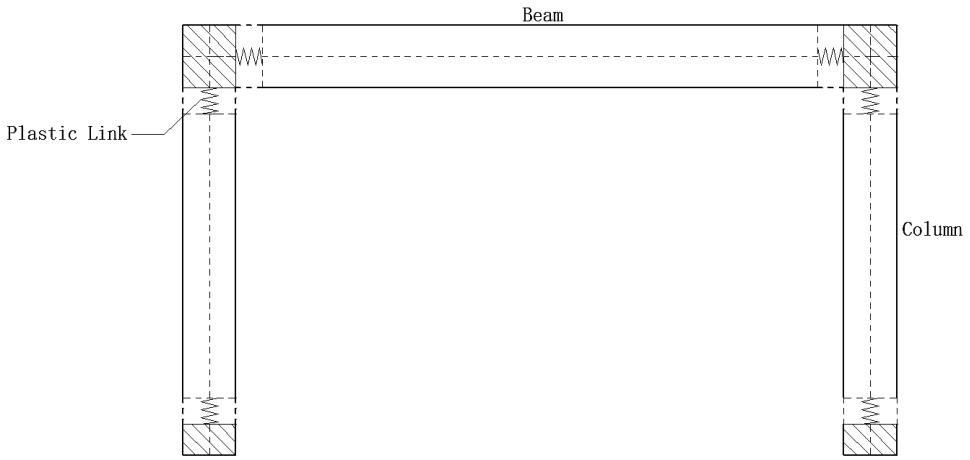

Figure 3.4: Placement of Plastic Links in Frame Elements

Multi-Linear Force-Deformation Definition

	Rotation	Moment
1	-0.0217	-783486.
2	-1.308E-03	-783486.
3	0.	0.
4	1.308E-03	783486.
5	0.0217	783486.

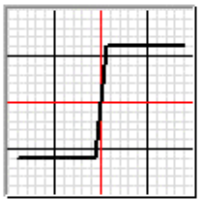

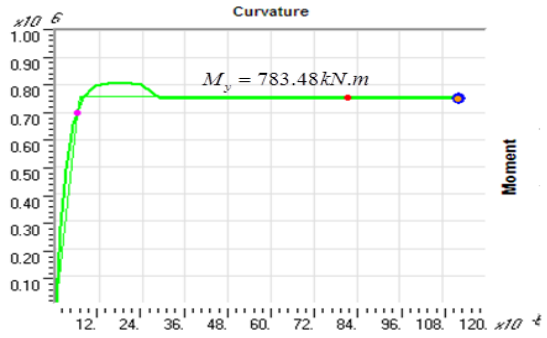

(a) Force-Deformation Definition of Links (b) Moment-Curvature Relationship of Reinforced Concrete

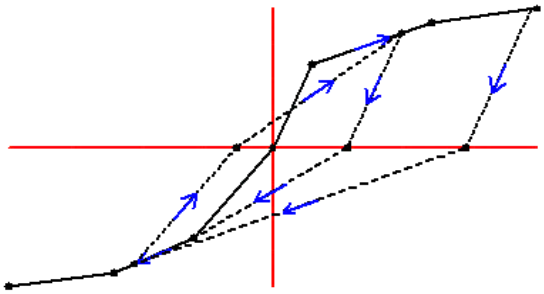

(c) Takeda's Hysteretic Model

Figure 3.5: Modeling Details of Multi-linear Plastic Links

Table 3.3: Effective Stiffness for Multi-linear Plastic Links in Six Principal Directions

Stiffness Coefficient	Formula
k_1 - Axial (U_1)	EA/L
k_2, k_3 - Translation (U_2, U_3)	$12EA/L^3$
k_4 - Torsion (R_1)	GJ/L
k_5, k_6 - Flexure (R_2, R_3)	EI/L

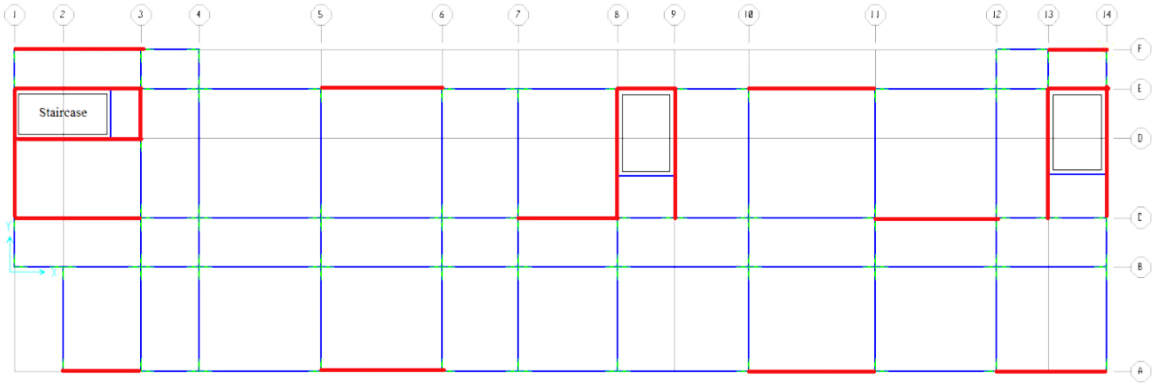

Figure 3.6: Placement of Grouted Walls

Table 3. 4: Properties of the Autoclaved Aerated Concrete Masonry

Dry Density (kg/m^3)	Compressive Strength (Mpa)	Tensile Strength (Mpa)	Elastic Modulus(Mpa)
500.00	3.00	0.30	1.50

3.3.3 Modeling of Masonry Walls

Part of the external walls and the walls forming the elevator shaft and stairwells at every floor of the building (shown as red lines in Figure 3.6) were grouted to enhance the lateral stiffness of the superstructure. Because the precise properties of the concrete masonry units used in the building could not be found, the autoclaved aerated concrete (AAC) masonry units that are widely used in China was assumed. Their properties are shown in Table 3.4. It is noteworthy that the density of the AAC masonry (500 kg/m^3) was quiet low compared with the density of regular concrete masonry (1700 to 2000 kg/m^3). The low density of masonry reduced the self-weight of the building, consequently lowering the bearing loads on the isolators and the initial forces caused by the ground excitation.

The infill wall was modeled in SAP2000 by two diagonal struts having the same thickness as the infill panel. The equivalent width of the strut (w) was calculated as $w = 0.175 d_{\inf} (\lambda_h H_{\inf})^{-0.4}$, where ($H_{\inf}$) is the height and ($d_{\inf}$) is the diagonal length of the infill wall [23,24]. Approximately, the strut width could be taken as equal to one-fourth of the diagonal wall length. The properties of the AAC masonry were assigned to the struts, except that the density was specified as zero, because the weight of the infill walls was incorporated as equivalent distributed loads on the beams. Because the struts were

intended to simulate diagonal compressive forces developing in infill walls, the joints connecting the struts to the beam-column joint was defined as pin connections to release the moments (M_x, M_y, M_z) at the strut ends. Also, the tension capacity was set to zero as struts could not resist tensile forces associated with diagonal tension in unreinforced masonry infills. At any given time during earthquake response, one of the two diagonal struts modelling an infill panel would be under compression while the other would experience zero tension, i.e., only one strut would be effective. Axial hinges were assigned at both ends of struts to simulate strength degradation of concrete masonry beyond crushing. The plasticity of axial hinges was modelled with the force-displacement behaviour of infill walls, shown in Figure 3.7. After the peak point (Point B) was reached, the resistance rapidly drops to zero, indicating failure of the infill (Point E).

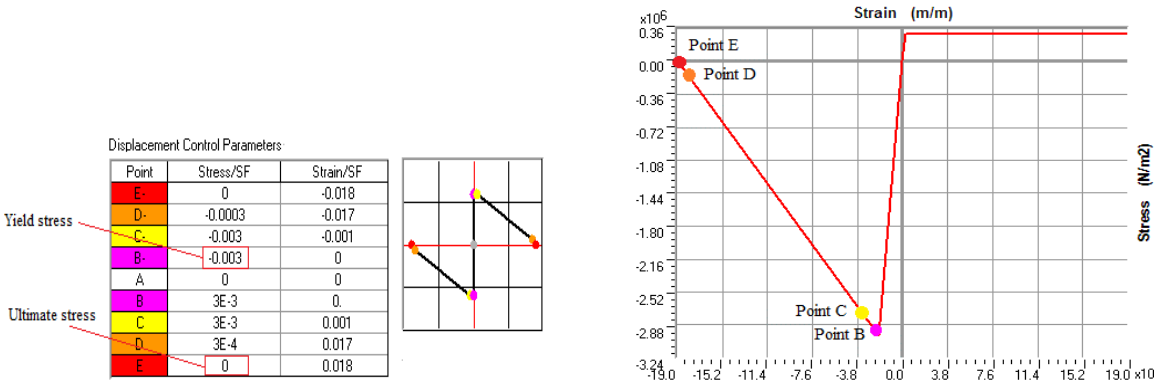

(a) Force-Deformation Definition of Axial Hinge (b) Force-Deformation Relationship of Masonry

Figure 3.7: Definition of Axial Hinge

3.4 Modeling of Rubber Bearings

Hysteretic isolator links were used to simulate rubber bearings in SAP2000. An isolator link was assigned to each column at the foundation level as a single joint element to connect the superstructure to the ground. Two types of isolator links were used; LRB links and LLRB links were applied to simulate laminated rubber bearings and lead rubber bearings, respectively. A small mass should normally be assigned to isolator links, empirically equal to about 100 times less than the supported superstructure mass. That being said, the isolator masses would have no critical effect on the overall dynamic

performance of the structure, though it might slightly influence the convergence of the modal analysis. In the current project, mass and rotational inertia properties of LBR and LLRB link elements were set to zero to reduce the complexity of calculations.

The behaviour of link elements in SAP2000 is defined in the Link/Support Property. Only the properties for axial deformation (U_1), shear deformations (U_2, U_3) and torsional deformation (R_1) were specified. All internal deformations of the isolator links are assumed to be independent of each other. The LRB and LLRB links had linear effective-stiffness properties for axial and torsional deformations. For shear deformations, the LRB links used elastic properties owing to the strong elasticity of the rubber material while the LLRB links had coupled plasticity properties associated with the hysteretic lateral performance of the lead plugs. Although the shear deformation of the LLRB links was defined as nonlinear, the linear properties such as the effective stiffness and the effective damping were still needed. This is because the model analysis that starts from zero initial condition uses the effective stiffness rather than the actual nonlinear stiffness to calculate the natural period of structural models.

Table 3.5: Parameters Assigned to Rubber Isolator Links

Properties	LLRB	LRB#1	LRB#2
Vertical Load Capacity (kN)	2367	2367	3393
Vertical Stiffness (kN/mm)	1030	1030	1678
Torsional Stiffness (kN/mm)	28407	28407	50894
Elastic Stiffness (kN/mm)	7.03	0.909	1.131
Post-yield Stiffness (kN/mm)	0.909	Non	Non
Yield Strength (kN)	40.5	Non	Non
Allowable lateral Deformation (mm)	167	167	200

The design properties assigned to the link elements are listed in Table 3.5, calculated according to the formulas given in Table 3.6. The formulas reveal the contribution of individual factors that affect link properties. For instance, the shear stiffness of LRB links is proportional to the diameter of rubber layer, and inversely proportional to its thickness. With regard to the LLRB links, the elastic shear stiffness is equal to the sum of the rubber stiffness and the lead stiffness, so the diameters of the rubber layer and the lead plugs

both matter, while the post-yield stiffness is solely dependent on the dimension of the rubber layer because after yielding of the lead plug only the rubber perform elastically.

Table 3. 6: Formulas for the Key Parameters in the Design of the Rubber Bearings

Key Parameters	Formula	Description
Vertical load Carrying Capacity	$A^{'}G_rS\gamma_w$	$A^{'}$: The area between the top and bottom faces of the bearings; G_r : The shear modulus of the rubber ; γ_w : The allowable shear strain under vertical load; S : The shape factor of the rubber layer;
Vertical Stiffness	$\frac{6G_rS^2A_r\kappa_r}{h_r(6G_rS^2+\kappa_r)}$	A_r : The rubber layer area; h_r : The total rubber height; G_r : The shear modulus of the rubber ; κ_r : The compression modulus of the rubber; S : The shape factor of the rubber layer;
Torsional Stiffness	GJ/l	G_r : The shear modulus of the rubber ; J : The torsional constant of the isolator ; l : The link length;
Lateral Stiffness for LRBs	G_rA_r/h_r	G_r : The shear modulus of the rubber ; A_r : The rubber layer area; h_r : The total rubber height;
Elastic Stiffness for LLRBs	$(G_rA_r+G_pA_p)/h_r$	G_r : The shear modulus of the rubber ; A_r : The rubber layer area; G_p : The shear modulus of the lead ; A_p : The lead corn area; h_r : The total rubber height;
Post-yield Stiffness for LLRBs	G_rA_r/h_r	G_r : The shear modulus of the rubber ; A_r : The rubber layer area; h_r : The total rubber height;
Yield Strength	$\tau_pA_p(1+G_rA_r/G_pA_p)$	G_r : The shear modulus of the rubber ; A_r : The rubber layer area; G_p : The shear modulus of the lead ; A_p : The lead corn area; τ_p : The shear yield strength of the lead;
Allowable Isolator Deformation	$0.8D(1-A^{'}/A_r)$	D : The area between the top and bottom faces of the bearings; $A^{'}/A_r$: The overlap factor ;

Furthermore, in terms of behaviour under vertical loads, the vertical stiffness and the allowable lateral deformation for both LBR and LLBR links are highly related to the isolator diameter. The isolator properties calculated based on the formulas from Table 3.6 are compared with those obtained from tests, shown earlier in Table 2.1, indicating excellent correlations.

Figure 3.8 shows biaxial hysteretic properties of shear deformation for the LLRB links. Upon reaching the yield force (F_y) the lateral stiffness of the link element is instantly dropped to one tenth of the initial stiffness and remain the same until reaching the maximum lateral displacement ($X_{\max}$). The energy dissipation capacity of the LLRB links was determined by the area of the hysteresis loops, which is highly dependent on the yield force and the elastic stiffness. Normally, the hysteresis loop area is proportional to the yield strength of the links, but a considerably large yield force may cause adverse effects on energy dissipation. A possible reason is that, the yield force might be so high that it could hardly be reached especially under small ground motions. As a result, plastic deformations would hardly occur, leading to a lower damping in the isolator links that barely dissipate energy. Since both the shear deformations of the LLRB links were defined to be nonlinear, a coupled force-deformation relationship for these shear deformations was obtained. This is shown below:

$$\begin{aligned} f_{u2} &= ratio_2 k_2 d_{u2} + (1 - ratio_2) yield_2 z_2 \\ f_{u3} &= ratio_3 k_3 d_{u3} + (1 - ratio_3) yield_3 z_3 \end{aligned} \tag{3.5}$$

Where k_2 and k_3 are the elastic stiffness, $yield_2$ and $yield_3$ are the yield force, $ratio_2$ and $ratio_3$ are the ratio of the post-yield stiffness to the elastic stiffness, and z_2 and z_3 are the internal hysteretic variables.

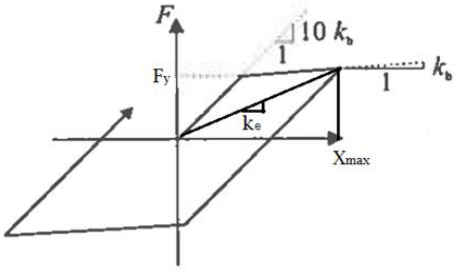

Figure 3.8: Hysteretic Property for the Shear Deformation of Rubber Isolator Links

These variables should satisfy $\sqrt{z_2^2 + z_3^2} \le 1$ with the yield surface represented by $\sqrt{z_2^2 + z_3^2} = 1$. The initial values of z_2 and z_3 are zero. Subsequently, they can be determined according to the following equations:

$$\begin{Bmatrix} \dot{z}_2 \\ \dot{z}_3 \end{Bmatrix} = \begin{bmatrix} 1 - a_2 z_2^{\,2} & -a_3 z_3 z_3 \\ -a_2 z_2 z_3 & 1 - a_3 z_3^{\,2} \end{bmatrix} \begin{Bmatrix} \dfrac{k_2}{yield_2} \dot{d}_{u2} \\ \dfrac{k_2}{yield_2} \dot{d}_{u3} \end{Bmatrix} \tag{3.6}$$

Where:

$$a_2 = \begin{cases} 1 & if \ \dot{d}_{u2} z_2 > 0 \\ 0 & otherwise \end{cases}$$

$$a_3 = \begin{cases} 1 & if \ \dot{d}_{u3} z_3 > 0 \\ 0 & otherwise \end{cases} \tag{3.7}$$

3.5 Modeling of the friction pendulum bearing system

The friction isolator links simulate the friction pendulum bearings in SAP2000. The mass and rotational deformation of the isolator links are set to be zero initially. Similarly as in the case of modeling of the rubber bearing system, only the link properties for axial deformation, two shear deformations and the torsional deformation are specified. The friction isolator link has nonlinear behaviour for the axial deformation; coupled friction properties for the two shear deformations; and linear effective-stiffness properties for the torsional deformation. As for the axial behaviour, a high stiffness is required to support the weight of the structure. This is determined as the isolator's length divided by its cross sectional area times the elastic modulus. The vertical stiffness of the friction isolator link must be positive and the axial force must be negative (compression). This is because the friction isolator links can only take axial compression for the purpose of generating shear forces. In addition, a damping coefficient is defined in order to reduce the numerical scatter that might happen during nonlinear analysis. The damping coefficient is calculated based on the formula $c = 2r\sqrt{km}$, where r is the damping ratio, which was assumed to be 5% in the current simulation and m is the tributary mass of the isolators estimated as the supported vertical loads divided by the acceleration of gravity. Since the additional

damping coefficient was specified, the total axial force was equal to the sum of the stiffness force and the damping force. However, only the stiffness force acted on the sliding surface and contributed to shear resistance; the damping force did not generate shear forces.

The friction isolator links had nonlinear behaviour in two shear deformation directions. The nonlinear shear forces in the link elements consist of friction forces and pendulum forces, which are both directly proportional to the axial compression in elements. The frictional force displacement relationship for each shear deformation was determined as $f_{u2,3f} = -p\mu_{u2,3}z_{2,3}$, where p is the axial force acted on the bearing surface, $\mu_{u2,3}$ is the friction coefficient and $z_{2,3}$ is the internal hysteretic variable. The friction coefficient is related to the sliding velocity determined as $\mu_{u2,3} = fast_{2,3} - (fast_{2,3} - slow_{2,3})e^{-\gamma v}$, where $slow_{2,3}$ and $fast_{2,3}$ are friction coefficients at zero velocities and at high velocities, which are directly specified in SAP2000. v is the resultant velocity of sliding, defined as $v = \sqrt{\dot{d}'^{2}_{u2} + \dot{d}^{2}_{u3}}$; and γ is the effective inverse velocity given by $\gamma = (rate_2 \dot{d}^{2}_{u2} + rate_3 \dot{d}^{2}_{u3}) / v^2$. Also, the internal hysteretic variables were determined as:

$$\begin{Bmatrix} \dot{z}_2 \\ \dot{z}_3 \end{Bmatrix} = \begin{bmatrix} 1 - a_2 z_2^{\,2} & -a_3 z_3 z_3 \\ -a_2 z_2 z_3 & 1 - a_3 z_3^{\,2} \end{bmatrix} \begin{Bmatrix} \frac{k_2}{p\mu_{u2}} \dot{d}_{u2} \\ \frac{k_2}{p\mu_{u2}} \dot{d}_{u3} \end{Bmatrix} \tag{3.8}$$

Where k_2 and k_3 are the initial shear stiffness of the FP isolator before sliding, and

$$a_2 = \begin{cases} 1 & if\ \dot{d}_{u2} z_2 > 0 \\ 0 & otherwise \end{cases}$$

$$a_3 = \begin{cases} 1 & if\ \dot{d}_{u3} z_3 > 0 \\ 0 & otherwise \end{cases}$$

SAP 2000 allows certain sliding before the shear forces in the link elements exceeds the maximum static friction ($p\mu$). To minimize sliding at lower shear forces, a large value of elastic shear stiffness was required, and specified as $p\mu/d_e$, where d_e is the lateral

displacement of the FPBs occurred before the static friction is overcome, normally with an order of magnitude of $10^{-4}m$ to $10^{-3}m$.

The pendulum force deformation relationship of the friction isolator links was obtained by $f_{u2,3p} = -p\,d_{u2,3}/radius_{2,3}$, where p is the axial compression force in the isolator links and $radius_{2,3}$ is the effective pendulum length, equal to the radius of the sliding surface minus the distance from the bearing surface to the articulation point of the isolators. The total shear force in the friction isolator links equals to the sum of the friction force and the pendulums force. It is computed by equation 3.9.

$$f_{u2,3} = -p(\frac{1}{radius_{2,3}} + \frac{\mu_{u,3} z_{2,3}}{d_{u2,3}})d_{u2,3} \tag{3.9}$$

Obviously, the lateral stiffness of the friction isolator links is proportional to the axial force in the element. As a result, the period of the friction isolation system becomes unrelated to the weight of the modeled structures as per $T = 2\pi\sqrt{\frac{W}{gk}} = 2\pi\Big/\sqrt{g(\frac{1}{radius} + \frac{\mu}{d_{\max}})}$. The properties assigned to the friction isolator links are shown in Table 3.7.

Table 3.7: Parameters Assign to the Friction Isolator Links

Supported Weight (kN)	1571
Radius of Sliding Surface (mm)	2300
Friction Coefficient, slow	0.04
Friction Coefficient, fast	0.06
Initial Stiffness (kN/mm)	942.6
Post-yield Stiffness (kN/mm)	0.683
Effective Stiffness (kN/mm)	1.154
Radius of Sliding Surface (mm)	2300

Figure 3.9 shows the hysteretic properties of shear deformations for friction pendulum isolators. The FP system has a large initial stiffness (k_e) and the system is near rigid until the shear force reaches the yield value of μp . Then, the force increase is proportional to the yield stiffness of the FPBs (k), specified as $p/radius$. Also, an effective stiffness (k_{eff}) is given by $P(1/radius + \mu/d_{\max})$, where $d_{\max}$ is the maximum lateral displacement. The hysteresis loop area can be used to estimate the energy dissipation capacity of the FP

system. Usually, the FP system with a high friction coefficient would produce a large hysteresis loop and thus dissipates a great value of seismic energy. Also, the energy dissipation capacity of the FPB system is directly proportional to the structural weight supported by bearings, since a large axial force in the isolator could generate a high yield force, creating a large area under the hysteresis loop.

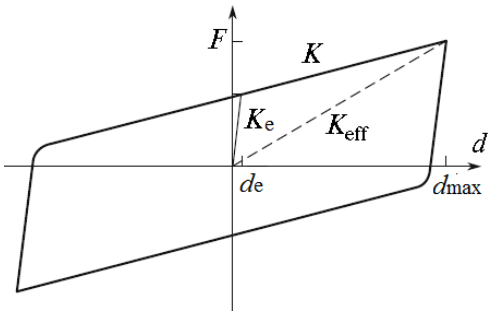

Figure 3.9: Hysteretic Property for the Shear Deformation of the Friction Isolator Links

3.6 Modeling of the supplemental viscous damper system

The damper links were used to model the supplemental viscous dampers in SAP2000, attached to the isolator links to provide additional viscous damping. Only the link properties for two shear deformations were specified. The behaviour of the damper link followed the Maxwell model of viscoelasticity (Malvern, 1969), which has an exponent viscous damper in series with a linear spring, as shown in Figure 3.10. The force deformation relationship of the damper link was determined as $f = kd_k = cv^{c\exp}$, where k is the spring constant, d_k is the deformation in the spring, c is the damping coefficient, $c\exp$ is the damping exponent and v is the velocity of the damper. The practical range of the damping exponent is 0.2 to 2.0; a small value of the damping exponent is recommended for the purpose of avoiding immense damping force at large velocities. It is importan to note that the damper links use linear damping properties if the damping exponent is set to be 1.0. Otherwise, nonlinear damping properties are to be specified.

Figure 3.10: Maxwell Damper Model

Table 3.8 lists the damper link element properties. The damping exponent was set equal to 1.0; hence the force deformation relationship was linear. The main reason for using linear damping is that it introduces little interaction between linear damping forces and structural forces in the model. Also, linear damping is easy to model and unlikely to excite higher modes of the structure. The critical damping coefficient of the modeled structure was obtained by $4\pi m/T$, where m is the structural mass and T is the natural period of the modeled structure. The damping coefficient of the damper link was specified as 30% of critical damping according to the displacement response spectra of the modeled structure. The displacement threshold of the isolated structure could dictate the estimation of the required viscous damping. Figure 3.11 indicates that, with the viscous damping of 30% of critical damping, the spectral displacement is reduced to the allowable isolator displacement, which is approximately equal to one-third of the isolator diameter.

Table 3.8: Parameters Assign to the Damper Links

Structural Mass (kg)	9137506
Natural Period of Structure (s)	2.09
Critical Damping Coefficient ($kN.s/m$)	54940.3
Viscous Damping Coefficient ($kN.s/m$)	16482.1
Damping Exponent	1

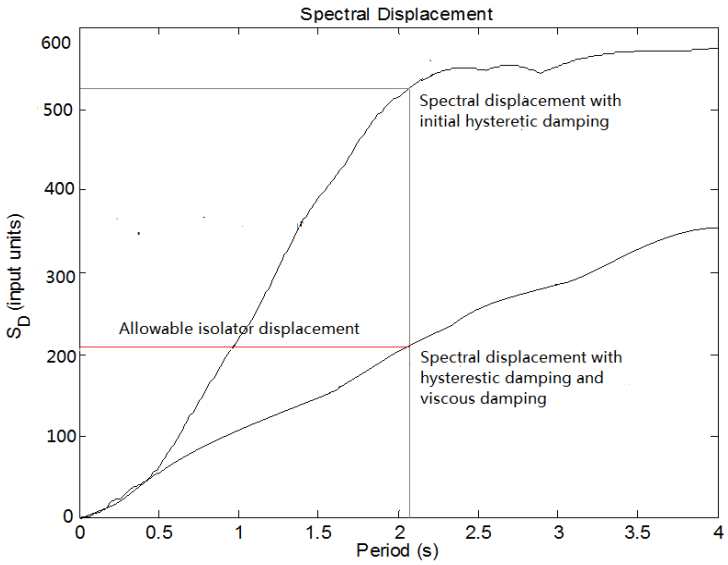

Figure 3.11: Spectral Displacements of Modeled Structure with Different Damping Levels

3.7 Load Cases

The load case defines how the loads are applied and how the structure responds to the loading. Several load cases were specified including the dead load case, live load case, modal load case, gravity load case and acceleration load case, as introduced in the followings.

Modal Load Case

The modal analysis is used to determine the vibration modes and the fundamental period of the modeled structure. The modal load case may use the structural stiffness from the initial conditions or at the end of a previous nonlinear analysis. In the current project, the modal load case was based on the stiffness of the full unstressed structure (using initial conditions). Thus, the modal analysis used linear properties only, regardless of whether nonlinear properties were specified or not. Moreover, the Ritz-vector analysis was selected, rather than the Eigenvector analysis, to create a basis for the subsequent time history analysis. The Eigenvector analysis is used for determining the undamped free-vibration mode shapes; the Ritz-vector analysis is used to find modes that are excited by a particular loading. Previous research showed that for the same number of modes, the dynamic analyses based on a set of Ritz vectors could generate better results than that

based on the natural mode shapes. This is because the Ritz-vector analysis account for the spatial distribution of dynamic loading, which is neglected by the Eigenvector analysis. The definition of the modal load case in SAP2000 is shown in Figure 3.12(a).

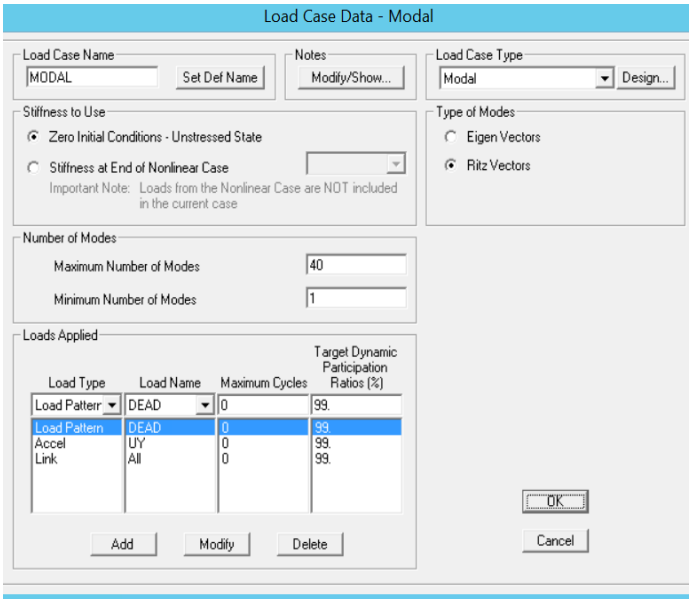

(a) Modal Load Case

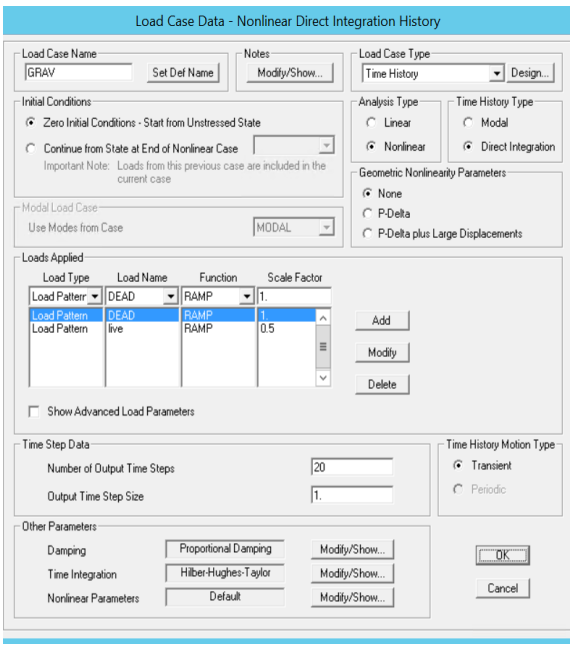

(b) Gravity Load Case

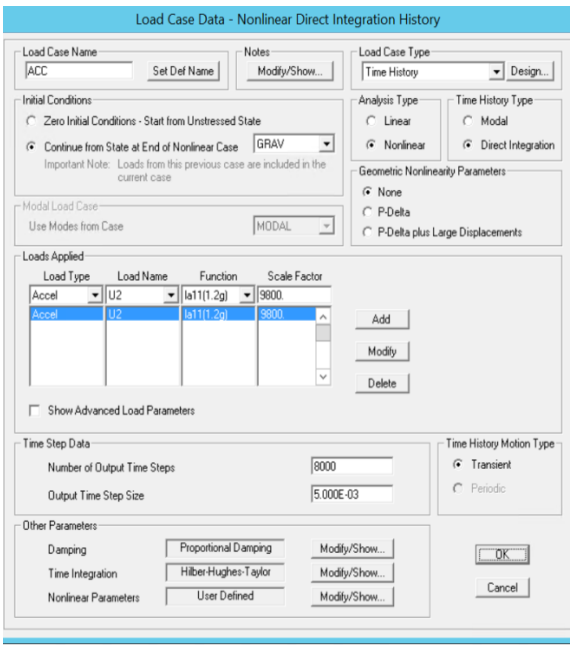

(c) Acceleration Load Case

Figure 3.12: Definition of Load Cases in SAP2000

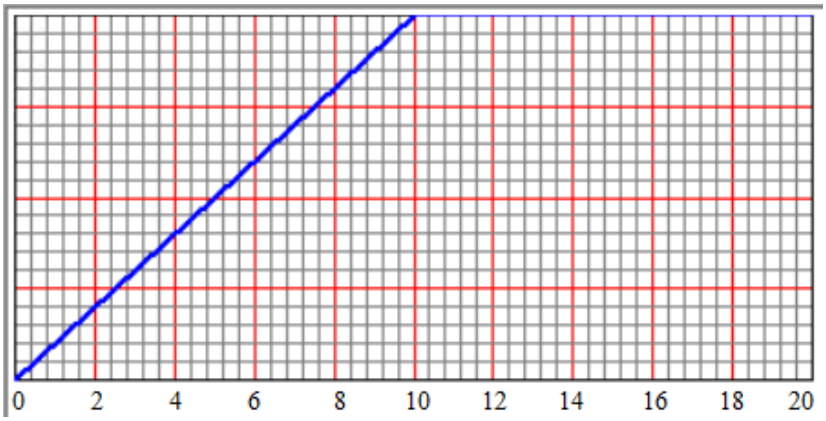

Figure 3.13: Ramp Time-history Function

Gravity Load Case

The dead load and half of the live load were applied to the structure in the gravity load case. Although the gravity loading was static in nature, the direct-integration time history analysis was used in this load case rather than the nonlinear static analysis. This is because the nonlinear static analysis did not always generate an exclusive solution for the models with plastic link elements, and thus, causing problems in convergence. In the time-history analysis, the gravity load was applied very slowly to minimize its dynamic effects, following the ramp time-history function shown in Figure 3.13. The ramp function increased the gravity load to its full value over 10 seconds and then held the load for an additional 10 seconds. The slow application of gravity loads guaranteed the efficiency of the Ritz vectors generated for gravity. Commonly, the Ritz vector is used for loaded DOFs that have mass in dynamic analysis. However, in this load case the Ritz vector was assigned for massless DOFs. As a matter of fact, the gravity load generated an insignificant dynamic effect that had minor impact on the efficiency of Ritz vector. The gravity load case used for the structural stiffness from the initial condition (the unstressed state) and the definition of this load case was shown in Figure 3.12(b).

Acceleration Load Case

In this load case, ground accelerations were applied to the structure in the horizontal Y-direction to generate earthquake forces. Nonlinear direct-integration time-history analysis was used for this load case because the nonlinear link elements would be active only if

the structural response was solved with the direct integration method. Also, the output time step size of the analysis was set to be 0.005s. The number of output time steps was set at 8000, which corresponded to input ground motion records that have a time-step of 0.005s and a total duration of 40s. The structural stiffness at the end of the gravity load case was used for the acceleration load case to combine the gravity load effects with the effects of ground excitation when computing structural response. This approach of load combination generated the most accurate results since both the loading sequence and the nonlinearity from factored loading (1D+0.5L+1Q) were accounted for. The definition of the acceleration load case in SAP2000 is presented in Figure 3.12(c).

3.8 Earthquake Records

Four ground motions, labelled as La11-005#1, La11-005#2, La11-005#3 and La11-005#4, were used in the horizontal Y-direction. The four earthquake records with the same frequency content but with an increasing intensity were selected to eliminate ground motion frequency content as a parameter. The earthquake record selected was the original 1940 Imperial Valley Earthquake (EI Centro) record (La11-005) specified in fractions of g, with a time-step of 0.005s and a total duration of 40s. The peak ground accelerations (PGA) of the four input motions were scaled to match 0.5g, 0.67g, 0.9g and 1.2g. These records were labelled as La11-005#1 to La11-005#4, respectively. The acceleration time-history of these records are presented in Figure 3.14 and their displacement and acceleration response spectra based on 15% structural damping are shown in Figure 3.15.

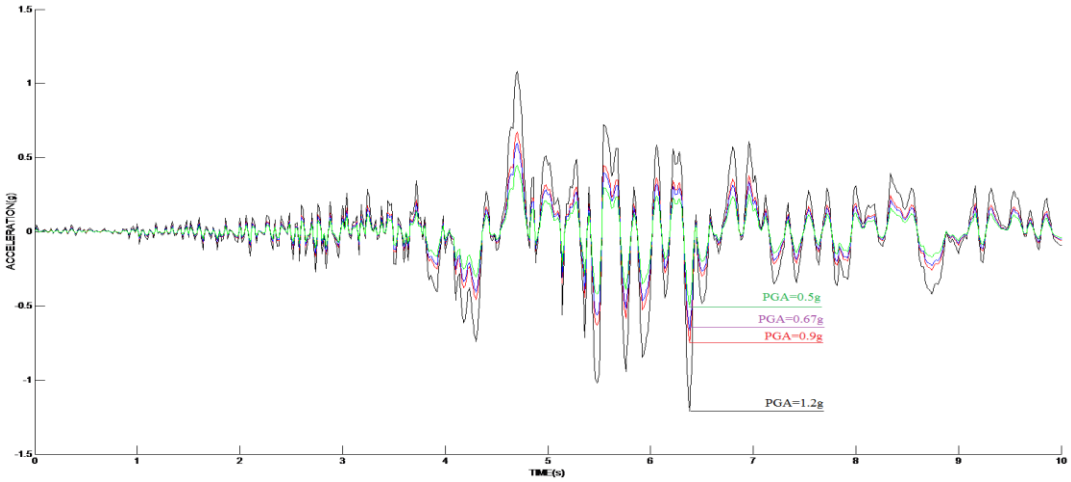

Figure 3.14: Acceleration Time-history of Four Input Motions

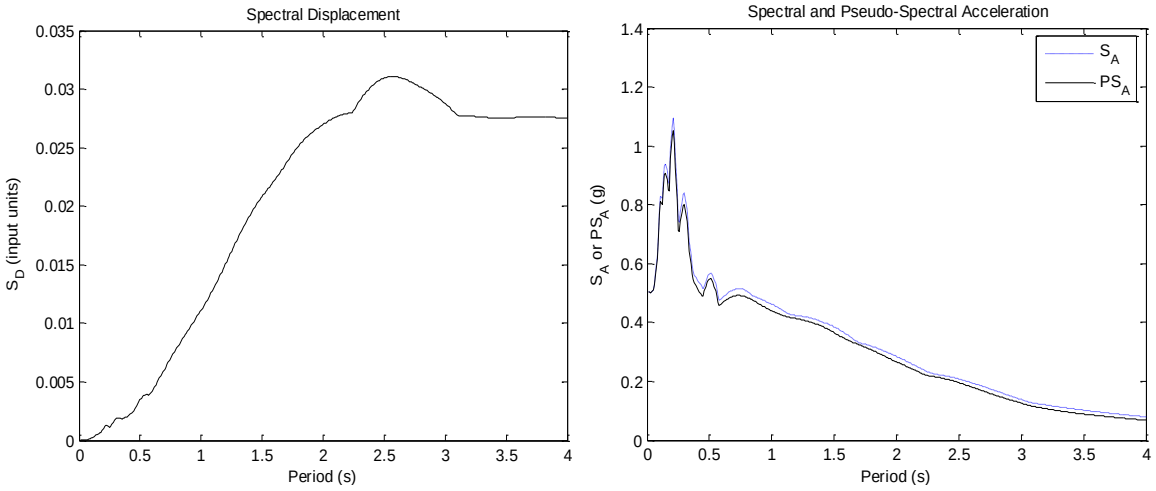

(a) Ground motion record: La11-005#1 (PGA=0.5g)

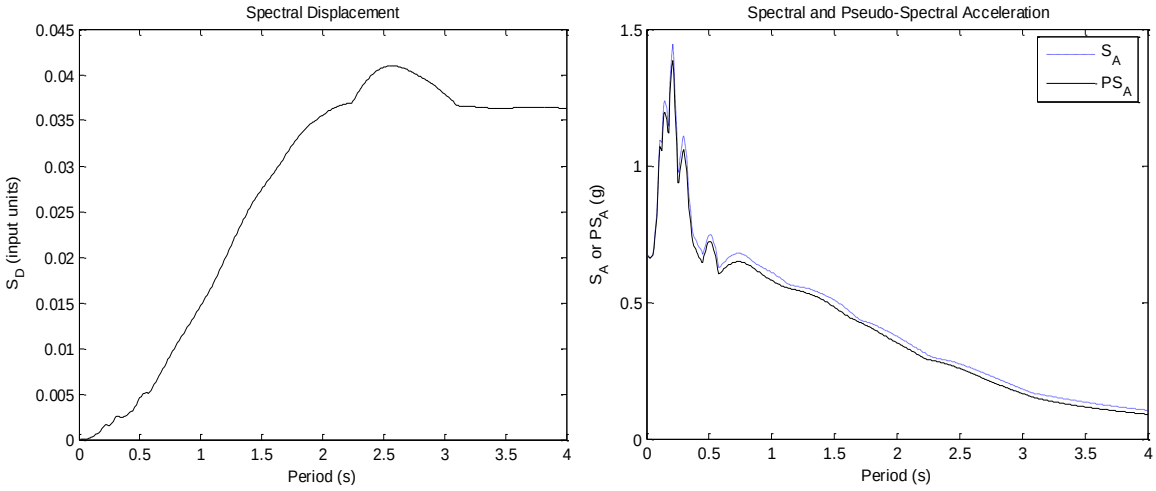

(b) Ground motion record: La11-005#2 (PGA=0.67g)

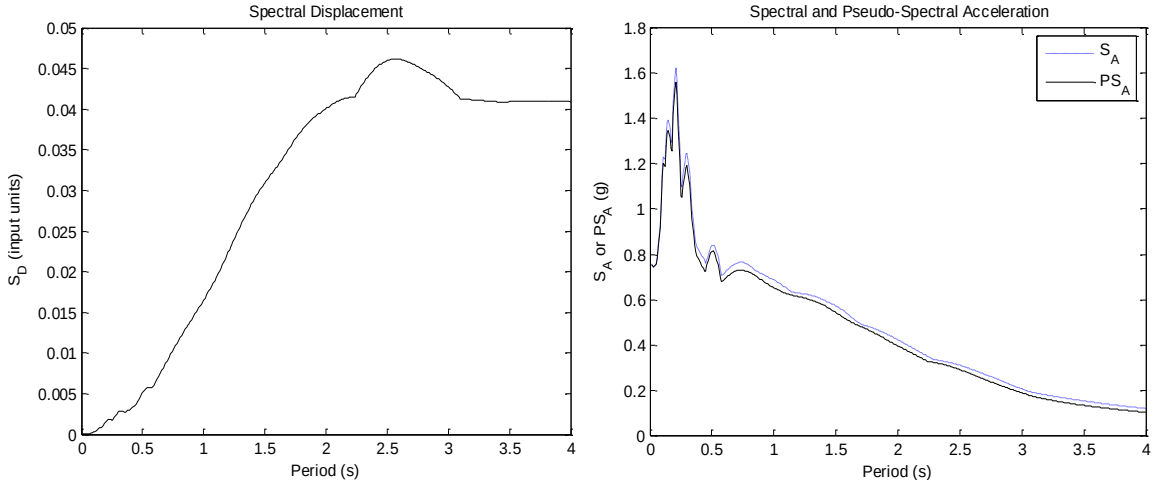

(c) Ground motion record: La11-005#3 (PGA=0.9g)

Figure 3.15: Displacement and Acceleration Response Spectra for Four Input Motions

(The input unit for spectra displacement is 10^{-4} m)

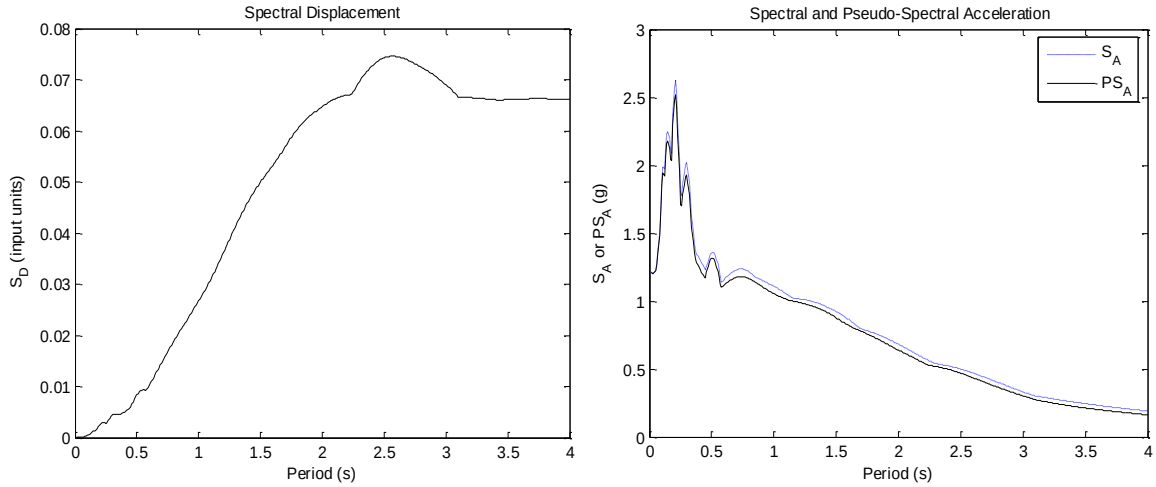

(d) La11-005#4 (PGA=1.2g)

Figure 3.15: Displacement and Acceleration Response Spectra of Four Input Motions

(The input unit for spectra displacement is 10^{-4} m)

Chapter 4

Results of Dynamic Analysis and Performance of Base Isolation Systems

4.1 General

The structural models (for both the base-isolated and the fixed base buildings) were analyzed using SAP2000 under different intensities of earthquake record. The seismic performance of the building without the isolation system was first conducted. The mode shapes and the fundamental period of the non-isolated model with and without the infill walls were obtained based on modal analysis and responses history analysis. The results showed that the masonry infill walls significantly affected structural performance. The dynamic inelastic response history analysis was conducted on isolated buildings to evaluate the effectiveness of different isolation systems (the rubber isolation system, the friction pendulum isolation system and the hybrid isolation system composed of bearings and dampers). The performances of the isolated structure were compared with that of the fixed-base structure in terms of lateral drift ratios, peak absolute accelerations and residual drifts. The influence of the isolator properties (such as the lead plug diameter for the LLRBs, the friction coefficient for the FPBs and the damping level for the viscous dampers) on the efficiency of the isolation system was assessed through a parametric study. In addition, the modeling and ground motion aspects, like the earthquake intensity, large isolator displacements and the contribution of vertical loading to isolator stiffness were also investigated. Particular attention was given to the high level damped LLRB system and viscous damper supplemented isolator systems, especially when the isolated structure was subjected to far-field excitations. The results for all three seismic isolation

systems were collected, analyzed and compared to provide insight into the design and use of the isolation systems considered in practice.

4.2 Seismic Performance Criteria

The primary focus of the current research is to investigate the effectiveness of the seismic isolation system in enhancing structural performance during earthquake. As such, the peak inter-storey drifts, the residual drifts and the peak absolute horizontal accelerations were used as the performance criteria, introduced subsequently.

Peak Inter-storey Drifts:

The peak inter-storey drift, defined as the maximum relative lateral displacement at each floor level divided by the floor height, is an indicator of both structural and non-structural damage. Normally, the building experiencing a drift ratio between 0.0% to 0.5% practically develops no damage in structural and non-structural elements. A drift ratio ranging between 0.5% and 1.0% is indicative of minor non-structural damage, but no structural damage. If drift ratio is 1.0% to 2.0%, major non-structural damage as well as minor to moderate structural damage is expected. The building is considered seriously damaged when the drift ratio is over 2.0%, and likely experience partial collapse when the drift ratio is in excess of 4%.

Residual Drifts:

The residual drift, caused by inelastic response, reflects the suitability of the building for occupancy and potential repair. Previous studies suggest that the building with a residual drift between 0.0% and 0.6% is likely usable from an occupancy perspective. Building that sustains a residual drift over 0.6%, structural repairs may be necessary for safety considerations. However, residual drifts beyond a certain level are perceivable and may justify the repair cost even though the main structure remains robust. Buildings that have over 1% residual drift could be considered as a total loss, and a complete rebuilding may be required.

Peak Absolute Horizontal Acceleration:

Peak absolute horizontal acceleration could significantly affect the performance of non-structural elements, such as suspended ceilings, light fixtures and mechanical equipment, because horizontal inertia forces at each floor level are proportional to the absolute acceleration of the building. Accelerations that are less than 0.5g cause little damage to non-structural elements. Accelerations between 0.5g to 1.0g may cause some damage to internal building components. If accelerations increase beyond 1.0g, the interior building space may be completely in shamble, and severe damage of sensitive equipment is expected.

The horizontal displacement at the isolator level is also critical. Several isolated buildings subjected to earthquakes revealed that the horizontal isolator displacement could become considerably large when the building was subjected to strong ground excitations. A large isolator deformation could severely damage the bearings, and may cause the collapse of the isolated structure even if the superstructure remains otherwise sound. Therefore, the allowable lateral displacement of the bearing should be kept in mind in selecting and designing the isolation system, especially if the building is expected to experience strong earthquake motions.

4.3 Performance of Buildings without Base Isolation

4.3.1 Fundamental Period

Two building models were considered to investigate the performance of the prototype frame building. These consist of a bare frame without the infill walls, and the building as designed with infill walls interacting with the frames. The first six periods of the infilled and bare frame models are listed in Table 4.1. The presence of infill walls resulted in a considerable stiffness increase, reducing the first mode period by approximately 50%; from 1.295sec to 0.635sec. The acceleration response spectra of the earthquake records showed higher spectral accelerations for reduced periods, as expected. As a result, the infilled frame was expected to experience higher seismic forces.

Table 4.1: First Six Periods of the Infilled and Bare Frame Models (sec)

	Infilled Model	Bare Model
Mode1	0.635	1.295
Mode2	0.623	1.184
Mode3	0.551	0.415
Mode4	0.213	0.388
Mode5	0.210	0.243
Mode6	0.189	0.237

4.3.2 Peak Inter-storey Drift

Figure 4.1 show the comparison of maximum inter-storey drifts at each floor level for the two non-isolated structural models, with and without the infill walls under the four ground motions considered. Figures 4.1(a) through 4.1(d) include the comparison of bare and infilled frames under gradually increasing levels of ground motion intensity. Figures 4.1 (e) and (f) show the effect of earthquake intensity on bare and infilled frames, respectively. The maximum peak inter-storey drifts occurred at the first two storey levels in both buildings, as also tabulated in Table 4.2. The inter-storey drifts were larger under higher earthquake intensity, as expected. Under the La11-005#1 record with the lowest intensity (PGA=0.5g), the maximum peak inter-storey drifts of infilled and bare frame models varied between 0.5% and 1%, suggesting a slight damage to non-structural elements. When the structures were subjected to La11-005#2 and La11-005#3 records with higher intensities (PGA of 0.67g and 0.9g) the maximum peak inter-storey drifts increased to 1.2% to 1.8%, indicating possible damage in structural elements. Earthquake record La11-005#4 with the highest intensity (PGA=1.2g) resulted in considerably large inter-storey drifts, approaching 3% to 4% for infilled and bare frames, respectively. The large drifts were indicative of severe damage to structural and non-structural systems with a potential for building collapse. It is noteworthy that the inter-storey drifts for the infilled frame were much less than those for the bare frame because of the stiffening effects of masonry infill walls. The frame building, even with grouted masonry walls experienced high inter-storey drifts, indicating potential damage and needs for seismic isolation.

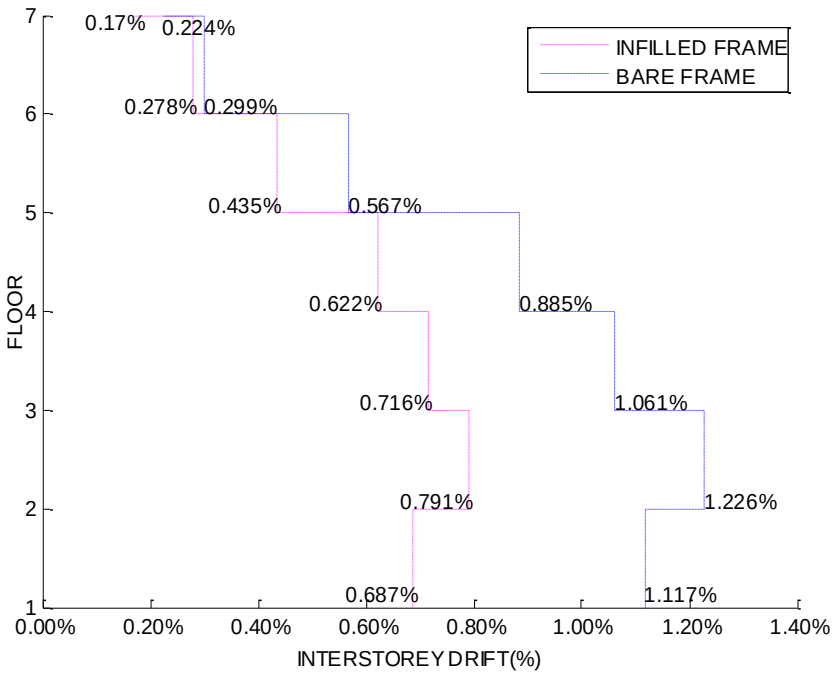

(a) Ground motion record: La11-005#1

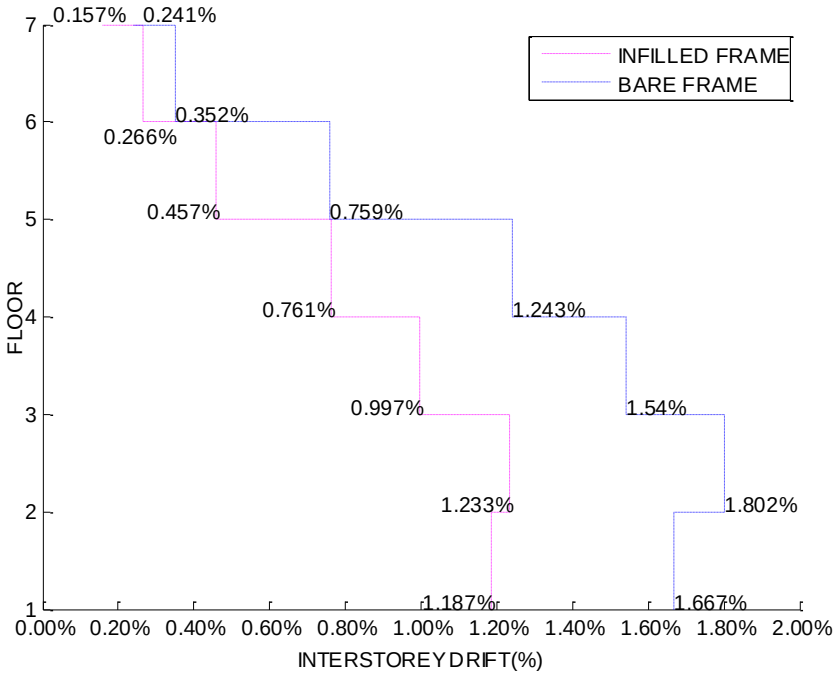

(b) Ground motion record: La11-005#2

Figure 4.1: Inter-storey Drift Envelopes for Non-isolated Frame Building with and without Infill Walls under Four Ground Motion Intensities

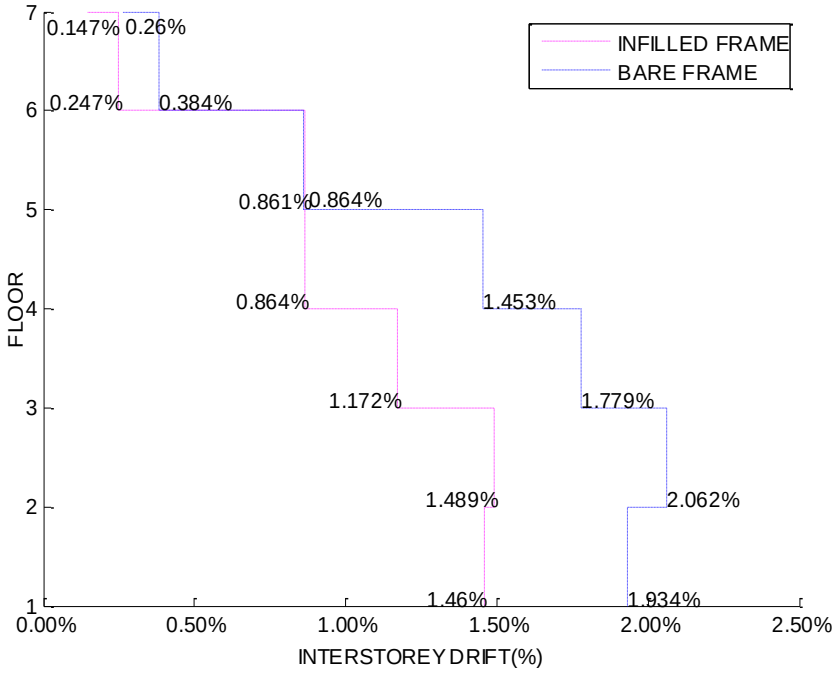

(c) Ground motion record:La11-005#3

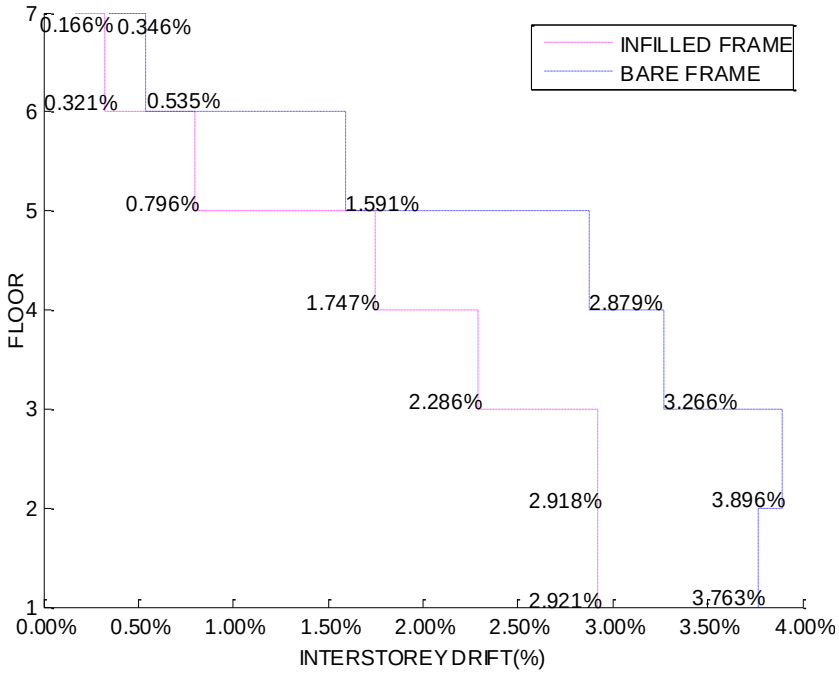

(d) Ground motion record: La11-005#4

Figure 4.1: Inter-storey Drift Envelopes for Non-isolated Frame Building with and without Infill Walls under Four Ground Motion Intensities

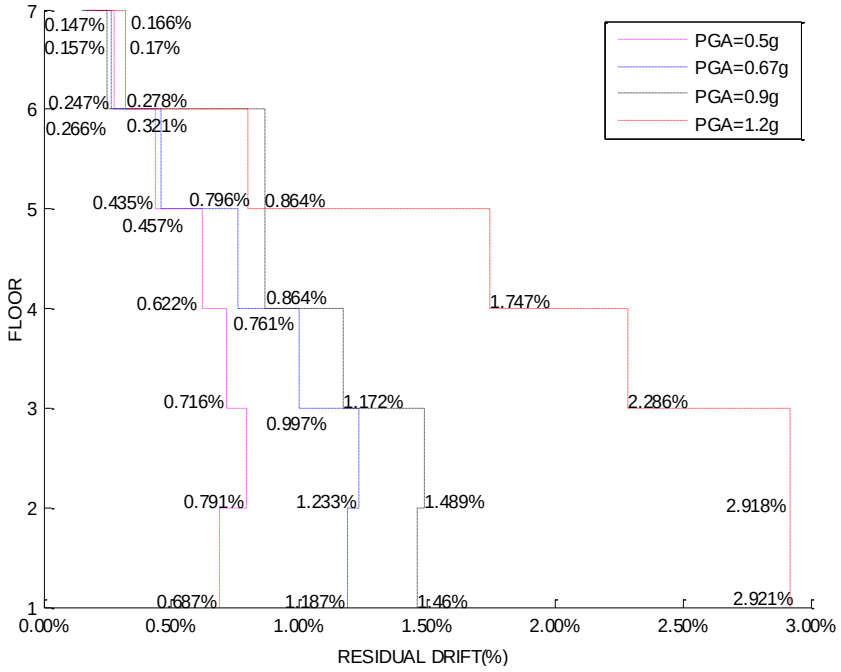

(e) Infilled structure subjected to the four ground motions

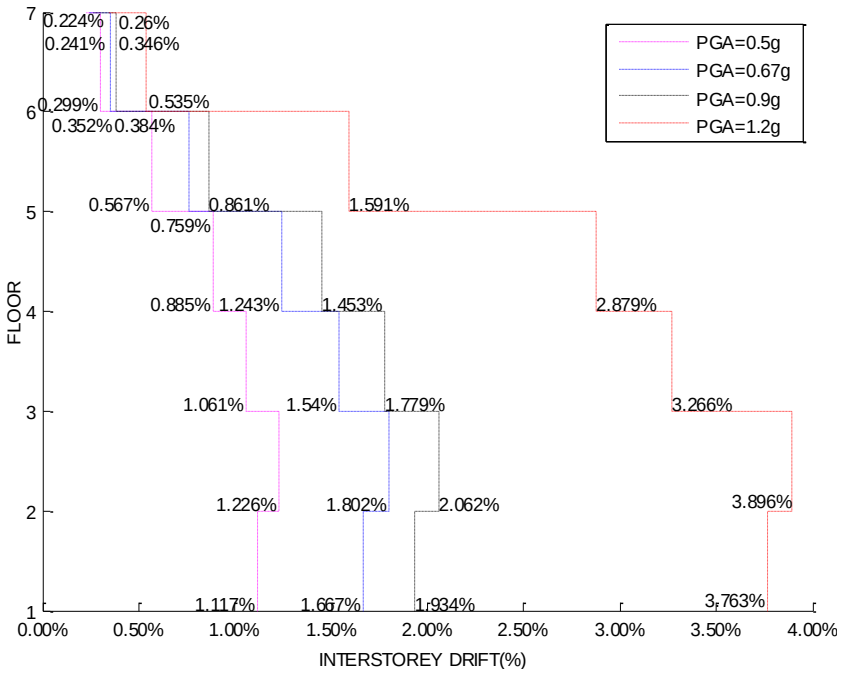

(f) Bare structure subjected to the four ground motions

Figure 4.1: Inter-storey Drift Envelopes for Non-isolated Frame Building with and without Infill Walls under Four Ground Motion Intensities

Table 4.2: Maximum Inter-storey Drifts of the Infilled and Bare Structural Models

	Infilled Model	Bare Model
PGA=0.5g	0.791%	1.226%
PGA=0.67g	1.187%	1.667%
PGA=0.9g	1.460%	1.934%
PGA=1.2g	2.921%	3.763%

4.3.3 Residual Drift

The maximum residual storey drifts, recorded during response, are shown in Fig. 4.3 for both frame buildings, with and without the infill walls. The results indicate less than 0.6% drift ratio in both buildings, suggesting the survival of the buildings without a significant effect on the operational capacity during seismic response. While these results are meaningful when the structural components do not develop strength decay because of limited ductility demands, or when they are well-designed and detailed with structural elements not experiencing strength decay. The hysteretic model used for the members had stiffness degradation capabilities, but not strength decay. Therefore, the results under high intensity ground motions, exhibiting low residual drifts may not reliable. These buildings may have experienced significant damage when their ductility capacities are exceeded beyond 2% lateral drift, hence also expected to develop excessive residual drift. Another reason for obtaining small residual drift is because the dynamic analysis continued beyond the maximum lateral drift, and recovered the excessively high value that may have occurred earlier. Therefore, even though the lateral drift may be over 2%, indicating structural damage, the dynamic analysis will still continue until the end of the earthquake input, often recovering previously experienced large drifts, resulting in small residual drifts.

Figure 4.3 indicates that the presence of infill walls reduced residual drifts slightly. It further indicates that residual drift demands were highest at the first floor level.

Table 4.3: Maximum Residual Drifts of the Infilled and Bare Structural Models

	Infilled Model	Bare Model
PGA=0.5g	0.098%	0.119%
PGA=0.67g	0.141%	0.148%
PGA=0.9g	0.161%	0.172%
PGA=1.2g	0.501%	0.505%

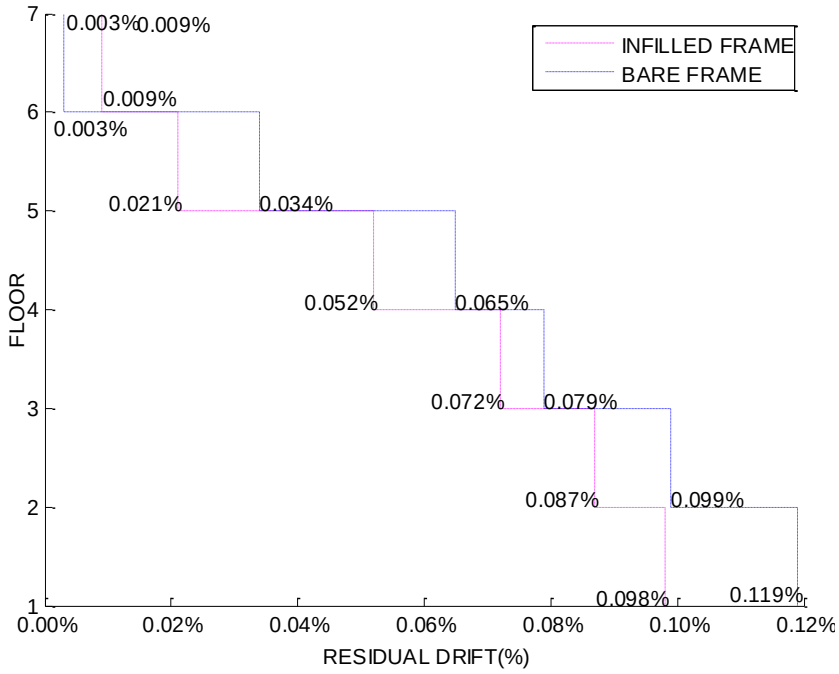

(a) Ground motion record: La11-005#1

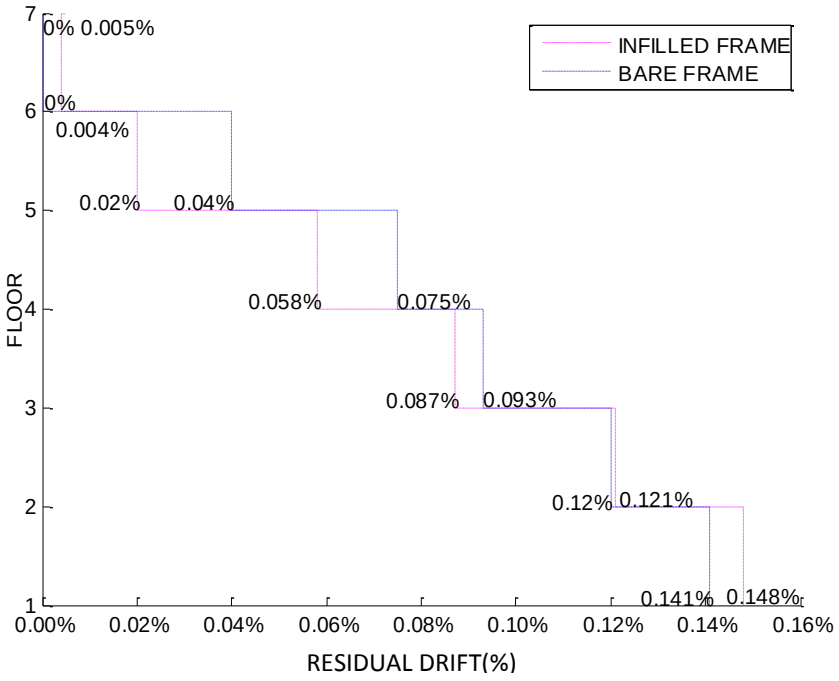

(b) Ground motion record: La11-005#2

Figure 4.2: Residual Drift Envelopes for Non-isolated Frame Building with and without Infill Walls under Four Ground Motion Intensities

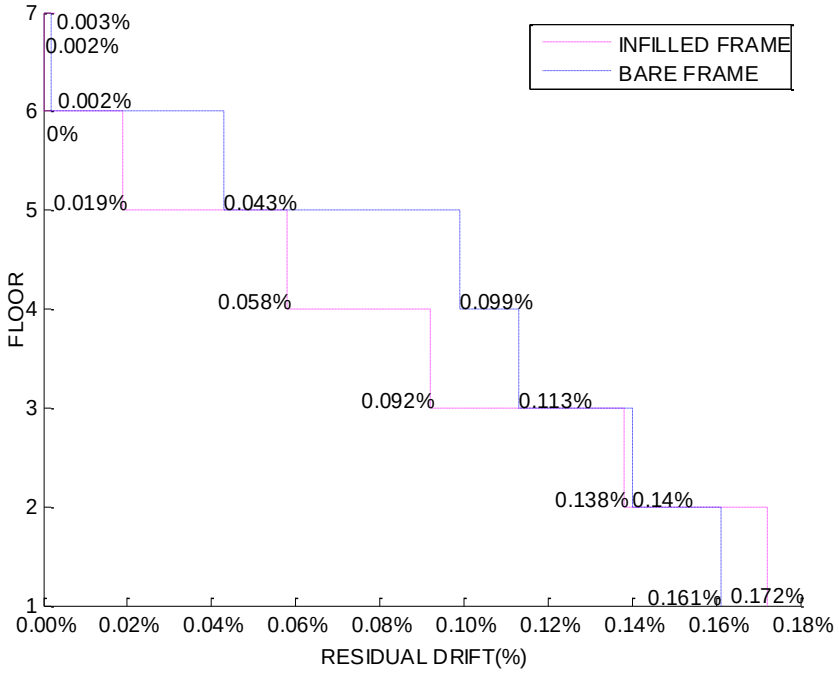

(c) Ground motion record: La11-005#3

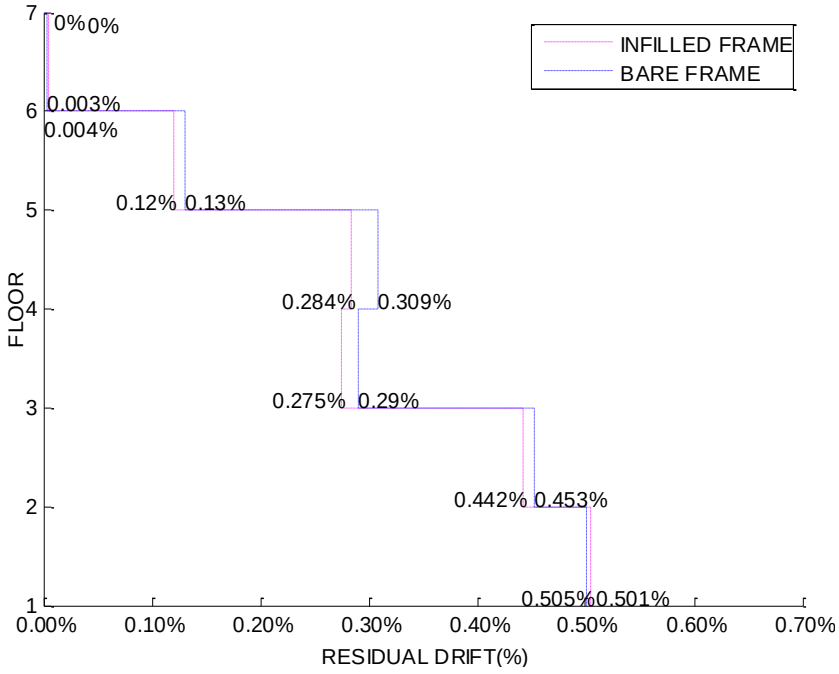

(d) Ground motion record: La11-005#4

Figure 4.2: Residual Drift Envelopes for Non-isolated Frame Building with and without Infill Walls under Four Ground Motion Intensities

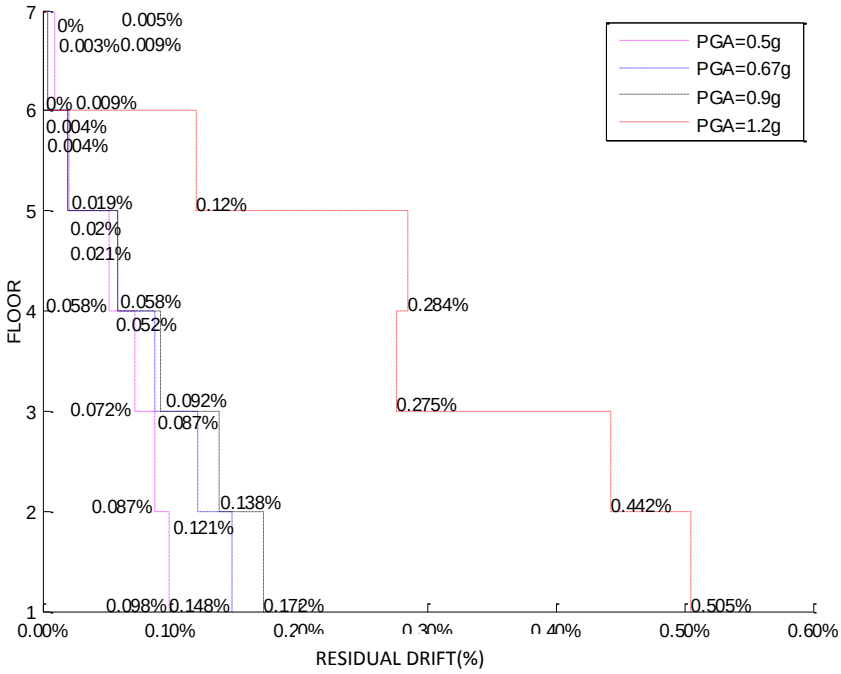

(e) Infilled structure subjected to the four ground motions

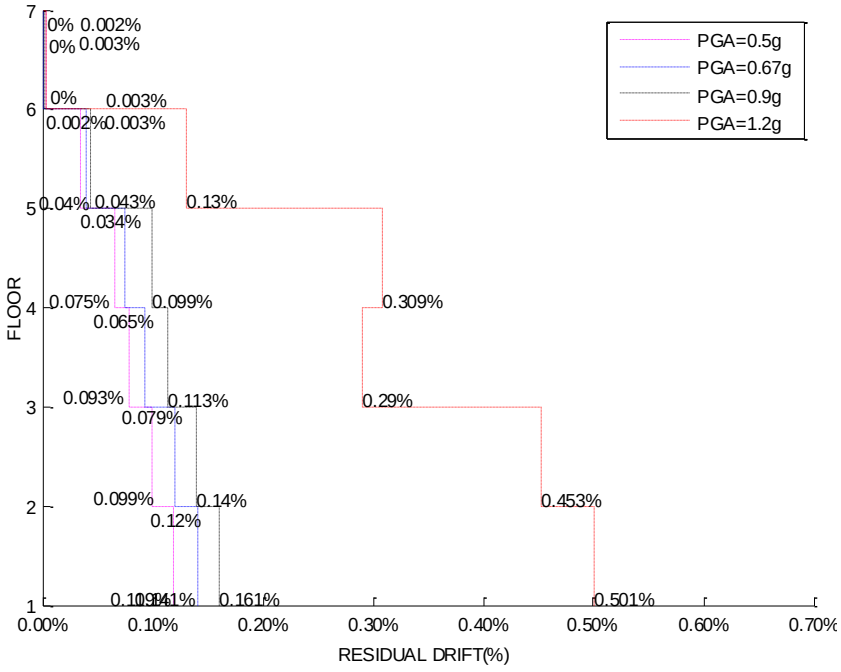

(f) Bare structure subjected to the four ground motions

Figure 4.2 : Residual Drift Envelopes for Non-isolated Frame Building with and without Infill Walls under Four Ground Motion Intensities

4.3.4 Peak Absolute Horizontal Acceleration

Peak absolute horizontal accelerations at each floor of the non-isolated buildings, with and without masonry infill walls, are illustrated in Figure 4.3. The peak floor accelerations at lower storeys decreased with building height up to about mid-height (4^{th} floor), and then increased quite substantially towards the top of the building. This observation was true for both buildings with and without the infill walls. The maximum peak accelerations are summarized in Table 4.4. They ranged between 0.5g and 1.0g for bare frame building and building with infill walls, respectively. This suggests that building contents, as well as operational and functional components are potentially subjected to severe accelerations with serious potentials for damage. The expected damage to building content and non-structural elements of a similar fixed base building was validated by the observation of serious destruction of non-structural elements of the old outpatient building of the Lushan People Hospital, which was not base isolated. This is shown in Figure 2.6.

It is important to note that the frame building with infill walls experienced higher floor accelerations as compared with the companion building with bare frames. Figure 4.3 shows that the frame model with infill walls developed larger floor accelerations than the bare frame model. This can be explained by the change of building period that is resulted from the presence of infill walls as stiffening elements. The increased structural stiffness translated into a reduction in structural period and consequent increase in building response as indicated by the acceleration response spectra. This increase in floor accelerations could generate higher inertia forces at each floor level, resulting in diagonal tension cracking in masonry infill walls. Also, the increased spectral acceleration would increase shear forces in the frame elements, such as columns. Hence, the presence of infill walls on one hand reduces inter-storey drift and controls damage associated with excessive deformations, but at the same time increases seismic forces on structural elements and may pose vulnerability associated with force capacities.

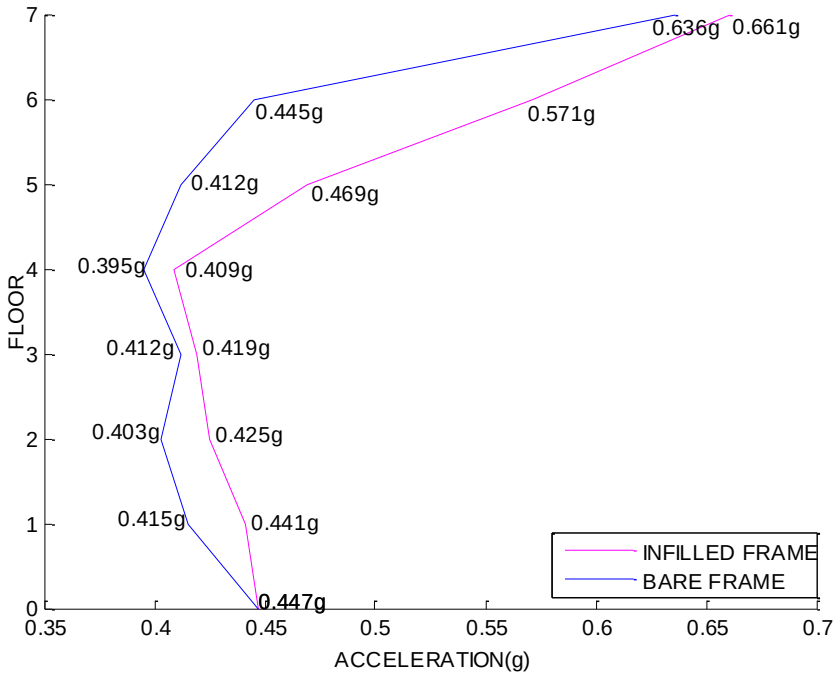

(a) Ground motion record: La11-005#1

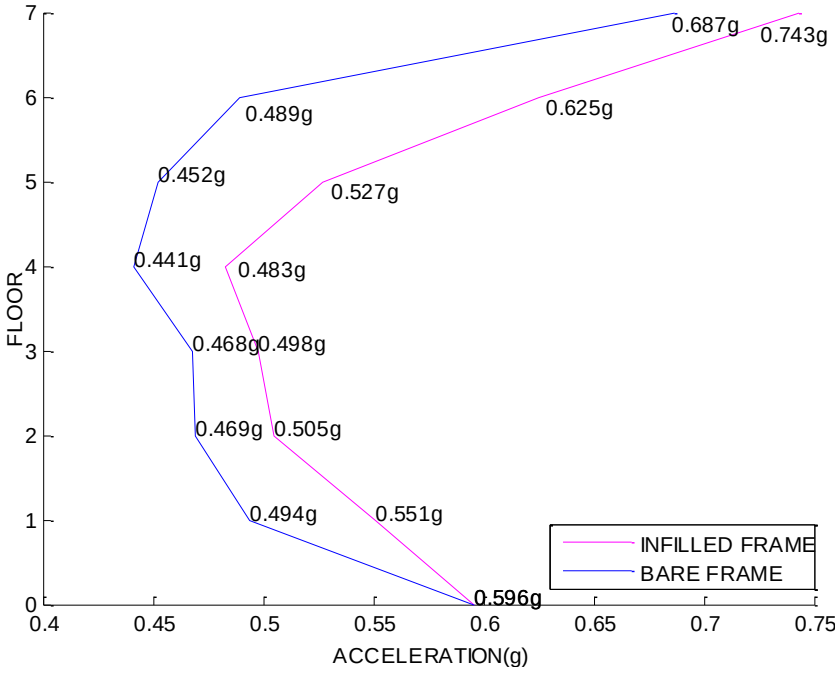

(b) Ground motion record: La11-005#2

Figure 4.3: Floor Acceleration Envelopes for Non-isolated Frame Building with and without Infill Walls under Four Ground Motion Intensities

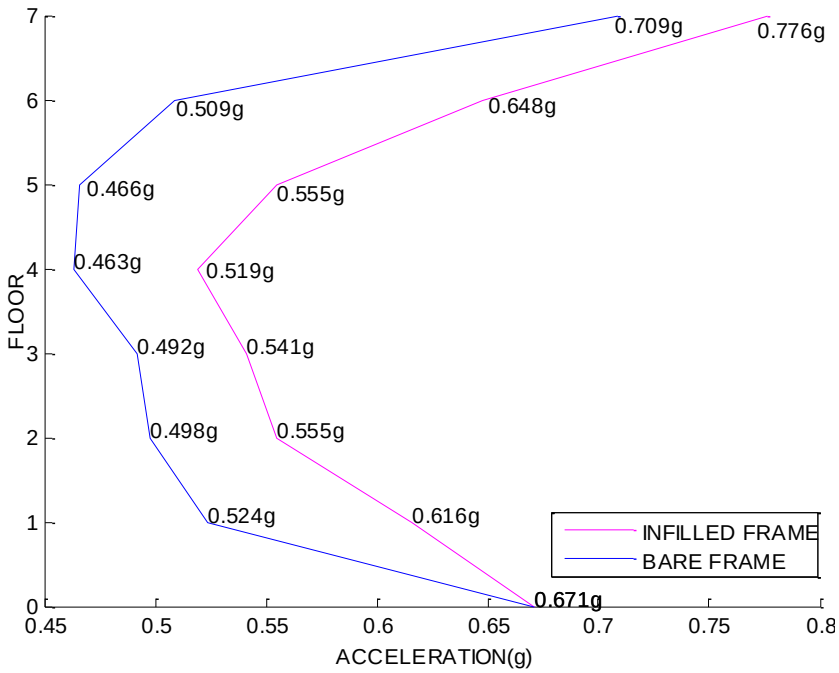

(c) Ground motion record: La11-005#3

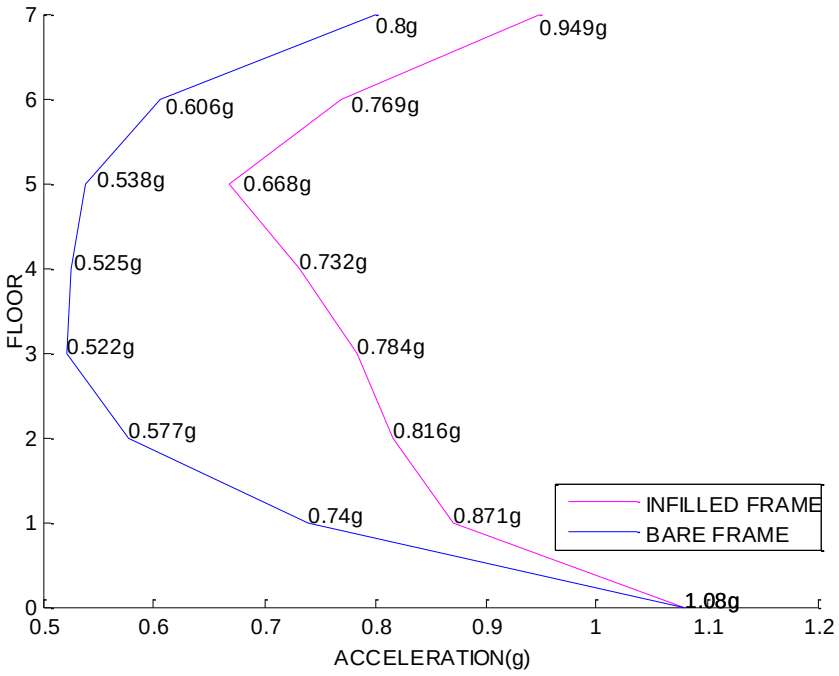

(d) Ground motion record: La11-005#4

Figure 4.3: Floor Acceleration Envelopes for Non-isolated Frame Building with and without Infill Walls under Four Ground Motion Intensities

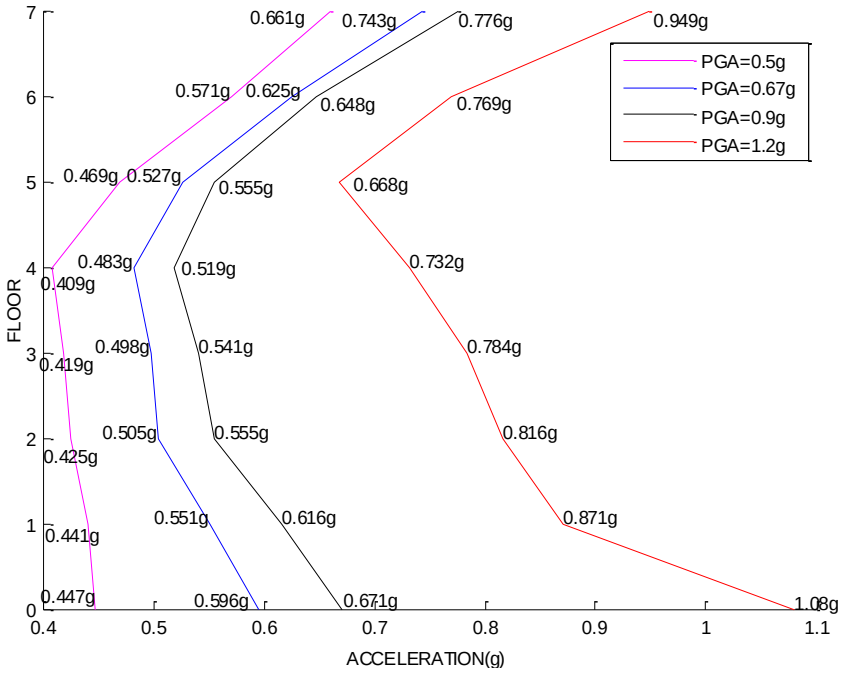

(e) Infilled structure subjected to the four ground motions

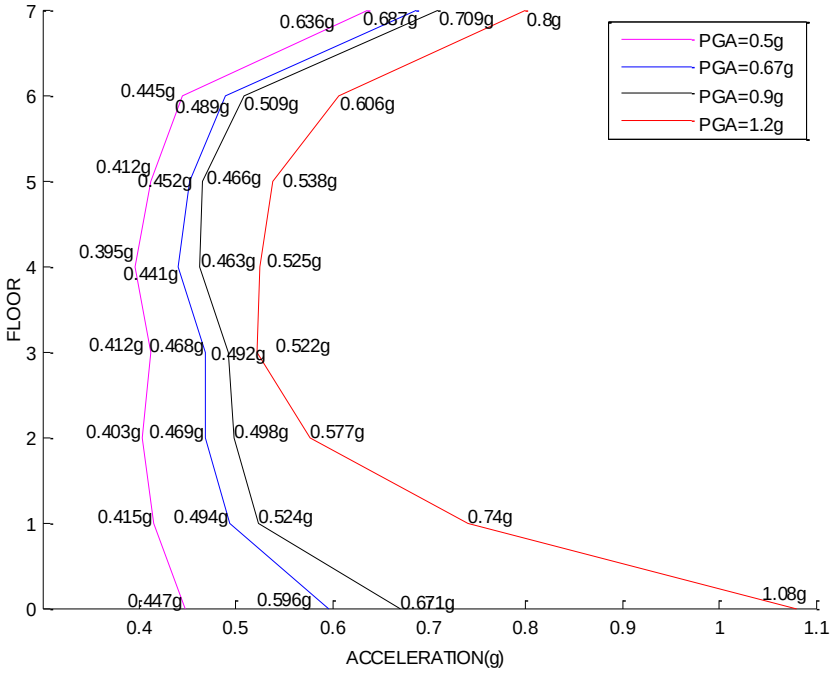

(f) Bare structure under the four ground motions

Figure 4.3: Floor Acceleration Envelopes for Non-isolated Frame Building with and without Infill Walls under Four Ground Motion Intensities

Table 4.4: Maximum Floor Accelerations of the Infilled and Bare Structural Models

	Infilled Model	Bare Model
PGA=0.5g	0.661g	0.636g
PGA=0.67g	0.743g	0.687g
PGA=0.9g	0.776g	0.709g
PGA=1.2g	0.800g	0.909g

4.3.5 Axial Forces in Diagonal Struts

The axial forces of the plastic hinge elements at the ends of the diagonal struts were examined to estimate the crushing of masonry infill walls during seismic response. Figure 4.4 presents the time history of axial forces at hinge No. 23 under Earthquake Record La11-005#3, where a compression strut, with a dimension of $2100mm \times 240mm$ is connected at the first storey level. As previously mentioned, the compressive strength of the concrete masonry used in this project is 3.0Mpa. Therefore, the maximum axial force (specified as the yield force for the purpose of modelling) for the diagonal strut is 1512kN, computed as the compressive strength times the strut area. No tensile force was resisted by the strut because the tension limit of the strut objects was set to zero. This can be observed in Fig. 4.4. The strut carried a large compressive force that exceeded the crushing strength of the masonry. The compression force resulted in the crushing of masonry infill wall, leading to sudden strength degradation (point A in Figure 4.4). However, the onset of crushing did not completely destroy the infill wall, and the wall continued to resist compression but with a lower compression resistance. The overall building response indicated that only a few wall struts were found to reach the crushing strength. This observation is consistent with the infill wall behaviour of the non-isolated old outpatient building whose infill walls partially crushed and also developed diagonal tension cracking.

4.3.6 Base Shear

Figure 4.5 depicts response time histories for base shear under the four earthquake intensities considered. The responses of both frame buildings, with and without infill walls, are shown. The results indicated that the base shear of the structure was higher for

the building that was stiffened by infill walls by 19.1%, 27.0%, 31.4% and 26.3%, respectively under the Earthquake Records La11-005#1, La11-005#2, La11-005#3 and La11-005#4. The increase in base shear was attributed to increased floor inertia forces associated with higher spectral accelerations attracted by more rigid building. As the total base shear is essentially equal to the summation of the inertia forces at each floor, the increased floor inertia forces in turn led to a larger structural base shear. Under the Earthquake Record La11-005#4 with the highest PGA of 1.2g, the dynamic analysis of the analytical model had convergence problems 12 seconds after the beginning of the analysis, possibly due to the excessive structural base shear (50976.93 kN) or the very large diagonal compression forces in some of the wall struts.

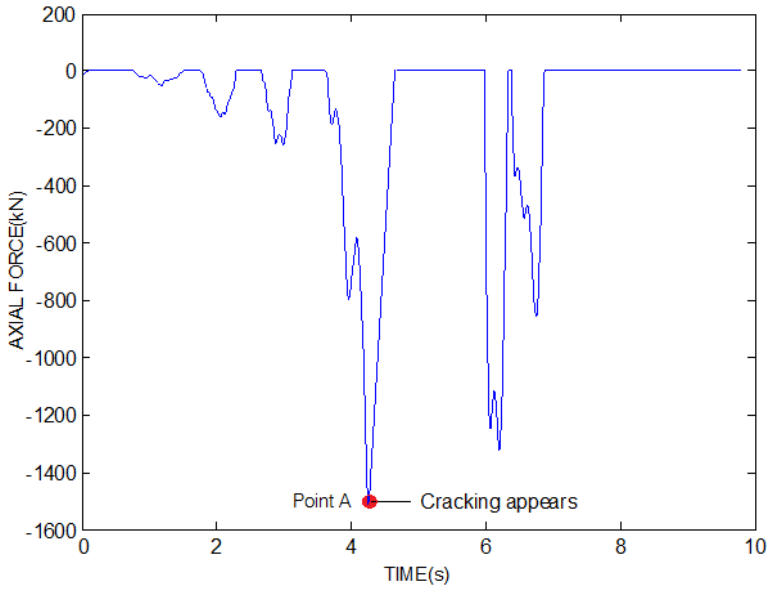

Figure 4.4: Axial Force Time History for the Hinge Element at the First-storey Strut under Earthquake La11-005#3

The presence of infill walls affected the performance of the frame elements. Two effects have become pronounced in terms of column response; i) increase in shear forces associated with increased spectral accelerations for the more rigid infilled building, and ii) the increase in column axial load and related increase in column bending moment capacity because of the vertical component of diagonal strut forces acting on the columns. To assess the significance of these changes in column behaviour, maximum shear forces in critical columns were reviewed. The results indicated that shear forces slightly

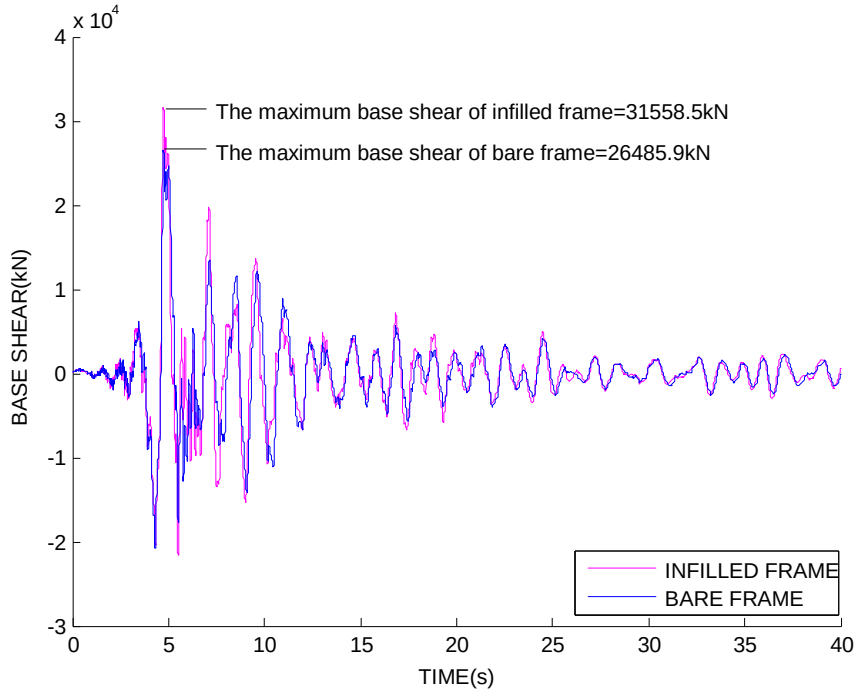

(a) Ground motion record: La11-005#1

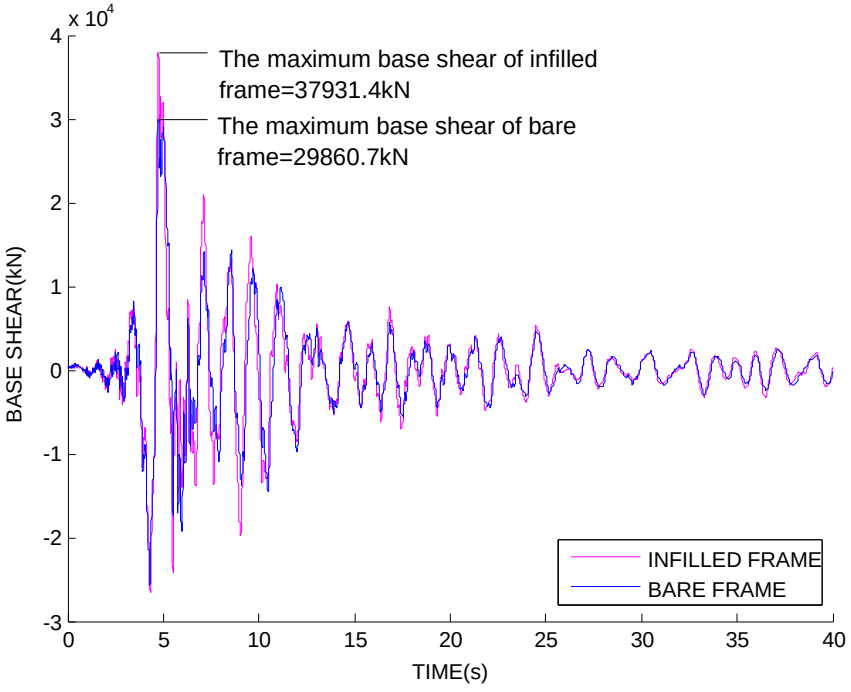

(b) Ground motion record: La11-005#2

Figure 4.5: Base Shear Time Histories for Non-isolated Frame Building with and without Infill Walls under Four Ground Motion Intensities

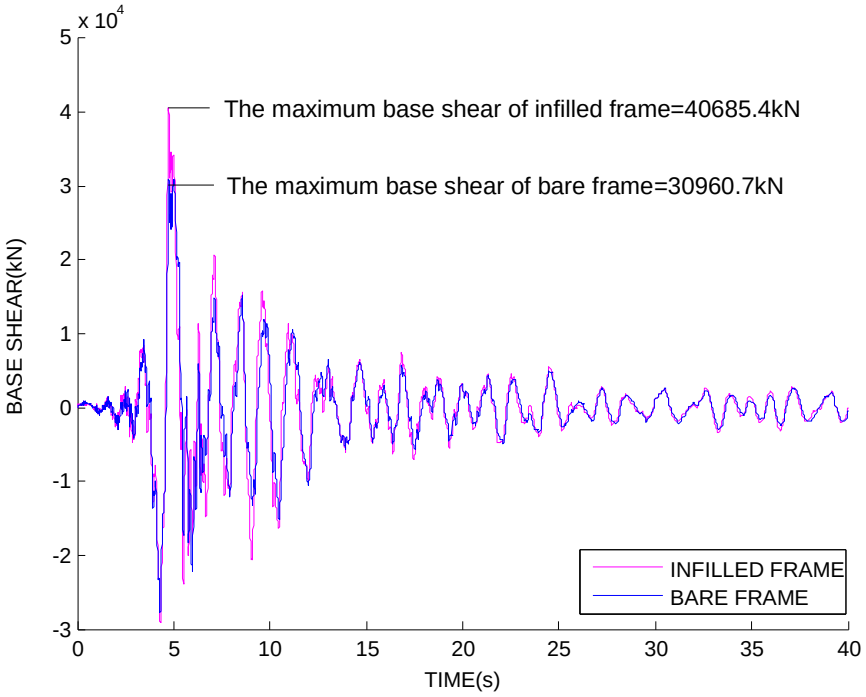

(c) Ground motion record: La11-005#3

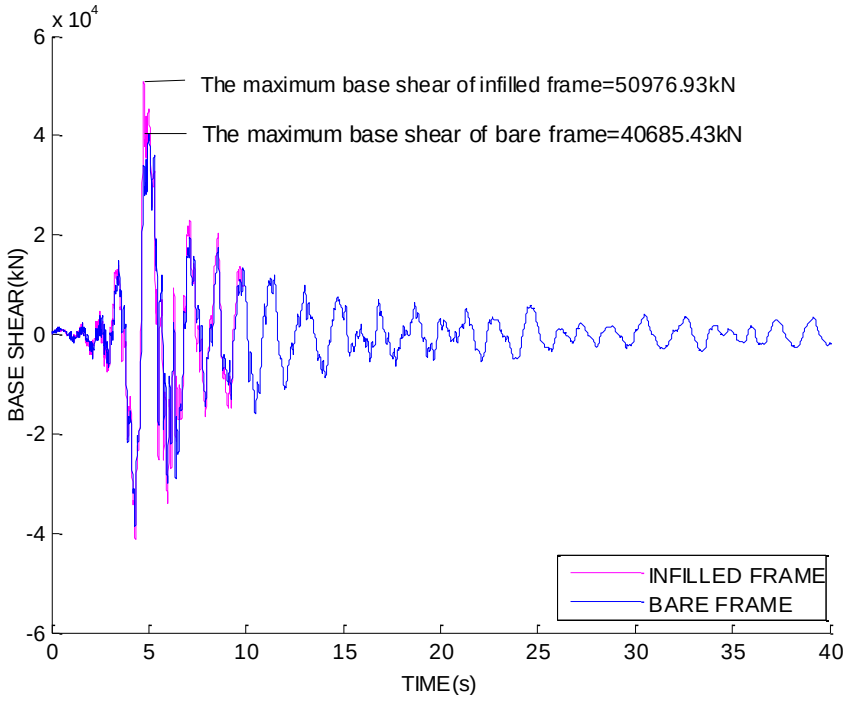

(d) Ground motion record: La11-005#4

Figure 4.5 : Base Shear Time Histories for Non-isolated Infilled and Bare Structures under Four Ground Motions Records

increased in some columns. This raised concerns that the increase in column shear forces might offset the beneficial effects of infill walls reducing inter-storey drifts. However, the adverse effects of increase column shear forces was found to be negligible, considering the significant improvement achieved on structural behaviour by reducing inter-storey drifts. The comparison of post-yield behaviour of the first-storey columns between bare frame and infilled frame structures showed that fewer columns were found to yield in the infilled frame model than those in the bare frame model. This is shown in Table 4.5. In conclusion, although the column shear forces were slightly increased, the use of the infill walls indeed contributed to a better overall structural performance.

Table 4.5: Number of Columns Experienced Yielding at the First Floor Level
(Total number of columns at the first storey: 57)

	Infilled Model	Bare Model
PGA=0.5g	0	17
PGA=0.67g	33	80
PGA=0.9g	40	42
PGA=1.2g	51	56

4.4 Performance of Building with Rubber Bearings

4.4.1 Bearing Configuration I

In this section, the structure with infills was equipped with rubber bearing isolators for seismic protection. The actual parameters of the rubber bearings used in the reference buildings (Lushan City Hospital outpatient building), shown in Table 2.1, were assigned to the isolators used for the building as "Bearing Configuration I." The structural performance of isolated infilled frame model under the selected earthquake records were analysed and compared with the behaviour of non-isolated infilled model. The comparison was made in terms of structural period, peak inter-storey drifts, residual drifts, peak floor accelerations and base shear.

Fundamental Period:

The first six periods of vibration for the infilled frame models with and without the rubber bearings are listed in Table 4.6. Because of the increased flexibility offered by the

isolators, the periods of vibration for the infilled frame model were significantly enlarged. As a result, the structural periods shifted outside the range where the most serious seismic responses occurred. Hence, it reduced the seismic energy transmitted to the superstructure.

Table 4.6: First Six Periods of vibration for the infilled building with and without base isolation

	Isolated Infilled Model (sec)	Non-isolated Infilled Model (sec)
Mode1	2.191	0.635
Mode2	2.111	0.623
Mode3	1.977	0.551
Mode4	0.448	0.213
Mode5	0.396	0.210
Mode6	0.365	0.189

Peak Inter-storey Drifts:

Peak inter-storey drift ratios at each floor level are compared in Figure 4.6 for the isolated and non-isolated infilled models under the four earthquake intensities considered. The maximum peak inter-storey drifts for both models are summarized in Table 4.7. The results clearly showed that the inter-storey drifts were significantly reduced by the use of rubber isolators. This is because the installation of seismic isolation system limited the transfer of the seismic energy to the superstructure, reducing dynamic response of the building significantly. The reduction in inter-storey drifts improved the overall structural behaviour by controlling damage to both structural and non-structural elements. The peak inter-storey drift for the isolated model were less than 1.0%, suggesting that the structural elements remained elastic and undamaged when subjected to earthquake records LA11-005#1, La11-005#2 and La11-005#3 with PGA varying between 0.5g and 0.9g. In contrast, the non-isolated model experienced approximately 1% to 2% inter-storey drift, potentially suffering from significant non-structural and some structural damage. Notably, the inter-storey drifts of the isolated model reached 2.0% when the structure was subjected to the largest earthquake La11-005#4. Although the drifts as such resulted in severe damage to the non-structural systems, the structural members were not significantly damaged and the building remained intact during and after the earthquake; however, this is not the case for the non-isolated frame with the very high inter-storey drifts, reaching approximately 3.0%.

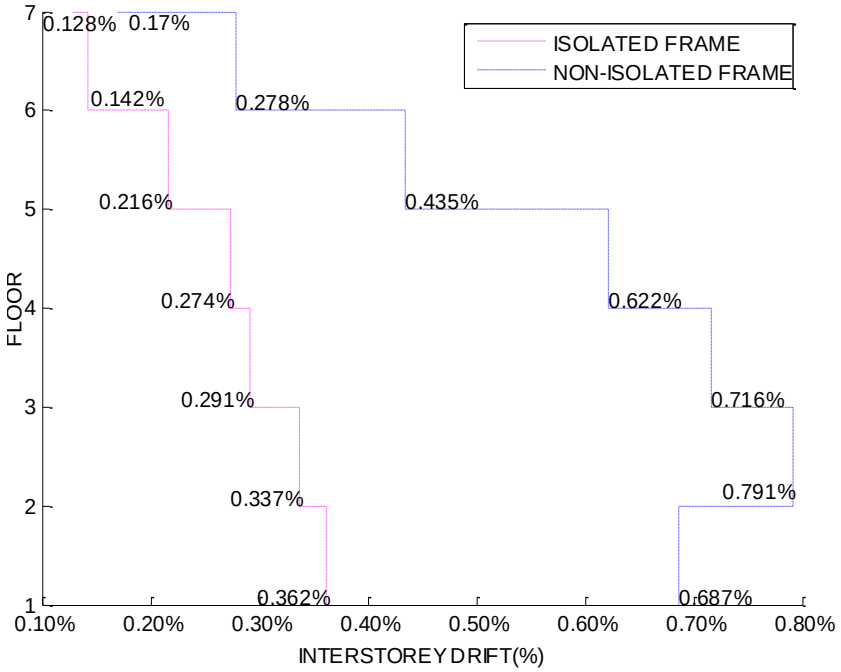

(a) Ground motion: La11-005#1

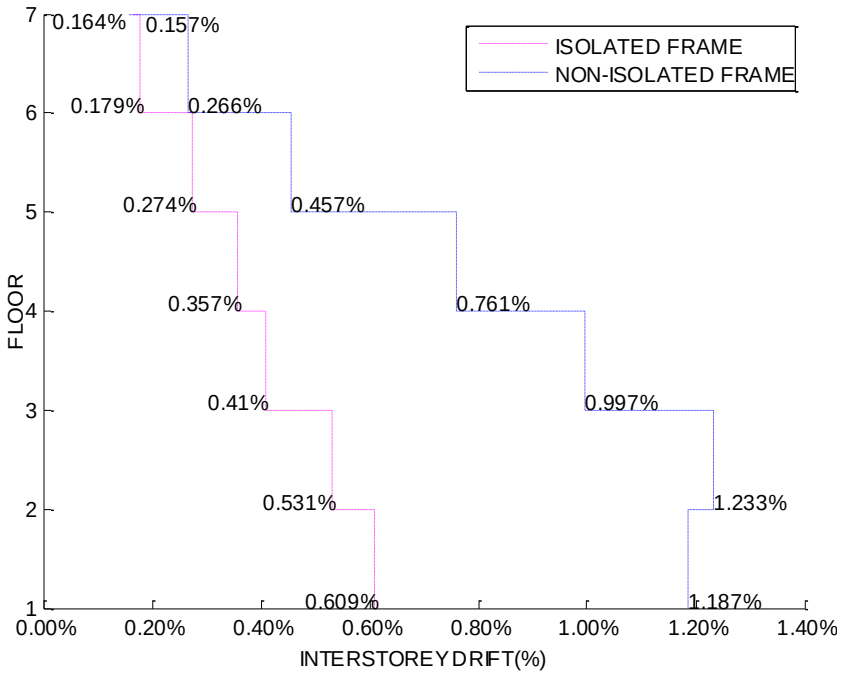

(b) Ground motion: La11-005#2

Figure 4.6: Inter-storey Drift Envelopes for Isolated and Non-isolated Infilled Structures under Four Ground Motion Intensities

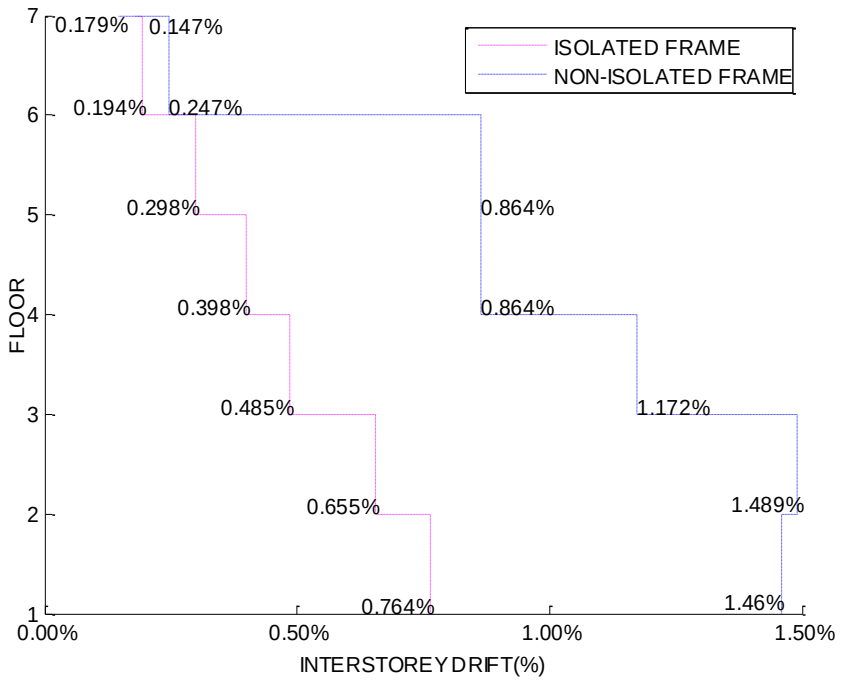

(c) Ground motion record: La11-005#3

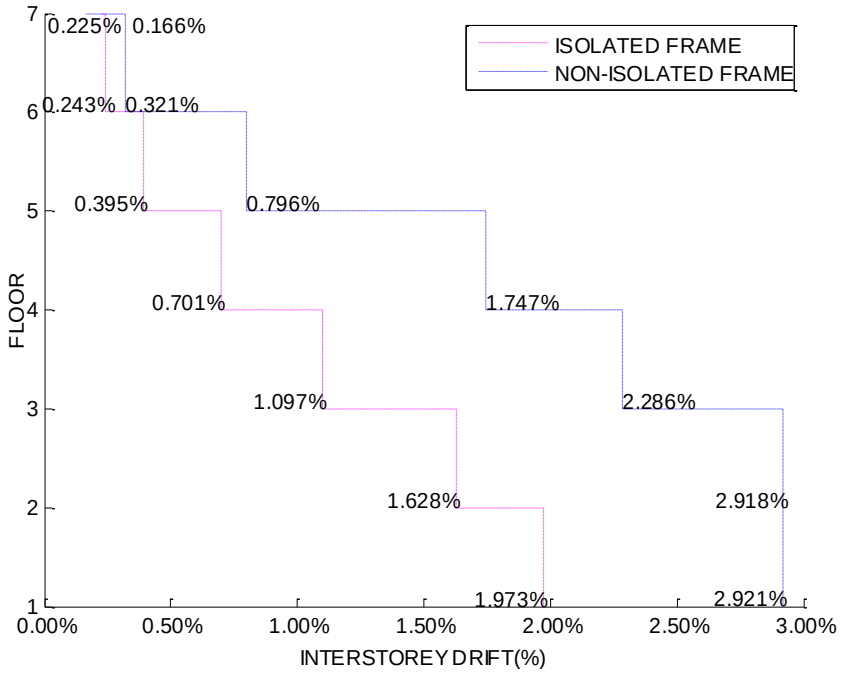

(d) Ground motion record: La11-005#4

Figure 4.6: Inter-storey Drift Envelopes for Isolated and Non-isolated Infilled Structures under Four Ground Motion Intensities

Table 4.7: Maximum Inter-storey Drifts of Isolated and Non-isolated Infilled Models

	Isolated Model	Non-isolated Model
PGA=0.5g	0.362%	0.791%
PGA=0.67g	0.609%	1.187%
PGA=0.9g	0.764%	1.460%
PGA=1.2g	1.973%	2.921%

Table 4.8: Maximum Residual Drifts of Isolated and Non-isolated Infilled Models

	Isolated Model	Non-isolated Model
PGA=0.5g	0.019%	0.098%
PGA=0.67g	0033%	0.141%
PGA=0.9g	0.026%	0.161%
PGA=1.2g	0.033%	0.501%

Residual Drifts:

The residual drift ratios at each floor level of the isolated and non-isolated infilled models are compared in Figure 4.7. The application of the rubber isolation system reduced the seismic loading experienced by the structure, resulting residual inter-storey drifts that are remarkably reduced. The residual inter-storey drift ratios for the superstructure remained below 0.1% as shown in Table 4.8, indicating no expected damage in the building.

Peak Absolute Horizontal Accelerations:

The peak absolute horizontal accelerations at each floor of the isolated and non-isolated structures with infills are presented in Figure 4.8 under different levels of earthquake intensity. The incorporation of the rubber isolation system played an important role in limiting the absolute horizontal accelerations. The flexible isolators shifted structural period to a higher value, which reduced the magnitude of floor acceleration response spectra. The reduction in structural accelerations controlled seismic damage to non-structural elements and building contents. The maximum peak floor accelerations for both isolated and non-isolated buildings are tabulated in Table 4.9. Base isolation resulted in a reduction of about 0.2g to 0.4g in floor accelerations, with the difference in reduction being higher under lower intensity earthquakes. Hence, it is expected that damage to operational and functional components in buildings would be reduced significantly due to base isolation.

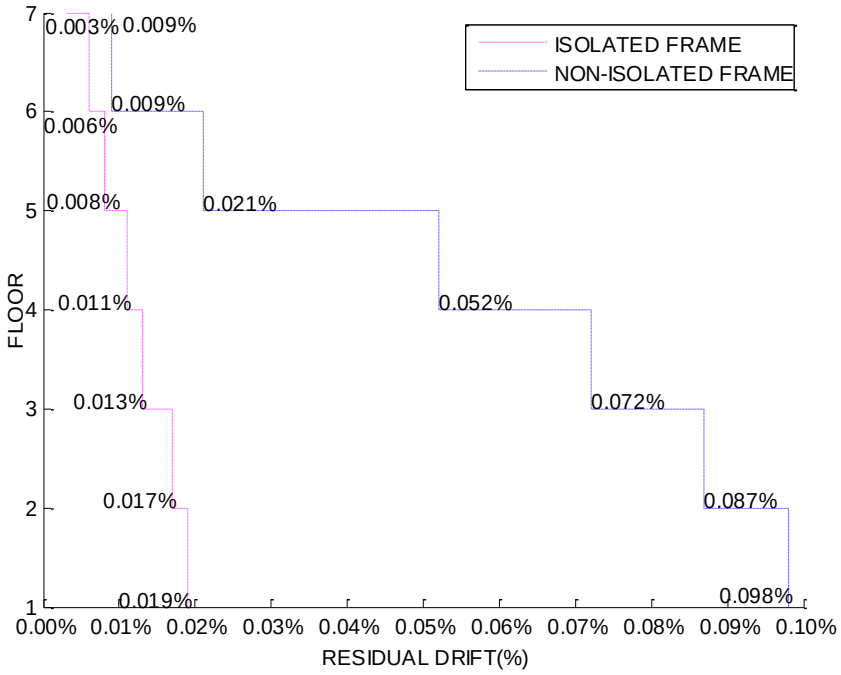

(a) Ground motion record: La11-005#1

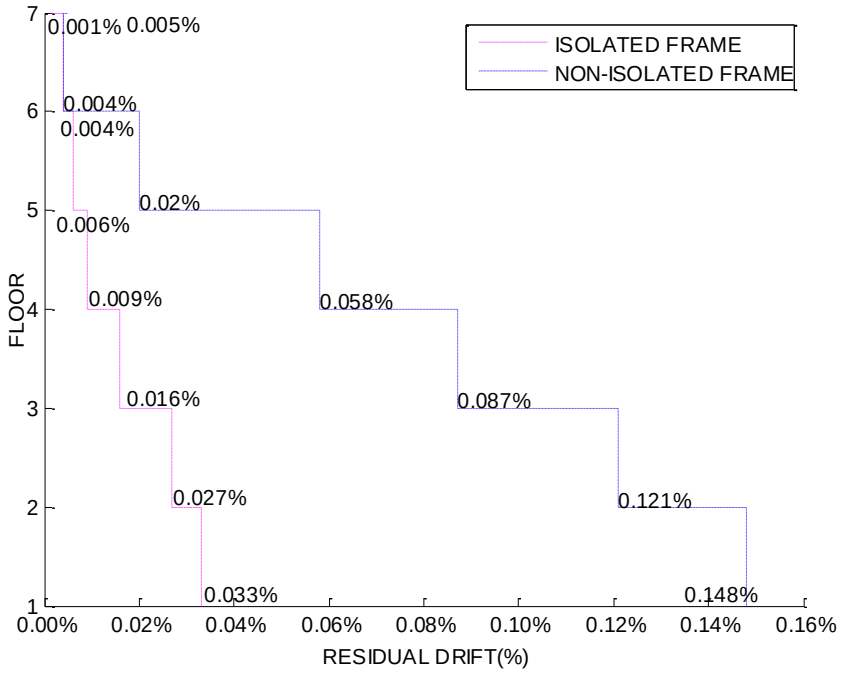

(b) Ground motion record: La11-005#2

Figure 4.7: Residual Drift Envelopes for Isolated and Non-isolated Infilled Structures under Four Ground Motion Intensities

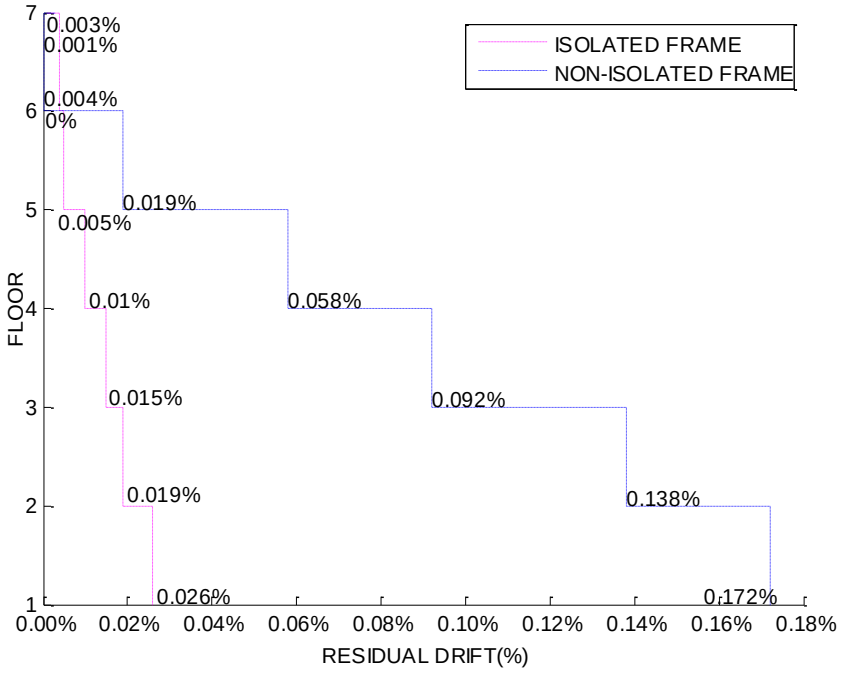

(c) Ground motion record: La11-005#3

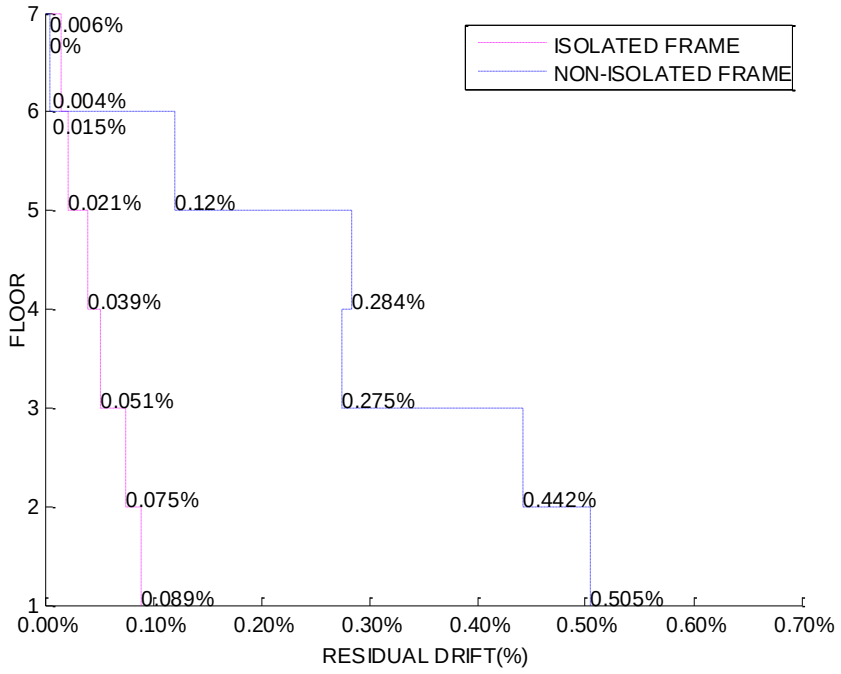

(d) Ground motion record: La11-005#4

Figure 4.7: Residual Drift Envelopes for Isolated and Non-isolated Infilled Structures under Four Ground Motion Intensities

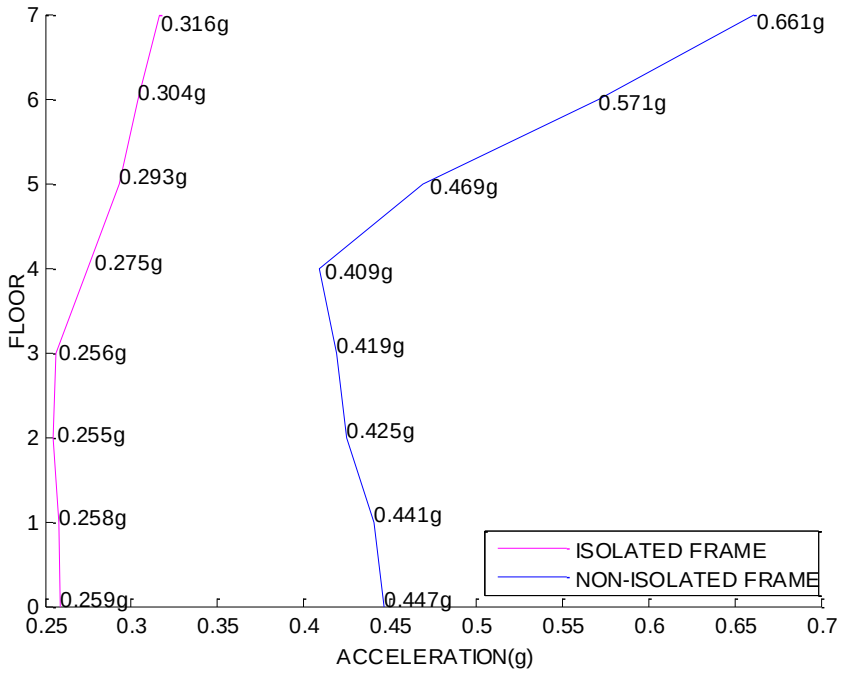

(a) Ground motion record: La11-005#1

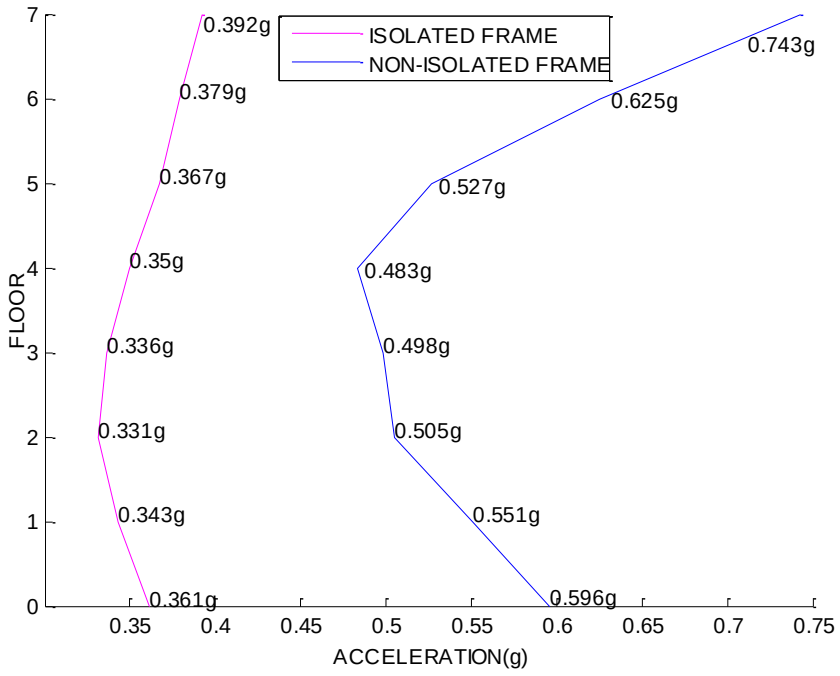

(b) Ground motion record: La11-005#2

Figure 4.8: Floor Acceleration Envelopes for Isolated and Non-isolated Infilled Structures under Four Ground Motion Intensities

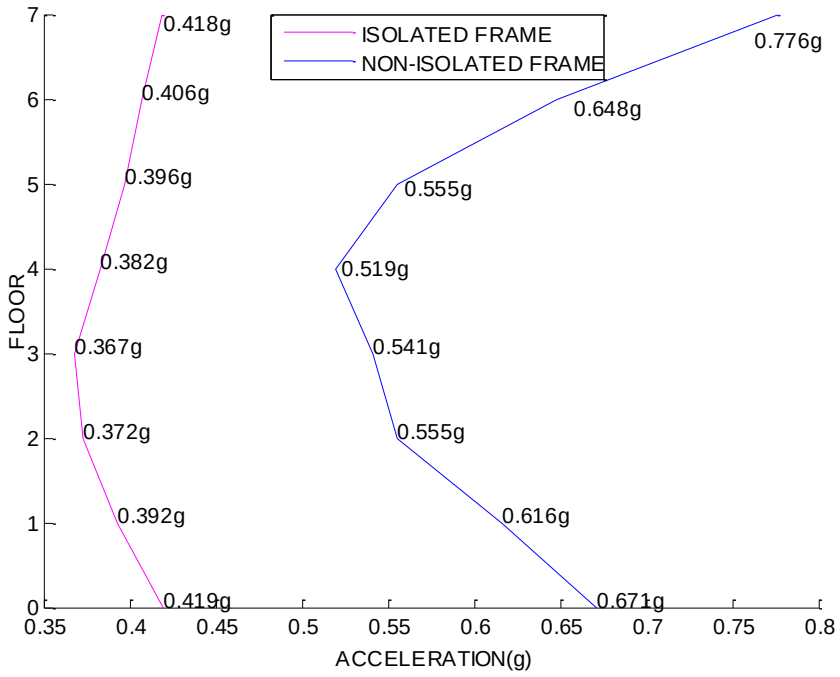

(c) Ground motion record: La11-005#3

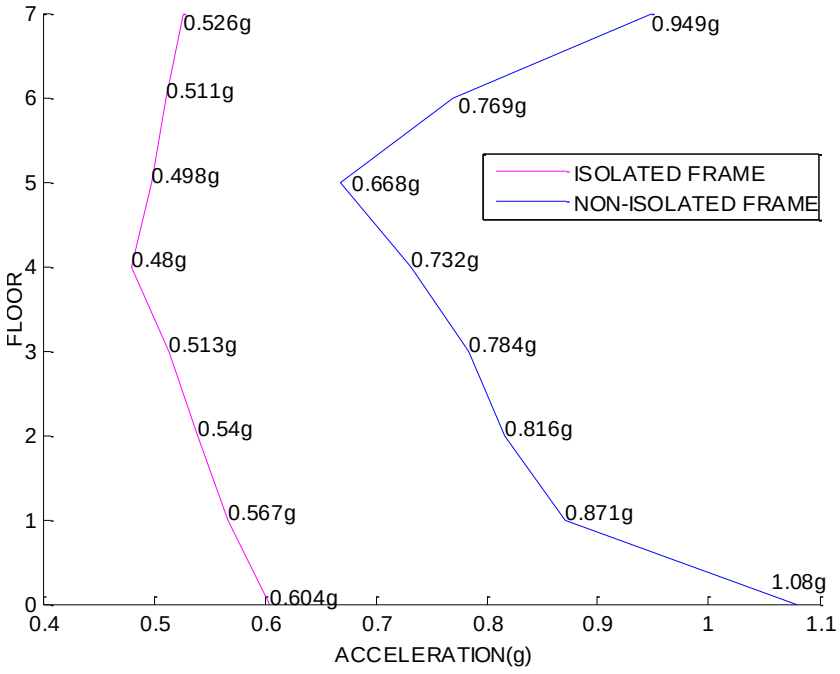

(d) Ground motion record: La11-005#4

Figure 4.8: Floor Acceleration Envelopes for Isolated and Non-isolated Infilled Structures under the Four Ground Motion Intensities

Table 4.9: Maximum Peak Floor Accelerations of Isolated and Non-isolated Infilled Models

	Isolated Model	Non-isolated Model
PGA=0.5g	0.259g	0.661g
PGA=0.67g	0.361	0.743g
PGA=0.9g	0.419g	0.776g
PGA=1.2g	0.604g	0.800g

Base Shear:

Base shear time histories of isolated and non-isolated buildings are shown in Figure 4.9. The building with infill walls, isolated by rubber bearings, experienced significant reductions in base shear forces. The reductions in base shear was 54%, 41%, 37% and 26%, respectively under the earthquake records La11-005#1, La11-005#2, La11-005#3 and La11-005#4. The decrease in base shear was directly related to reduced floor accelerations, which produced lower inertia forces at each floor level. A reduction in column shear was also observed because the decrease in base shear would translate directly to the reduction in column shears that make up the total base shear. This resulted in the yielding of fewer columns in the isolated structure, as summarized in Table 4.10.

Assessment of Bearing Configuration I

It was previously indicated that the rubber isolation system applied in the new outpatient building of the Lushan City Hospital (the prototype building) was very effective in controlling structural vibrations and seismic shear forces during the 2013 Lushan City Earthquake. Therefore, as the first bearing configuration the same type and size of isolators were adopted first, as presented in the preceding sections, with properties listed in Table 2.1. However, some bearings showed less than desirable performance during the earthquake. The rubber bearings must have sufficient vertical load carrying capacity to support the vertical loads transferred from the superstructure. The vertical load capacity of the rubber isolators used in the outpatient building was calculated to be 2466kN and was justified to be sufficient if the bearings solely supporting the structural weight. However, when the structure was subjected to earthquake, the vertical forces acting on the isolators became much larger than the structural weight due to the impact caused by the ground excitation. Considering this, the designed vertical load capacity of the isolation system was judged to be inadequate. The bearings might be damaged under

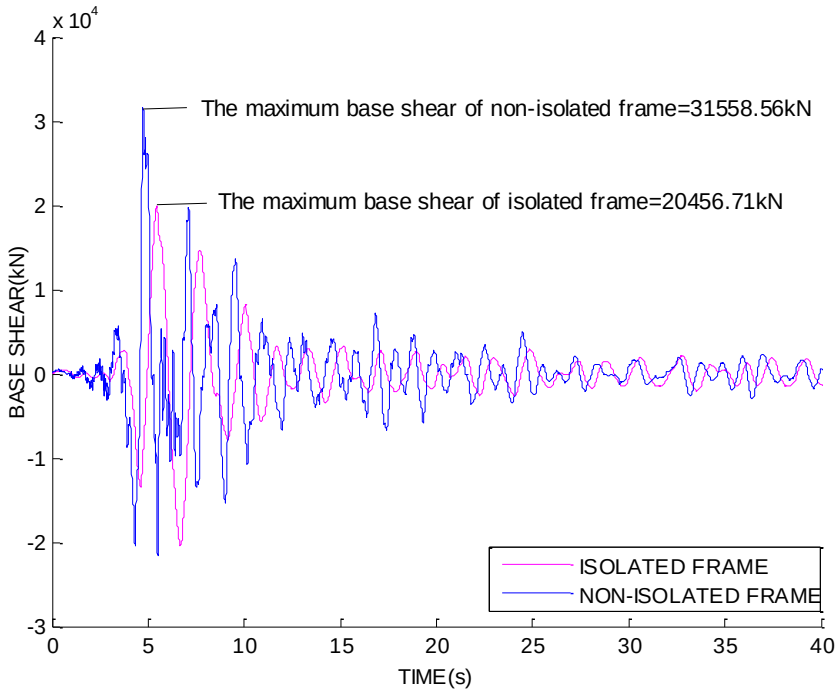

(a) Ground motion record: La11-005#1

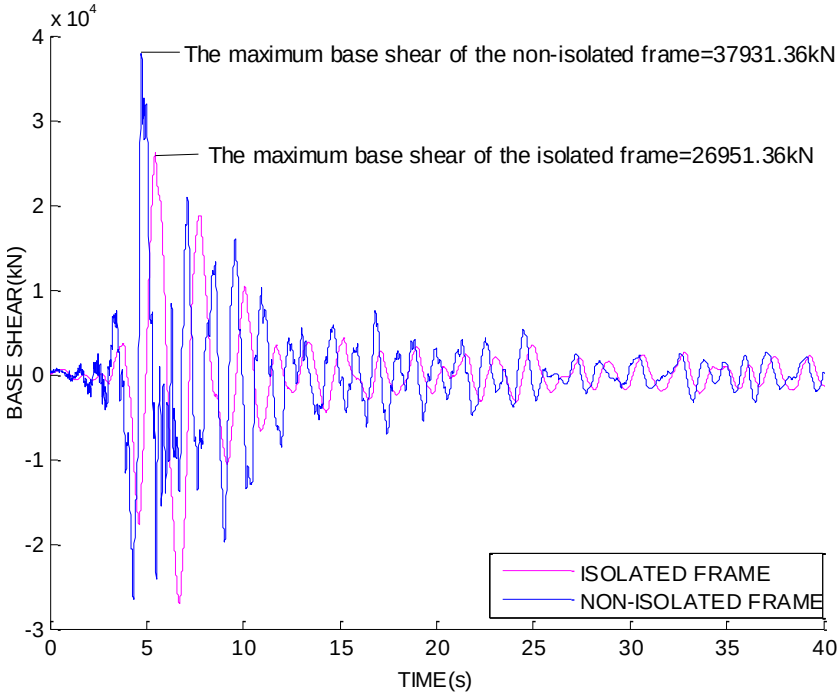

(b) Ground motion record: La11-005#2

Figure 4.9: Base Shear Time Histories for Isolated and Non-isolated Infilled Structures under Four Ground Motion Intensities

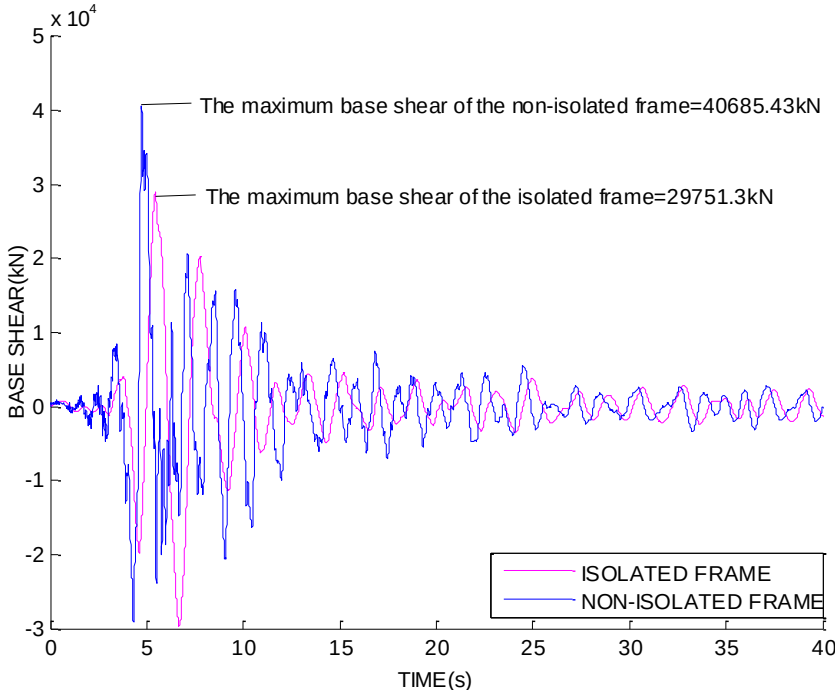

(c) Ground motion record: La11-005#3

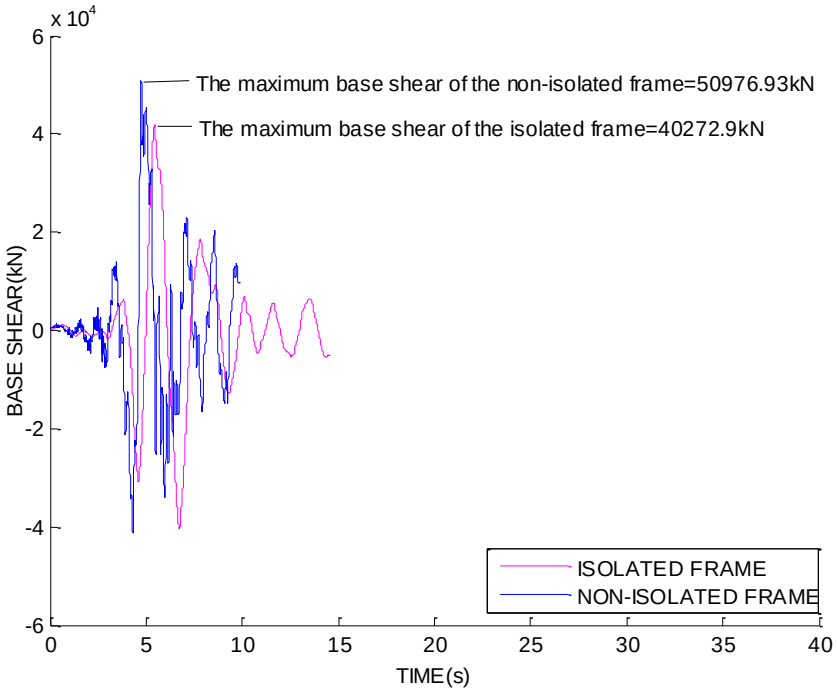

(d) Ground motion record: La11-005#4

Figure 4.9: Base Shear Time History for Isolated and Non-isolated Infilled Structures under Four Ground Motion Intensities

Table 4.10: Number of Columns Experienced Yielding at the First Storey Level
(Total number of columns at the first storey: 57)

	Isolated Model	Non-isolated Model
PGA=0.5g	0	0
PGA=0.67g	14	33
PGA=0.9g	20	40
PGA=1.2g	50	51

Table 4.11: Maximum Isolator Displacements under Four Different Intensities of Earthquakes (mm)

	PGA=0.5g	PGA=0.67g	PGA=0.9g	PGA=1.2g
Maximum Displacemnt (mm)	308	402	442	597

heavy axial forces and may not be able to support the superstructure in a stable manner. Another limitation for this rubber isolation system is the relatively large lateral displacements that they may experience. Table 4.11 indicates that lateral displacements at the isolator level reached 308mm under the smallest intensity earthquake, and increased to 597mm under the largest intensity earthquake. These isolator displacements greatly exceed the allowable displacement threshold (167mm), indicating severe damage in the rubber isolators. Hence, Bearing Configuration I was deemed to be unsatisfactory, likely leading to failures of the isolation system, even if the superstructure remains intact.

4.4.2 Bearing Configuration II

Bearing Configuration II consists of larger diameter isolators to overcome some of the shortcomings of Bearing Configuration I. In this configuration the diameter of isolator LLRB and LRB#1was enlarged from 500mm to 600mm to obtain the required vertical load capacity as the load carrying capacity is directly proportional to the isolator cross-section area. The modified isolator parameters were computed based on the formulas from Table 3.6. They are listed in Table 4.12 and represent enhancements relative to those listed in Table 2.1. With the new diameter the vertical load carrying capacity of isolators LLRB and LRB#1 were increased from 2367kN to 3927kN. The increased load capacity was verified to be adequate for the vertical loads experienced by bearings under the selected intensities of earthquake record. However, the increase in the isolator diameter in turn increased the elastic stiffness and post-yield stiffness of the isolation system. The increase in post-yield stiffness of isolators could intensify dynamic response

by attracting higher seismic forces to the structure. This might create an undesirable response in the modified isolated structure with Bearing Configuration II.

Table 4.12: Parameters of the Modified Isolation System for Bearing Configuration II

Design Properties	LLRB	LRB#1	LRB#2
Thickness of the Rubber Layer (mm)	86.4	86.4	100
Diameter of the Isolator (mm)	600	600	600
Area (cm^2)	2827	2827	2827
Vertical Load Capacity (kN)	3927	3927	3393
Vertical Stiffness (kN/mm)	2761	2761	2517
Elastic Stiffness (kN/mm)	7.430	1.309	1.131
Post-yield Stiffness (kN/mm)	1.309	Non	Non
Yield Strength (kN)	42.8	Non	Non
Allowable Lateral Deformation (mm)	200	200	200

Figures 4.10 to 4.13 compare inter-storey drifts, residual drifts, floor accelerations and base shear for the two isolated structural models having Bearing Configurations I and II with two different isolator diameters. As expected, the increase in isolator dimension resulted in larger deformations of the superstructure. The inter-storey drifts and residual drifts for the structure with Bearing Configuration II increased by approximately 25%, yet remained sufficiently low to ensure that the structure remained intact. Similarly, structural floor accelerations of the modified model increased by 9.4%, 8.9%, 16.7% and 14.1% respectively under the four intensities of ground excitations considered. The increased floor accelerations, although in the allowable range, could cause more damage in the non-structural elements attached to the main structure. As for the base shear, the modified structure experienced larger shear forces at the base due to increased inertia forces. This could potentially lead to shear damage in critical columns. The lateral displacements in isolators were slightly reduced due to the increased elastic stiffness of the isolation system. Despite this reduction they remained out of the acceptable range. The maximum isolator displacements of the two isolated structural models with Bearing Configurations I and II having 500 mm and 600 mm isolators, respectively are compared in Table 4.13.

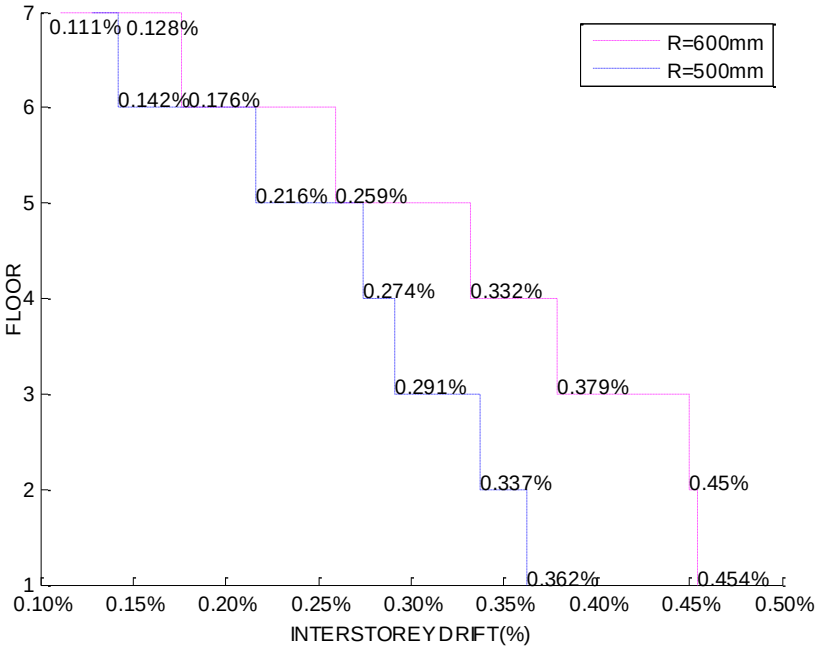

(a) Ground motion record: La11-005#1

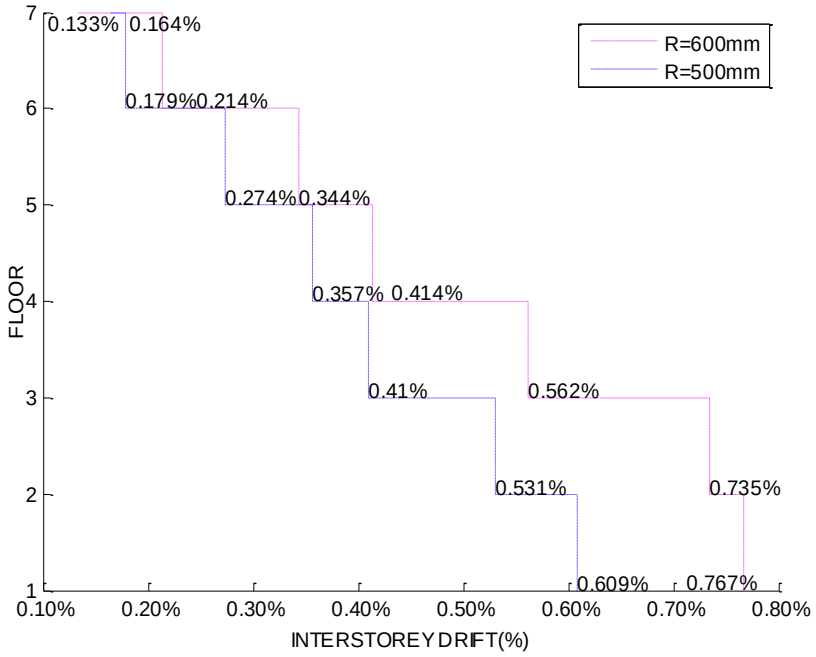

(b) Ground motion record: La11-005#2

Figure 4.10: Inter-storey Drift Envelopes for Isolated Structures with Configuration I (Isolator Diameter R=500 mm) and Configuration II (Isolator Diameter R=600mm)

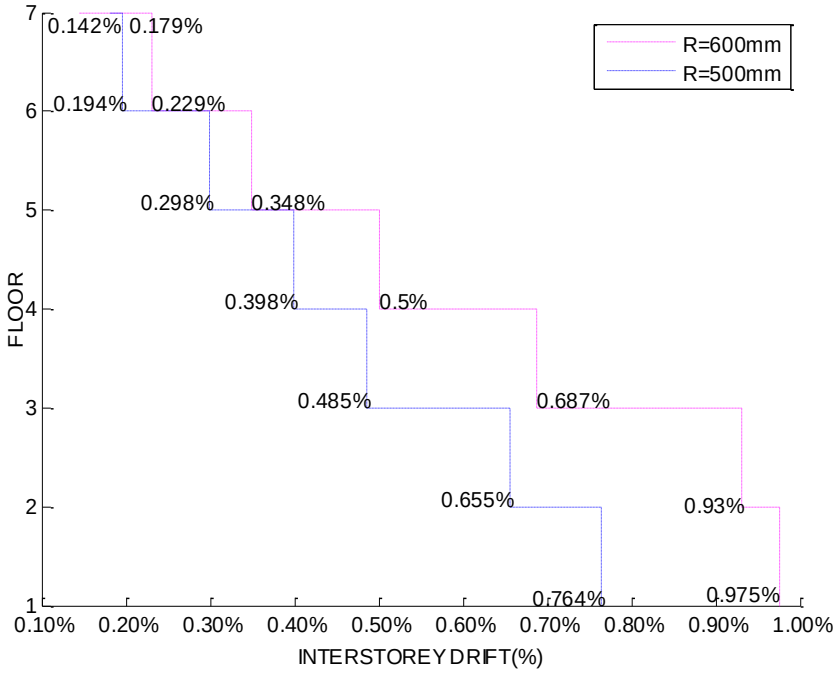

(c) Ground motion record: La11-005#3

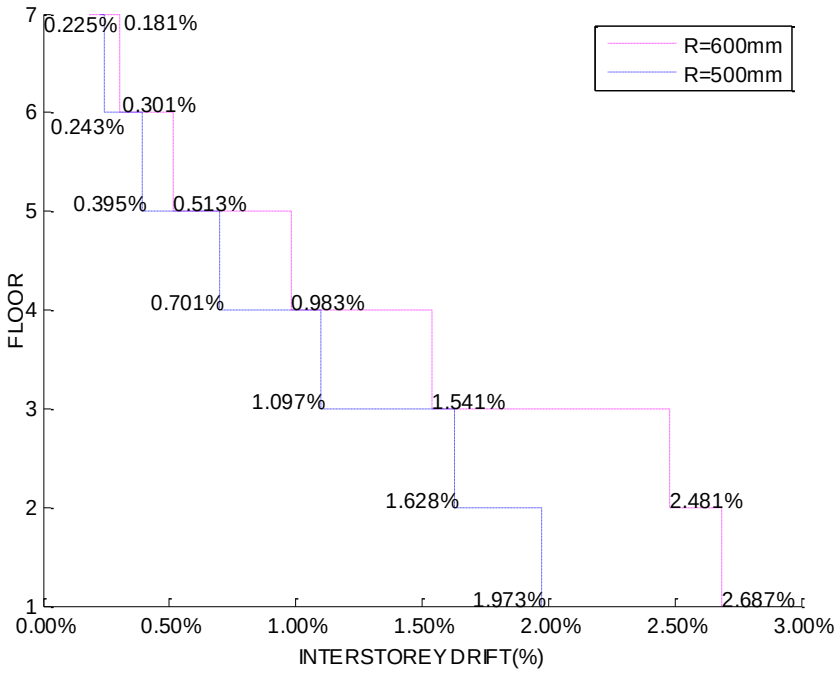

(d) Ground motion record: La11-005#4

Figure 4.10 : Inter-storey Drift Envelopes for Isolated Structures with Configuration I (Isolator Diameter R=500 mm) and Configuration II (Isolator Diameter R=600mm)

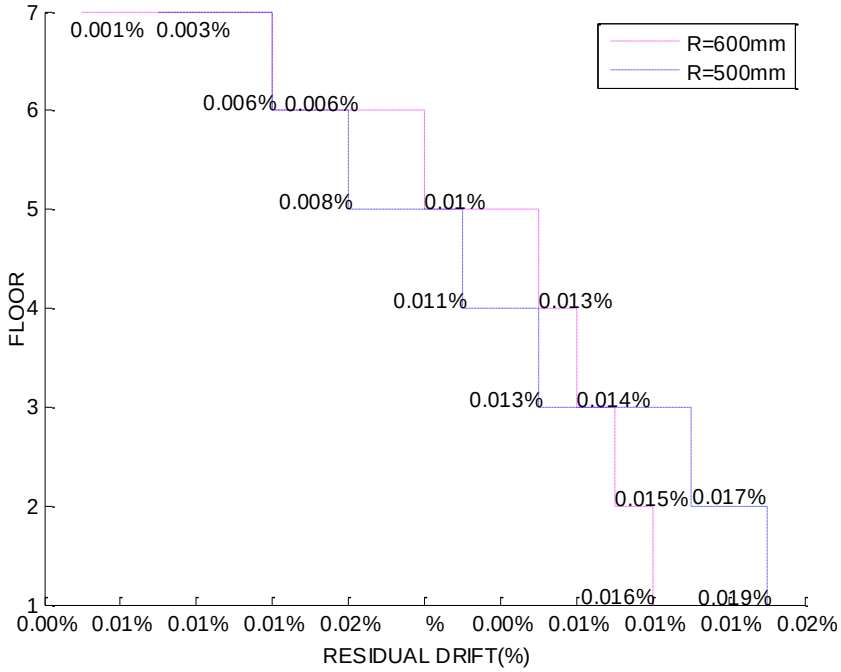

(a) Ground motion record: La11-005#1

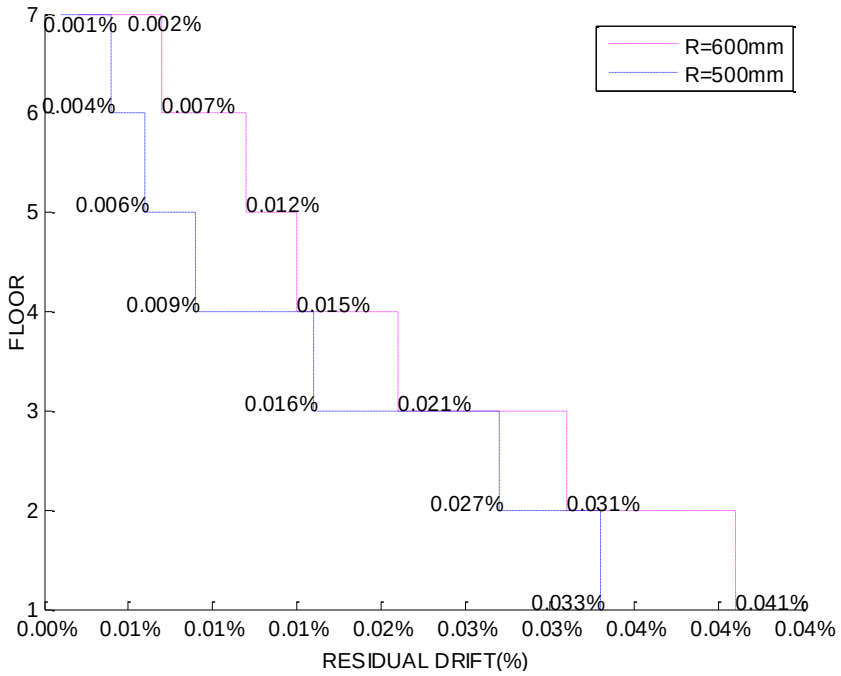

(b) Ground motion record: La11-005#2

Figure 4.11: Residual Drift Envelopes for Isolated Structures with Configuration I (Isolator Diameter R=500 mm) and Configuration II (Isolator Diameter R=600mm)

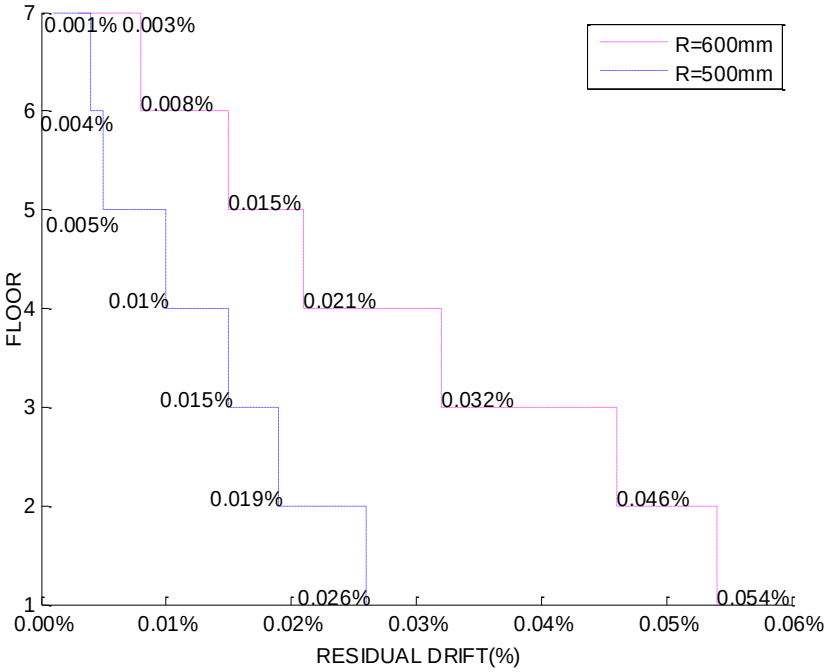

(c) Ground motion record: La11-005#3

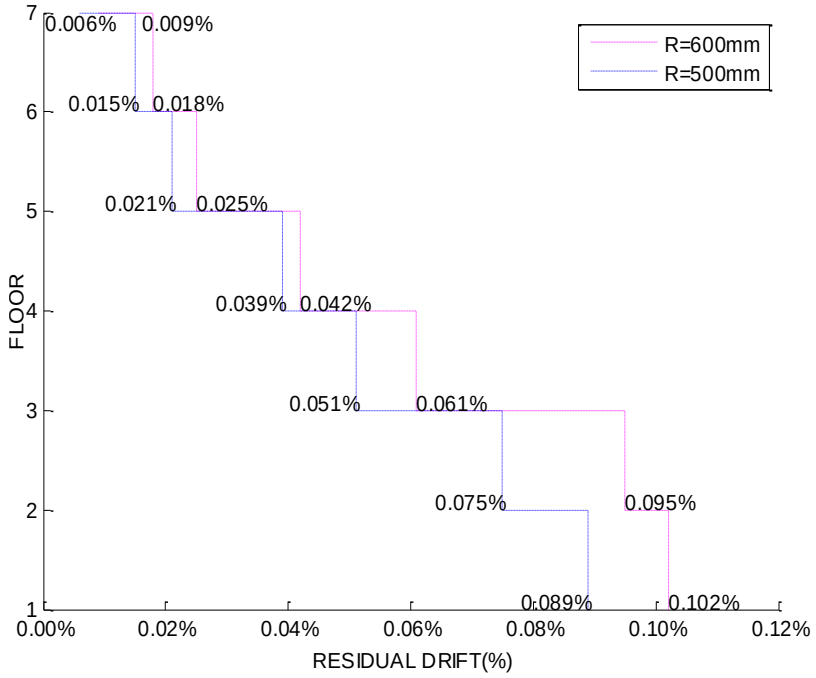

(d) Ground motion record: La11-005#4

Figure 4.11 : Residual Drift Envelopes for Isolated Structures with Configuration I (Isolator Diameter R=500 mm) and Configuration II (Isolator Diameter R=600mm)

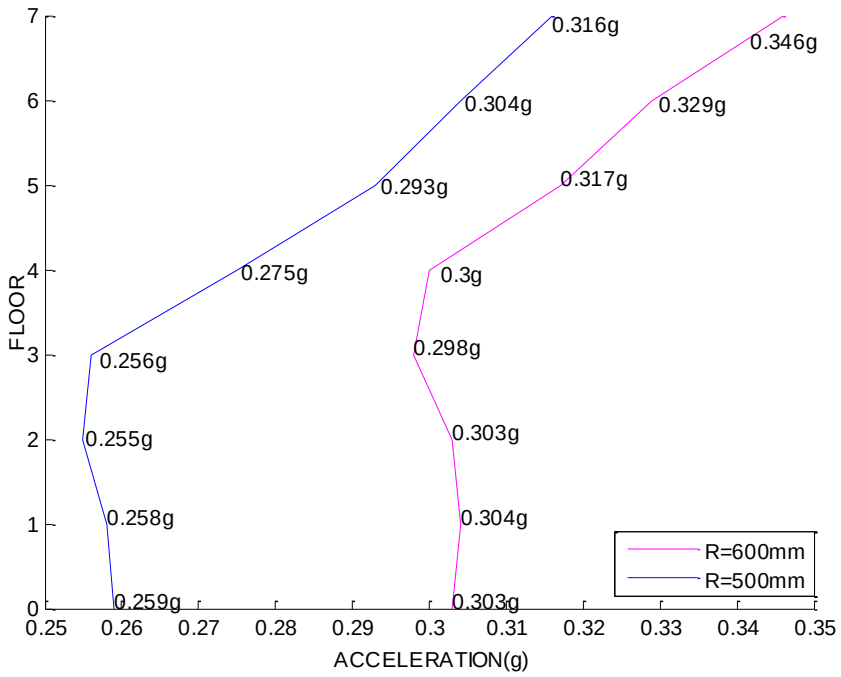

(a) Ground motion record: La11-005#1

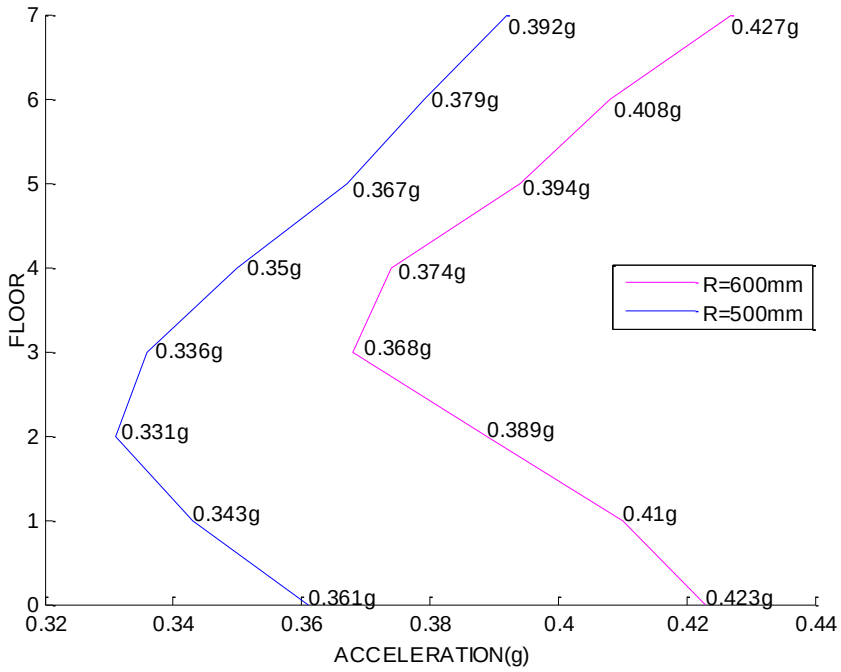

(b) Ground motion record: La11-005#2

Figure 4.12: Acceleration Envelopes for Isolated Structures with Configuration I (Isolator Diameter R=500 mm) and Configuration II (Isolator Diameter R=600mm)

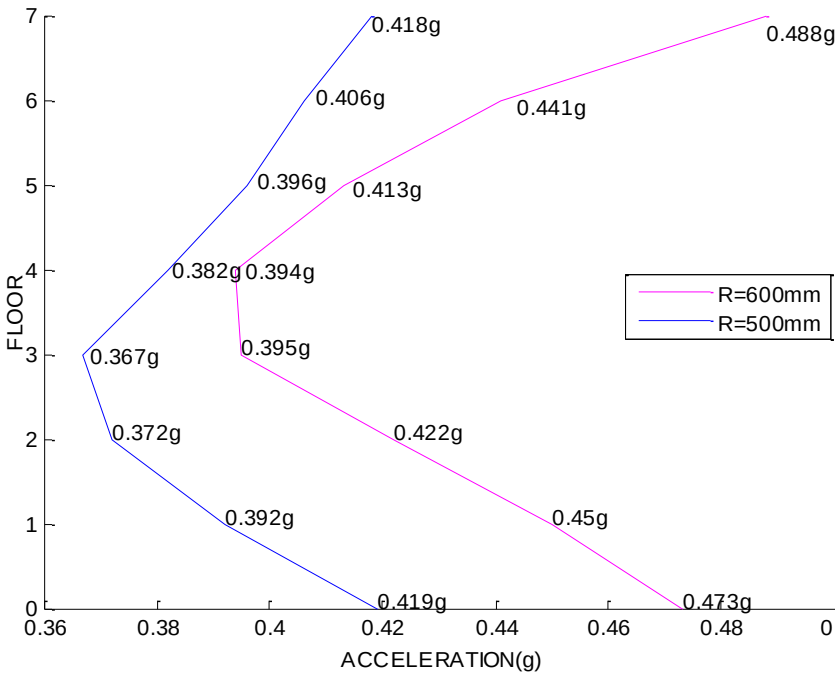

(c) Ground motion record: La11-005#3

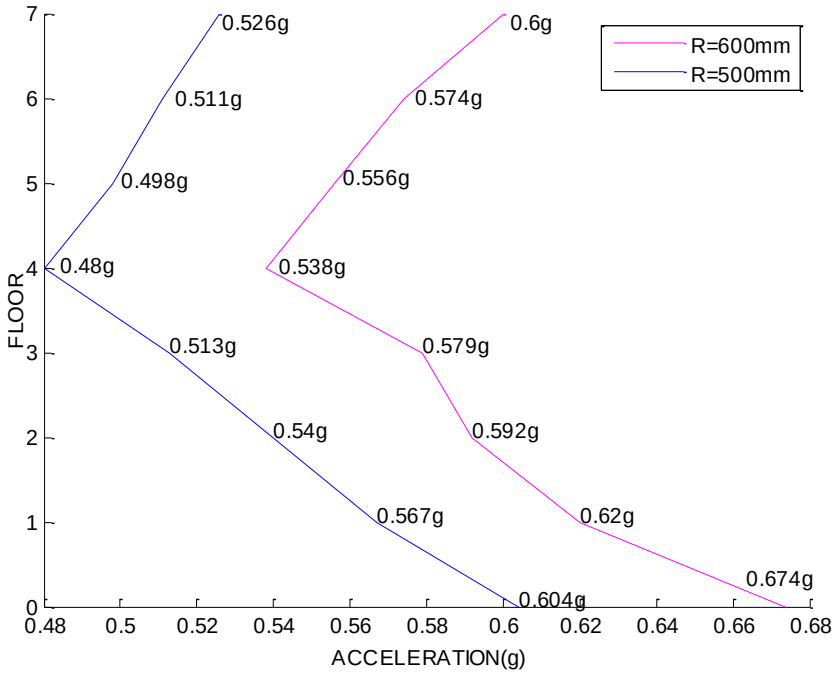

(d) Ground motion record: La11-005#4

Figure 4.12: Acceleration Envelopes for Isolated Structures with Configuration I (Isolator Diameter R=500 mm) and Configuration II (Isolator Diameter R=600mm)

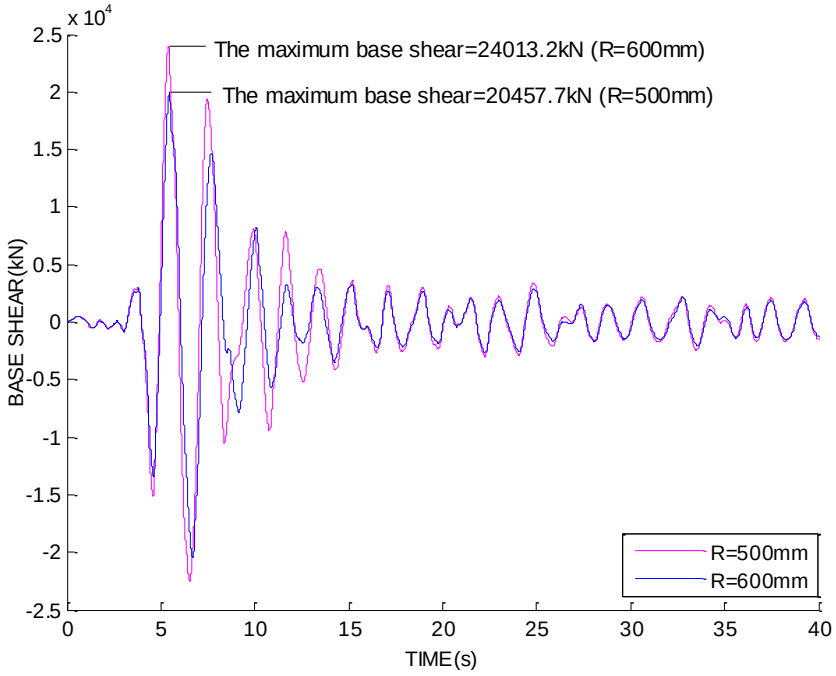

(a) Ground motion record: La11-005#1

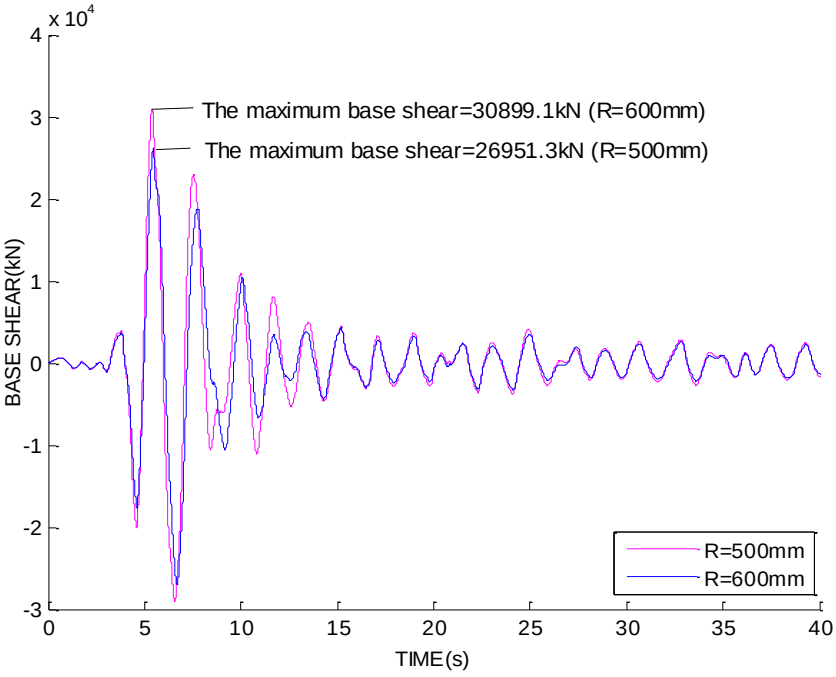

(b) Ground motion record: La11-005#2

Figure 4.13: Base Shear Time Histories for Isolated Infilled Structures with Configuration I (Isolator Diameter R=500 mm) and Configuration II (Isolator Diameter R=600mm)

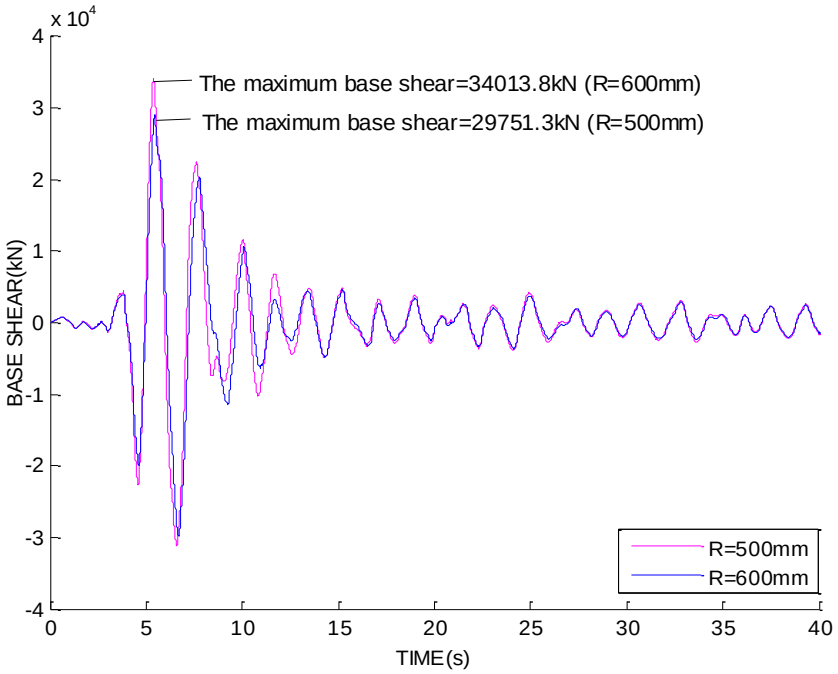

(c) Ground motion record: La11-005#3

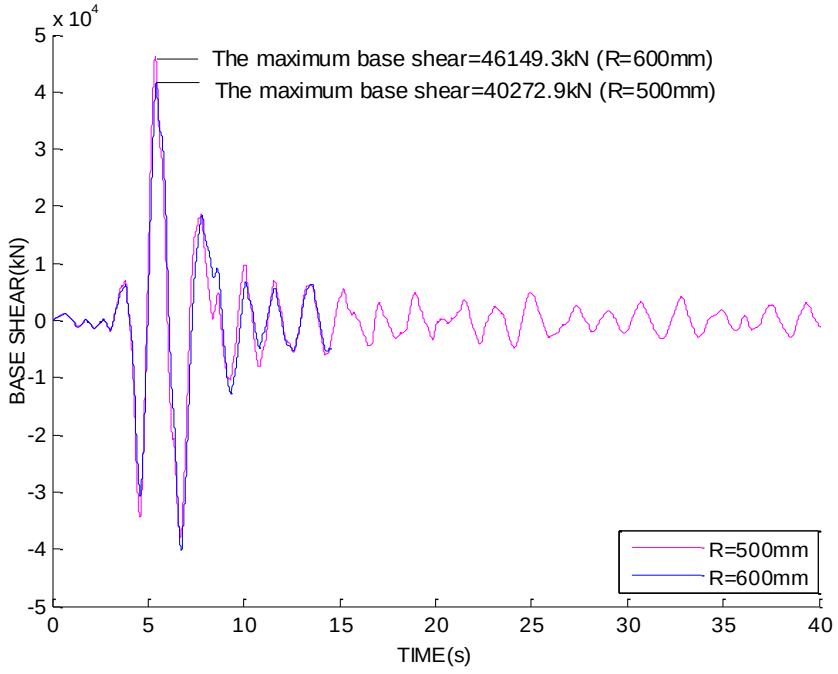

(d) Ground motion record: La11-005#4

Figure 4.13: Base Shear Time Histories for Isolated Infilled Structures with Configuration I (Isolator Diameter R=500 mm) and Configuration II (Isolator Diameter R=600mm)

Table 4.13: Maximum Isolator Displacements under Four Different Intensities of Earthquakes (mm)

	PGA=0.5g	PGA=0.67g	PGA=0.9g	PGA=1.2g
Configuration I (R=500mm)	308	402	442	597
Configuration II (R=600mm)	281	357	386	534

In conclusion, increasing the isolator diameter, as was done in Bearing Configuration II, could provide larger vertical load capacity for the isolation system, but it also amplifies the dynamic response of the superstructure. To obtain an optimum base isolation system further refinements have to be made on the isolation system for controlling structural response and isolator lateral displacements. This is done below as Bearing Configuration III.

4.4.3 Bearing Configuration III

Bearing Configuration III is intended to restrict the isolator displacement by either increasing the diameter of rubber layers and/or increasing the diameter of the lead plug in LLRBs. Increasing the isolator diameter would also enhance the post yield stiffness of isolators, which might increase the seismic responses. Therefore, it was deemed to be a superior approach to increase the diameter of the lead plug. This could increase the initial stiffness of the LLRBs for lateral displacement control, but more importantly, this would not affect the isolation efficiency as the lead plug would have already yielded and would provide no lateral resistance during response to ground excitations. Furthermore, previous studies showed that if the lead plug diameter was enlarged in a proper way, it could help restrict structural vibrations during response, although it might affect structural acceleration response to certain extent. It can be concluded that increasing the size of the lead plug is an optimum approach to simultaneously control both structural deformations and isolator displacements. Accordingly, in Configuration III, the diameter of the lead plug was enlarged from 67mm to 100mm first, and then to 170mm in increments of 100mm to establish the relationship between the lead plugs size and the isolator performance.

Figure 4.14 illustrates that lateral isolator displacements reduce significantly with increasing initial stiffness and damping of the isolators by increasing lead plug diameter. The results show that the maximum isolator displacement decreased by approximately 16%

to 19% under increasing earthquake intensities when the lead plug diameter increased from 67mm to 170mm. Despite the great reduction in the isolator displacement, the displacement under the ground motion La11-005#4 with PGA=1.2g exceeded the allowable displacement even with the highest diameter (170 mm) lead plug considered. This implies that changing only the size of the lead plug in LLRBs is impractical to control base displacement. Thus additional damping devices may be needed to reduce displacement demands for isolators.

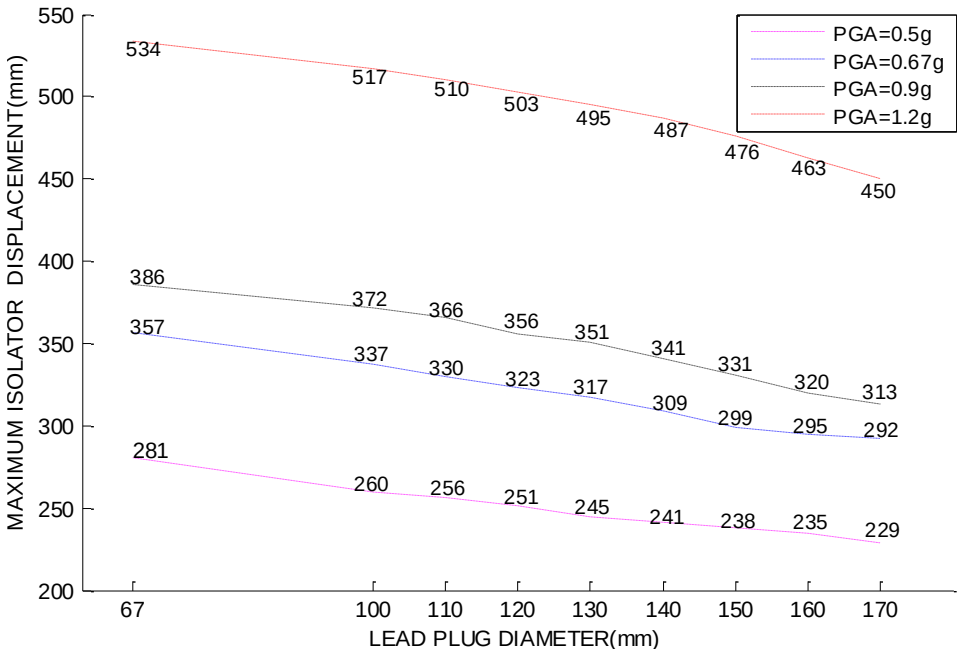

Figure 4.14: Variation of Maximum Base Displacement of Isolated Structure with Increasing Lead Plug Diameter

Table 4.14 and Figure 4.15 compare the inter-storey drifts of the isolated structure obtained from different analyses with different lead plug diameters. As expected, the superstructure drifts were significantly reduced due to the increase in lead plug diameter, which resulted in greater hysteretic damping, providing a higher energy dissipation capacity. By enlarging the diameter of the lead plug, a significant amount of seismic energy was dissipated in the isolation system rather than being transmitted to the superstructure. However, the effectiveness of lead plug diameter increase was lost after a certain diameter size. Beyond the lead plug diameter of 150 mm the inter-storey drift remained essentially unchanged and even slightly increased (cells with blue background

in Table 4.14). This can be attributed to two reasons. First, a sizable lead plug in the LLRBs could generate an unnecessary high level of hysteretic damping that would inappropriately restrain the isolator movement during earthquakes. This might stiffen the isolated structure, increasing inter-storey drifts for the superstructure. Second, the LLRBs with a large size lead plug would have high yield strength which could be hardly attained during response especially under low intensity ground motions. In this case, the LLRBs would act elastically most of the time, making the structure more rigid. This would reduce the effectiveness of the isolation system. In the current research, it was observed that the first reason dominated the behaviour.

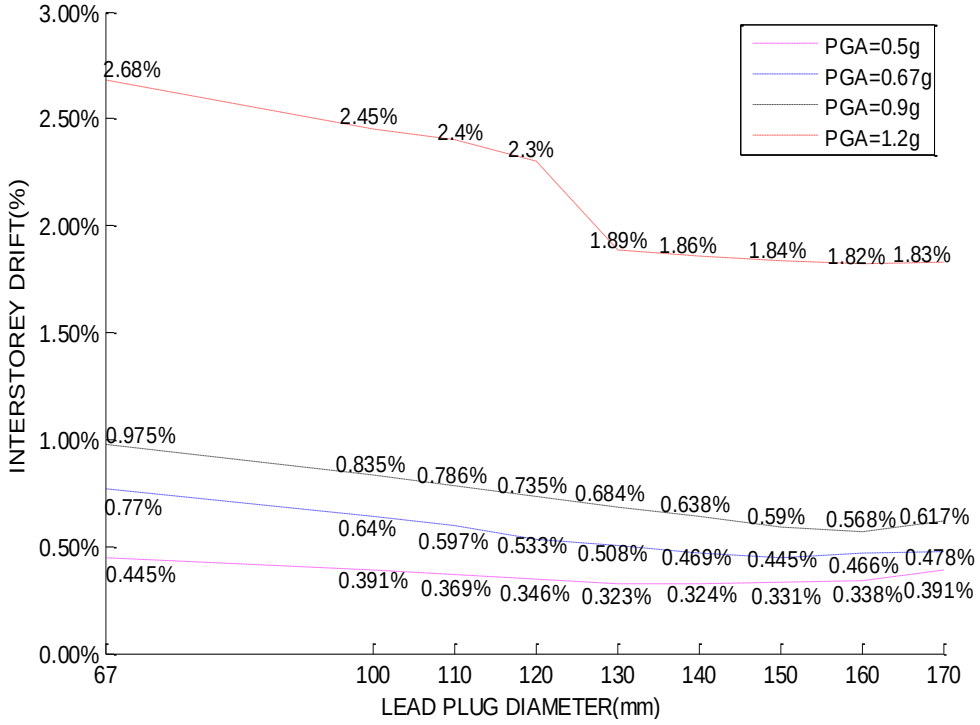

Figure 4.15: Vibration of Maximum Inter-storey Drift of Isolated Structure with Increasing Lead Plug Diameter

Table 4.14: Inter-storey Drifts of Isolated Structure with Different Lead Plug Diameters

(a) Ground motion record: La11-005#1(PGA=0.5g)

Lead plug diameter / Structure Floor	67mm	100mm	110mm	120mm	130mm	140mm	150mm	160mm	170mm
7th floor	0.111%	0.092%	0.097%	0.093%	0.088%	0.078%	0.070%	0.071%	0.102%
6th floor	0.176%	0.160%	0.154%	0.147%	0.140%	0.121%	0.109%	0.110%	0.142%
5th floor	0.259%	0.234%	0.225%	0.215%	0.204%	0.177%	0.164%	0.161%	0.210%
4th floor	0.332%	0.297%	0.284%	0.270%	0.255%	0.229%	0.220%	0.220%	0.257%
3rd floor	0.379%	0.332%	0.315%	0.297%	0.279%	0.263%	0.261%	0.264%	0.312%
2nd floor	0.450%	0.388%	0.366%	0.342%	0.319%	0.315%	0.319%	0.326%	0.345%
1st floor	0.454%	0.391%	0.369%	0.346%	0.323%	0.324%	0.331%	0.338%	0.390%

(b) Ground motion record: La11-005#2(PGA=0.67g)

Lead plug diameter / Structure Floor	67mm	100mm	110mm	120mm	130mm	140mm	150mm	160mm	170mm
7th floor	0.133%	0.125%	0.123%	0.119%	0.115%	0.111%	0.107%	0.094%	0.101%
6th floor	0.214%	0.201%	0.196%	0.191%	0.185%	0.178%	0.169%	0.149%	0.152%
5th floor	0.344%	0.297%	0.290%	0.281%	0.271%	0261%	0.245%	0.223%	0.229%
4th floor	0.414%	0.392%	0.379%	0.365%	0.349%	0.332%	0.312%	0.299%	0.311%
3rd floor	0.562%	0.476%	0.455%	0.432%	0.407%	0.383%	0.363%	0.362%	0.370%
2nd floor	0.735%	0.602%	0.566%	0.531%	0.497%	0.463%	0.444%	0.455%	0.461%
1st floor	0.767%	0.641%	0.597%	0.553%	0.508%	0.469%	0.445%	0.466%	0.482%

(c) Ground motion record: La11-005#3(PGA=0.9g)

Lead plug diameter / Structure Floor	67mm	100mm	110mm	120mm	130mm	140mm	150mm	160mm	170mm
7th floor	0.142%	0.134%	0.131%	0.128%	0.125%	0.122%	0.119%	0.113%	0.101%
6th floor	0.229%	0.215%	0.211%	0.206%	0.200%	0.195%	0.190%	0.180%	0.162%
5th floor	0.348%	0.322%	0.314%	0.306%	0.297%	0.288%	0.280%	0.264%	0.246%
4th floor	0.500%	0.442%	0.426%	0.410%	0.394%	0.378%	0.363%	0.347%	0.342%
3rd floor	0.687%	0.571%	0.543%	0.516%	0.487%	0.459%	0.433%	0.422%	0.432%
2nd floor	0.930%	0.761%	0.720%	0.675%	0.631%	0.587%	0.547%	0.541%	0.568%
1st floor	0.975%	0.835%	0.786%	0.735%	0.684%	0.635%	0.590%	0.568%	0.617%

(d) Ground motion record: La11-005#4(PGA=1.2g)

Lead plug diameter / Structure Floor	67mm	100mm	110mm	120mm	130mm	140mm	150mm	160mm	170mm
7th floor	0.181%	0.171%	0.168%	0.180%	0.161%	0.158%	0.155%	0.153%	0.151%
6th floor	0.301%	0.284%	0.278%	0.226%	0.266%	0.260%	0.255%	0.251%	0.248%
5th floor	0.513%	0.476%	0.464%	0.473%	0.439%	0.423%	0.411%	0.402%	0.399%
4th floor	0.983%	0.884%	0.850%	0.818%	0.783%	0.736%	0.706%	0.689%	0.682%
3rd floor	1.541%	1.349%	1.301%	1.252%	1.167%	1.112%	1.093%	1.076%	1.070%
2nd floor	2.481%	2.076%	2.007%	1.887%	1.652%	1.629%	1.598%	1.580%	1.578%
1st floor	2.687%	2.456%	2.402%	2.303%	1.894%	1.864%	1.839%	1.826%	1.829%

Tests showed that increasing the diameter of the lead plug in LLRBs would control the base displacement, but inevitably amplify the floor accelerations of the isolated structure. The same observation was made in the analyses conducted in the current investigation. Figure 4.16 shows the variation of maximum floor accelerations of modeled structures with lead plug diameter. The floor accelerations were first reduced as the lead plug diameter went from 67mm to 100mm, but started increasing thereafter. It should be pointed out that the magnitude of accelerations in the structure was affected by damping in the isolators, which depended on the diameter of the lead pug. At a low level of isolation damping, the slight increase in damping created by the enlarged lead plug diameter could dissipate more seismic energy, thereby reducing floor accelerations. However, as the lead plug diameter went up, the isolation damping became too much for the earthquakes considered and the high damping generated stiffened the isolation system at a certain degree, which could amplify the acceleration response of the isolated structure. The intensified structural acceleration would cause adverse effects on internal components and the equipment attached to the primary structure. This could have contradictory effects on base isolation because the main purpose of applying the isolation system is to protect the building and its contents.

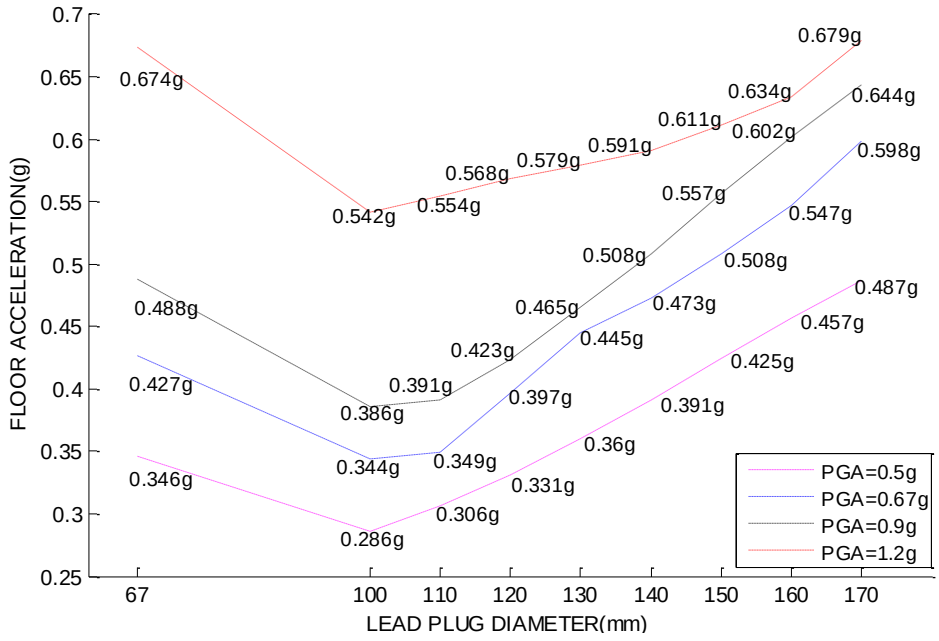

Figure 4.16: Variation of Maximum Floor Acceleration of Isolated Structure with Increasing Lead Plug Diameter

Table 4.15: Floor Accelerations of Isolated Structure with Different Lead Plug Diameters

(a) Ground motion record: La11-005#1(PGA=0.5g)

Diameter / Structure Floor	67mm	100mm	110mm	120mm	130mm	140mm	150mm	160mm	170mm
7th floor	0.346g	0.273g	0.260g	0.327g	0.360g	0.391g	0.425g	0.457g	0.487g
6th floor	0.329g	0.249g	0.235g	0.289g	0.318g	0.346g	0.375g	0.403g	0.428g
5th floor	0.316g	0.219g	0.204g	0.247g	0.268g	0.291g	0.315g	0.337g	0.357g
4th floor	0.300g	0.186g	0.176g	0.235g	0.236g	0.240g	0.251g	0.265g	0.292g
3rd floor	0.297g	0.191g	0.186g	0.258g	0.263g	0.268g	0.275g	0.280g	0.286g
2nd floor	0.302g	0.216g	0.215g	0.269g	0.275g	0.282g	0.288g	0.294g	0.299g
1st floor	0.304g	0.242g	0.248g	0.273g	0.276g	0.289g	0.300g	0.313g	0.330g
Base	0.303g	0.286g	0.306g	0.331g	0.359g	0.389g	0.414g	0.430g	0.452g

(b) Ground motion record: La11-005#2(PGA=0.67g)

Diameter / Structure Floor	67mm	100mm	110mm	120mm	130mm	140mm	150mm	160mm	170mm
7th floor	0.427g	0.342g	0.349g	0.376g	0.417g	0.461g	0.505g	0.547g	0.591g
6th floor	0.408g	0.315g	0.334g	0.336g	0.370g	0.405g	0.460g	0.515g	0.572g
5th floor	0.393g	0.282g	0.320g	0.325g	0.334g	0.341g	0.363g	0.384g	0.410g
4th floor	0.373g	0.246g	0.308g	0.317g	0.321g	0.324g	0.331g	0.343g	0.364g
3rd floor	0.368g	0.262g	0.327g	0.331g	0.336g	0.342g	0.348g	0.358g	0.395g
2nd floor	0.389g	0.283g	0.338g	0.343g	0.349g	0.354g	0.357g	0.362g	0.409g
1st floor	0.410g	0.307g	0.342g	0.346g	0.351g	0.361g	0.417g	0.453g	0.486g
Base	0.423g	0.344g	0.341g	0.397g	0.445g	0.473g	0.508g	0.543g	0.598g

(c) Ground motion record: La11-005#3(PGA=0.9g)

Diameter / Structure Floor	67mm	100mm	110mm	120mm	130mm	140mm	150mm	160mm	170mm
7th floor	0.488g	0.386g	0.375g	0.398g	0.442g	0.485g	0.530g	0.571g	0.609g
6th floor	0.441g	0.374g	0.363g	0.358g	0.395g	0.432g	0.470g	0.503g	0.534g
5th floor	0.413g	0.362g	0.350g	0.337g	0.344g	0.368g	0.395g	0.420g	0.444g
4th floor	0.393g	0.350g	0.339g	0.339g	0.340g	0.341g	0.344g	0.351g	0.365g
3rd floor	0.395g	0.354g	0.358g	0.363g	0.369g	0.374g	0.378g	0.384g	0.391g
2nd floor	0.421g	0.365g	0.371g	0.377g	0.383g	0.387g	0.393g	0.401g	0.410g
1st floor	0.450g	0.370g	0.377g	0.383g	0.385g	0.399g	0.426g	0.452g	0.478g
Base	0.473g	0.377g	0.391g	0.423g	0.465g	0.508g	0.557g	0.602g	0.644g

(d) Ground motion record: La11-005#4(PGA=1.2g)

Diameter / Structure Floor	67mm	100mm	110mm	120mm	130mm	140mm	150mm	160mm	170mm
7th floor	0.599g	0.482g	0.485g	0.489g	0.487g	0.532g	0.588g	0.649g	0.713g
6th floor	0.574g	0.465g	0.470g	0.473g	0.477g	0.514g	0.555g	0.601g	0.647g
5th floor	0.556g	0.448g	0.469g	0.460g	0.463g	0.486g	0.513g	0.542g	0.569g
4th floor	0.535g	0.452g	0.474g	0.459g	0.463g	0.470g	0.479g	0.486g	0.492g
3rd floor	0.578g	0.473g	0.491g	0.477g	0.485g	0.503g	0.515g	0.526g	0.531g
2nd floor	0.591g	0.476g	0.492g	0.501g	0.511g	0.526g	0.536g	0.544g	0.555g
1st floor	0.619g	0.497g	0.516g	0.531g	0.540g	0.547g	0.544g	0.587g	0.610g
Base	0.674g	0.542g	0.554g	0.568g	0.579g	0.591g	0.611g	0.634g	0.679g

The variation of maximum base shear force in isolated structure with lead plug diameter is shown in Figure 4.17. In contract to the amplification of floor accelerations, shear forces at the structure base slowly but steadily reduced as the diameter of the lead plug increased. This can be explained by the contributions of different modes of response, which result in a descending trend in base shear while maximum floor accelerations may increase after the optimum lead plug diameter shown in Fig. 4.16.

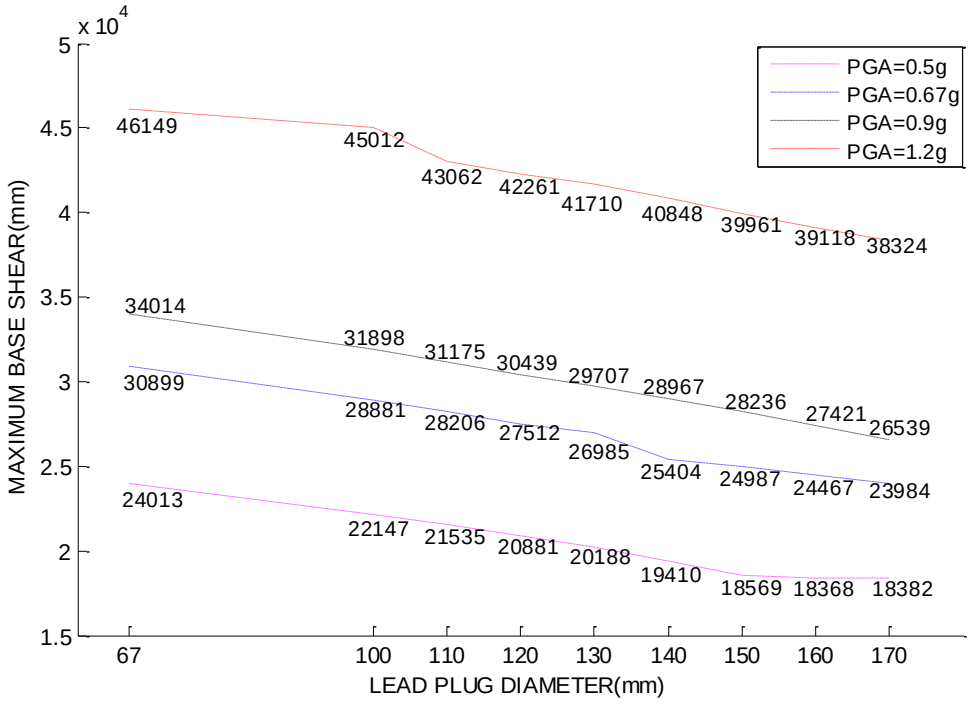

Figure 4.17: Variation of Maximum Base Shear of Isolated Structure with Increasing Lead Plug Diameter

In summary, increasing the diameter of the lead plug could effectively control displacements in isolators. If the choice of the lead plug diameter is properly made, sufficient reductions in structural drifts can be attained in the superstructure. Nonetheless, there is a trade-off between reducing structural response while controlling base displacements and an increase in floor accelerations, which would intensify seismic damage to non-structural elements and building contents. As a result, it is important to balance out the reduction of isolator displacements and the reduction of floor accelerations when deciding on the optimal size for isolators.

4.5 Performance of Buildings with Rubber Bearings and Viscous Dampers

The application of supplemental damping devices was investigated as a means of controlling excessive horizontal displacements at the base isolation level, under high intensity earthquakes. This mitigation technique was considered in place of enlarging the isolator dimension. Supplemental viscous dampers were implemented for additional damping, over and above those provided by rubber isolators. Five different designs of viscous damper were implemented in addition to the use of 600 mm diameter isolators and 100 mm diameter lead plugs. The designs varied in damping values, which varied from 10% to 50% of critical damping, as shown in Table 4.16.

Table 4.16: Viscous Damping Coefficients for Five Designs of Viscous Dampers

	10% Critical	20% Critical	30% Critical	40% Critical	50% Critical
Viscous Damping Coefficient (kN.s/m)	5494	10988	16482	21976	27470

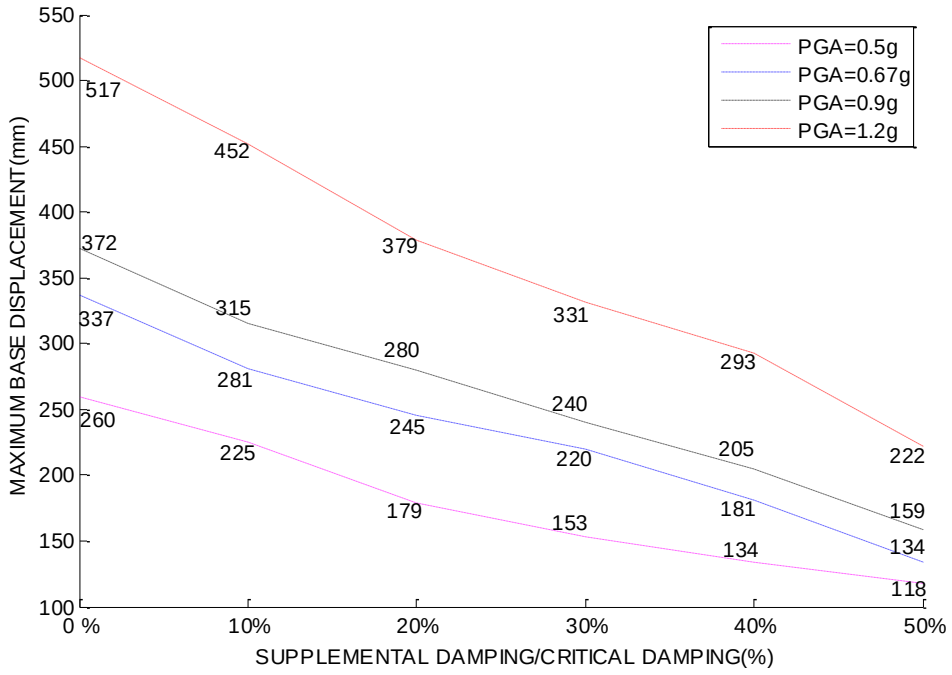

Figure 4.18: Variation of Maximum Base Displacement of Isolated Structure with Increasing Supplemental Viscous Damping

The results of dynamic analyses of isolated buildings with different viscous dampers are shown in Figure 4.18. The figure compares base displacements of buildings with different

supplemental viscous dampers. It was observed that base displacement was significantly reduced due to the implementation of supplemental damping. The trend for the reduction tended to be almost linear with the increase in damping coefficient. By adding viscous dampers with 50% of critical damping, the isolator displacements were successfully restrained within the allowable displacement threshold under all the four earthquake intensities considered. This therefore validated the effectiveness of viscous dampers in controlling isolator displacements. Nonetheless, such combination of large viscous damping might undesirably intensify structural response, amplifying the superstructure drifts and floor accelerations. To verify this, further investigation was undertaken to study the effects of adding supplemental dampers on structural response. Figure 4.19 and Table 4.17 show that the supplemental damping could effectively limit inter-storey drifts, but excessive damping could have an adverse effect. As an example, the maximum superstructure storey drift was reduced by approximately 20% to 30% when viscous damping was 30% of critical, and the earthquake PGA ranged between 0.5g and 1.2g. However, inter-storey drift remained approximately the same beyond a damping ratio of 30% of critical. This range is shown in blue in Table 4.17. Clearly, a proper level of supplemental damping helped reduce the energy transfer to the superstructure. On the other hand, large supplemental damping might severely stiffen the isolation system, resulting in the amplification of storey-drifts. It was observed, as depicted in Table 4.17, that this undesirable effect of highly damped supplementary device was prominent in the case of low intensity earthquakes (such as La11-005#1 and La11-005#2). This is because a relatively small ground excitation may be inadequate to trigger the isolators when the supplemental damping is high. One may then conclude from this observation that supplemental isolation damping is not always ideal for small earthquakes. Therefore, supplemental damping must be properly selected with due considerations given to design hazard spectra.

Table 4.17: Inter-storey Drifts of Isolated Structure with Various Levels of Supplemental Damping

(a) Ground motion record: La11-005#1(PGA=0.5g)

Viscous Damping / Structure Floor	No Damping	10% Critical	20% Critical	30% Critical	40% Critical	50% Critical
7th floor	0.092%	0.087%	0.085%	0.077%	0.069%	0.081%
6th floor	0.160%	0.154%	0.134%	0.121%	0.117%	0.125%
5th floor	0.234%	0.212%	0.195%	0.179%	0.171%	0.180%
4th floor	0.297%	0.256%	0.247%	0.231%	0.210%	0.226%
3rd floor	0.332%	0.298%	0.274%	0.227%	0.233%	0.252%
2nd floor	0.388%	0.345%	0.318%	0.260%	0.277%	0.296%
1st floor	0.391%	0.357%	0.325%	0.266%	0.284%	0.303%

(b) Ground motion record: La11-005#2(PGA=0.67g)

Viscous Damping / Structure Floor	No Damping	10% Critical	20% Critical	30% Critical	40% Critical	50% Critical
7th floor	0.125%	0.117%	0.111%	0.100%	0.098%	0.100%
6th floor	0.201%	0.187%	0.175%	0.153%	0.148%	0.150%
5th floor	0.297%	0.271%	0.258%	0.222%	0.210%	0.213%
4th floor	0.392%	0.356%	0.333%	0.292%	0.274%	0.281%
3rd floor	0.476%	0.423%	0.390%	0.304%	0.333%	0.342%
2nd floor	0.602%	0.532%	0.477%	0.422%	0.426%	0.433%
1st floor	0.641%	0.568%	0.488%	0.452%	0.461%	0.473%

(c) Ground motion record: La11-005#3(PGA=0.9g)

Viscous Damping / Structure Floor	No Damping	10% Critical	20% Critical	30% Critical	40% Critical	50% Critical
7th floor	0.134%	0.127%	0.121%	0.116%	0.111%	0.109%
6th floor	0.215%	0.204%	0.192%	0.184%	0.173%	0.166%
5th floor	0.322%	0.299%	0.284%	0.270%	0.254%	0.242%
4th floor	0.442%	0.401%	0.377%	0.355%	0.336%	0.338%
3rd floor	0.571%	0.504%	0.466%	0.433%	0.428%	0.431%
2nd floor	0.761%	0.682%	0.603%	0.553%	0.556%	0.564%
1st floor	0.835%	0.710%	0.658%	0.607%	0.613%	0.615%

(d) Ground motion record: La11-005#4(PGA=1.2g)

Viscous Damping / Structure Floor	No Damping	10% Critical	20% Critical	30% Critical	40% Critical	50% Critical
7th floor	0.171%	0.166%	0.160%	0.157%	0.156%	0.155%
6th floor	0.284%	0.271%	0.264%	0.257%	0.236%	0.254%
5th floor	0.476%	0.454%	0.433%	0.419%	0.417%	0.416%
4th floor	0.884%	0.812%	0.778%	0.746%	0.734%	0.761%
3rd floor	1.349%	1.269%	1.204%	1.149%	1.153%	1.179%
2nd floor	2.076%	1.964%	1.855%	1.668%	1.682%	1.718%
1st floor	2.456%	2.371%	2.293%	1.954%	1.974%	2.013%

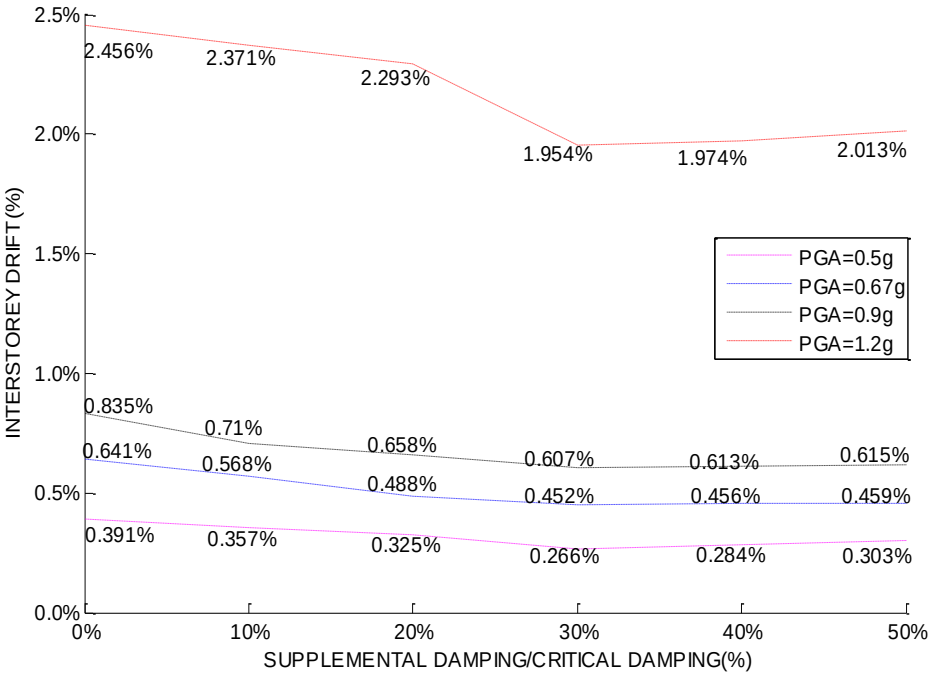

Figure 4.19: Variation of Maximum Inter-story Drift of Isolated Structure with Increasing Supplemental Viscous Damping

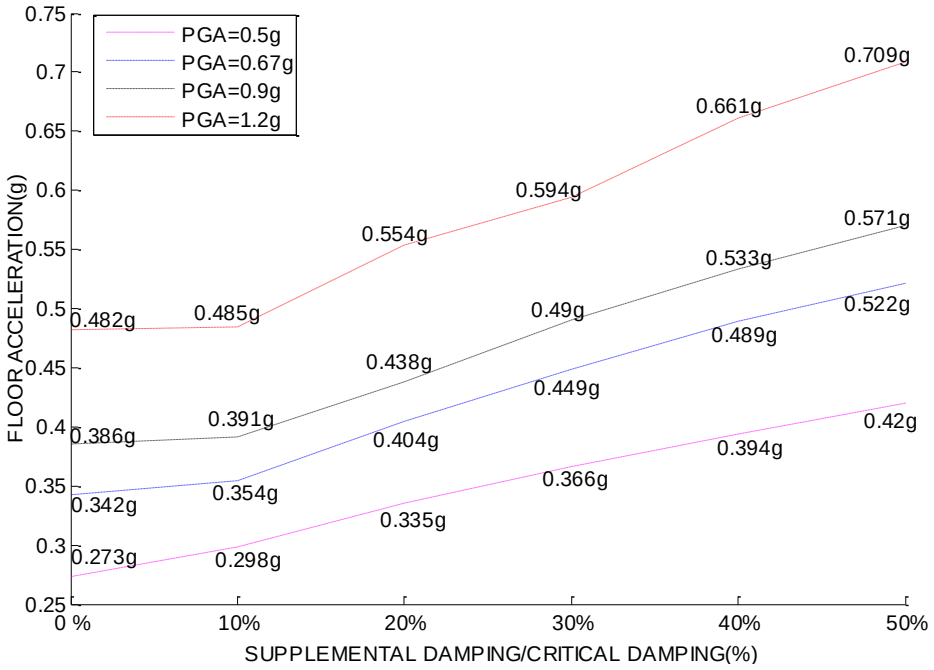

Figure 4.20: Variation of Maximum Accelerations at the Top Floor of Isolated Building with Increasing Supplemental Viscous Damping

Table 4.18, Figure 4.20 and Figure 4.21 present the effects of supplemental viscous damping on floor accelerations. The supplemental damping increased floor acceleration response. The top floor acceleration increased by about 50% as the supplemental damping increased to 50% of critical damping. This effect became more pronounced under less intense earthquake motions. The pattern changed in base floor accelerations completely, as illustrated in Figure 4.21, showing reductions in floor accelerations. This reduction is attributed to the reduction in horizontal displacements of the isolation system.

The supplemental damping would stiffen the isolation system, and more importantly, create higher mode effects. This would amplify upper floor accelerations. In some cases, however, the supplemental damping would increase floor accelerations to a degree such that the acceleration values become higher than those obtained from the undamped structural model under more intense earthquakes. In this respect, the level of supplemental damping should be carefully chosen in order to control isolator displacements, without adversely affecting (excessively increasing) floor accelerations.

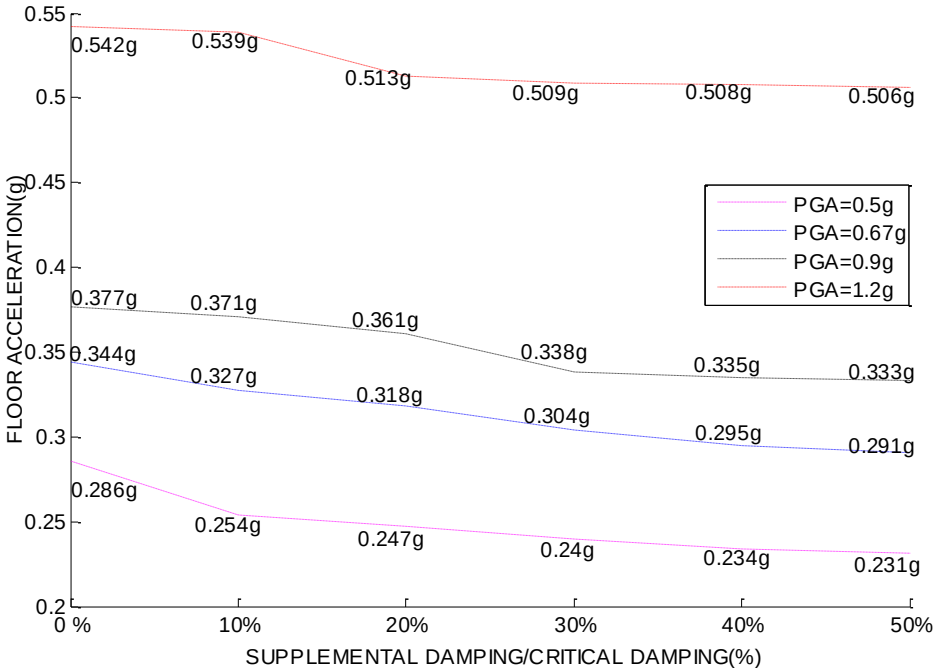

Figure 4.21: Variation of Maximum Accelerations at the Base Floor Level of Isolated Structure with Increasing Supplemental Viscous Damping

Table 4.18: Floor Accelerations of Isolated Structure with Supplemental Viscous Damping

(a) Ground motion level: La11-005#1(PGA=0.5g)

Viscous Damping / Structure Floor	No Damping	10% Critical	20% Critical	30% Critical	40% Critical	50% Critical
7th floor	0.273g	0.298g	0.335g	0.366g	0.394g	0.420g
6th floor	0.249g	0.265g	0.297g	0.324g	0.348g	0.371g
5th floor	0.219g	0.234g	0.255g	0.275g	0.292g	0.308g
4th floor	0.186g	0.239g	0.245g	0.252g	0.260g	0.267g
3rd floor	0.191g	0.257g	0.266g	0.276g	0.285g	0.294g
2nd floor	0.216g	0.264g	0.270g	0.278g	0.287g	0.293g
1st floor	0.242g	0.259g	0.261g	0.262g	0.263g	0.267g
Base	0.286g	0.254g	0.247g	0.240g	0.234g	0.231g

(b) Ground motion level: La11-005#2(PGA=0.67g)

Viscous Damping / Structure Floor	No Damping	10% Critical	20% Critical	30% Critical	40% Critical	50% Critical
7th floor	0.342g	0.354g	0.404g	0.449g	0.489g	0.522g
6th floor	0.315g	0.326g	0.361g	0.399g	0.460g	0.498g
5th floor	0.282g	0.311g	0.317g	0.340g	0.381g	0.418g
4th floor	0.246g	0.310g	0.318g	0.326g	0.360g	0.399g
3rd floor	0.262g	0.331g	0.343g	0.354g	0.366g	0.371g
2nd floor	0.283g	0.338g	0.346g	0.355g	0.363g	0.372g
1st floor	0.307g	0.329g	0.334g	0.335g	0.336g	0.339g
Base	0.344g	0.327g	0.318g	0.304g	0.295g	0.291g

(c) Ground motion level: La11-005#3(PGA=0.9g)

Viscous Damping / Structure Floor	No Damping	10% Critical	20% Critical	30% Critical	40% Critical	50% Critical
7th floor	0.386g	0.391g	0.438g	0.490g	0.533g	0.571g
6th floor	0.374g	0.381g	0.392g	0.435g	0.469g	0.497g
5th floor	0.362g	0.364g	0.369g	0.371g	0.392g	0.412g
4th floor	0.343g	0.350g	0.351g	0.357g	0.360g	0.368g
3rd floor	0.354g	0.363g	0.374g	0.384g	0.394g	0.407g
2nd floor	0.365g	0.372g	0.375g	0.387g	0.398g	0.409g
1st floor	0.370g	0.369g	0.368g	0.371g	0.372g	0.373g
Base	0.377g	0.371g	0.361g	0.338g	0.335g	0.333g

(d) Ground motion level: La11-005#4(PGA=1.2g)

Viscous Damping / Structure Floor	No Damping	10% Critical	20% Critical	30% Critical	40% Critical	50% Critical
7th floor	0.482g	0.485g	0.554g	0.594g	0.661g	0.709g
6th floor	0.465g	0.470g	0.523g	0.555g	0.592g	0.629g
5th floor	0.448g	0.462g	0.480g	0.505g	0.520g	0.533g
4th floor	0.452g	0.463g	0.475g	0.495g	0.510g	0.521g
3rd floor	0.473g	0.477g	0.502g	0.527g	0.536g	0.544g
2nd floor	0.476g	0.491g	0.518g	0.521g	0.523g	0.525g
1st floor	0.497g	0.513g	0.511g	0.500g	0.486g	0.472g
Base	0.542g	0.539g	0.513g	0.509g	0.508g	0.506g

Further assessment of the effects of supplemental damping is assessed by examining the variation of base shear. Figure 4.22 compares the variation of base shear with increasing level of viscous damping. The pattern observed resembles to that observed under increasing isolator lead plug diameter (shown in Figure 4.16). The shear force is reduced to 17.1%, 18.3%, 17.4% and 19.4% respectively from the earthquake ground motions La11-005#1 to La11-005#4 as the supplemental damping value increased up to 50% of critical damping. The trend in base shear variation appears to change, and decrease beyond 20% of critical damping. Despite the reduction in base shear, the application of viscous dampers generates higher inertial forces at floor levels, because of increased floor accelerations. The contradiction between reduced base shear and increased seismic forces at floor levels can be attributed to the supplemental damping, which could excite higher modes, generating inertial forces in the opposite direction. Thus, although the floor inertial forces were increased, it was possible to create a reduced total base shear.

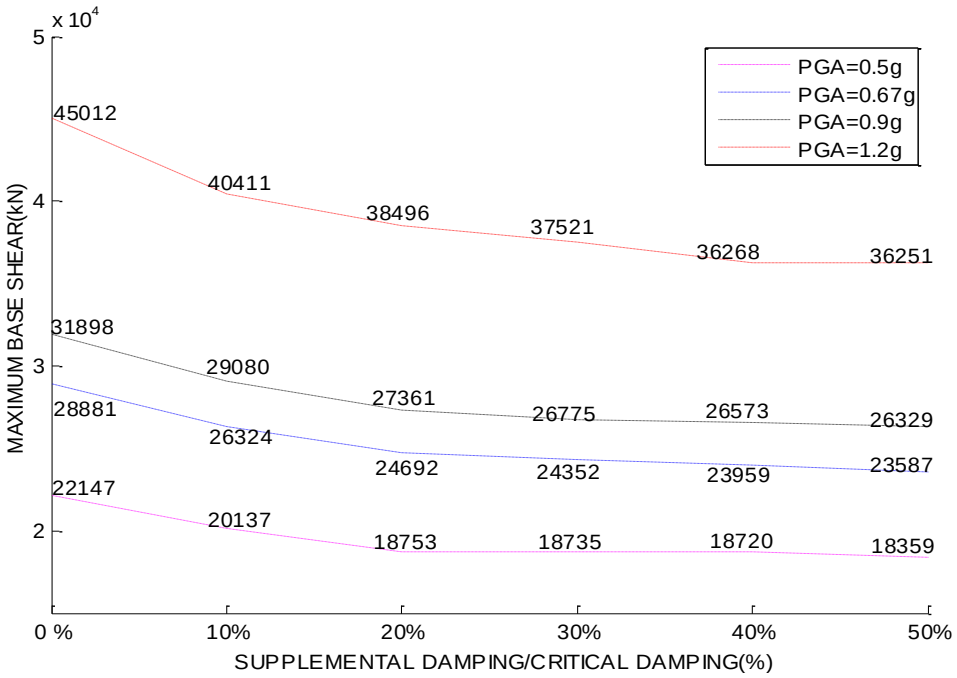

Figure 4.22: Variation of Maximum Base Shear of Isolated Building with Increasing level of Supplemental Damping

In summary, the incorporation of viscous dampers in the isolation system effectively controls the horizontal displacement of the base isolation system, provided the supplemental damping value which is carefully selected according to the expected

seismic hazard spectra of the region. Care should be exercised in adjusting the level of damping so that the floor accelerations and the superstructure inter-storey drifts remain low to realize full benefits of the isolation system.

4.6 Performance of Buildings with Friction Pendulum Bearings

Previous sections presented the results of dynamic analyses to assess the effectiveness of rubber bearing base isolation systems of different sizes and properties, with and without supplemental damping. Some of the shortcomings of the system were identified, especially under high-intensity ground motions. It was concluded that, while the rubber bearing systems can be used effectively as base isolation systems, excessive movements of the isolation system may occur under strong earthquakes. Increasing the diameter of the lead plug in LLRBs or introducing supplemental viscous damping to overcome this problem could trigger undesirable effects on structural response, especially as it affects floor accelerations. High levels of floor accelerations increase the risk of damage to non-structural elements and building contents. To overcome some of these shortcomings, the feasibility of using friction pendulum bearings (FPB) with rubber bearings was investigated in this section. The FPB bearings could provide high initial isolator stiffness and adequate energy dissipation. The FPBs were placed under the external columns of the reference buildings, while the rubber bearings were placed underneath the internal columns, as illustrated in Figure 4.23. The analysis results obtained from the use of FPB are compared with previously obtained results from the use of rubber bearing only, with rubber bearing isolator diameters of 600 mm and lead plug diameter of 100 mm, with and without the supplemental viscous damping of 30% of critical damping.

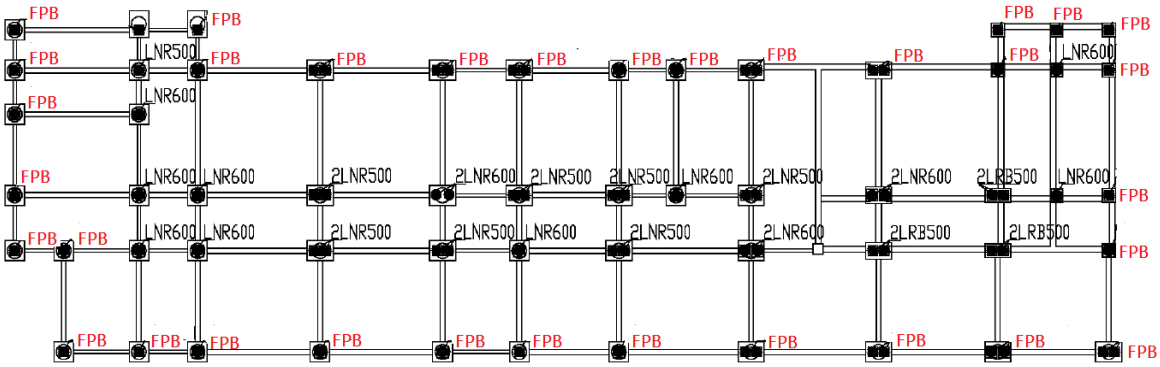

Figure 4.23: Placement of Friction Pendulum Bearings (FPB) and Rubber Bearings

Table 4.19 summarizes the cases considered in the comparison, while providing a summary of maximum lateral displacements obtained at the isolator level. The incorporation of FPB bearings remarkably restricted lateral displacements at the isolator level without the need for supplementary damping. The base displacement was reduced by 43.8%, 39.7%, 37.1% and 28.4% respectively for the earthquake motions La11-005#1 to La11-005#4 with increasing intensity. The improvement obtained was similar to that obtained from the use of supplemental damping at 30% of critical damping. The FPB bearings have the additional advantages of large allowance on the isolator horizontal displacement and self-centring capacity to control residual displacements, thereby improving the stability of the rubber isolation system during large movements.

Figure 4.24 provides comparisons for superstructure inter-storey drift between the fixed-base structure and the isolated structures with three isolation systems (rubber bearings, rubber bearings with the dampers and rubber bearings with the FPBs). All the isolation systems were able to attenuate structural vibrations. Among them, the friction pendulum bearings coupled with rubber bearings resulted in the best drift control, successfully limiting inter-storey drifts to 1.0%, under the four earthquake intensities considered. This led to significant improvements in structural performance and produced elastic response in the superstructure. This favourable performance was attributed to the outstanding energy dissipation capacity provided by FPB bearings, as the FPBs could convert seismic energy into heat and potential energy, which are more efficient than consuming the energy through plastic deformations of isolators and viscous damping.

Table 4.19: Maximum Isolator Displacements (mm)

	Rubber bearings Solely	Rubber Bearings & Dampers	Rubber Bearings & FPBs
PGA=0.5g	260	154	146
PGA=0.67g	337	204	203
PGA=0.9g	372	229	234
PGA=1.2g	517	331	370

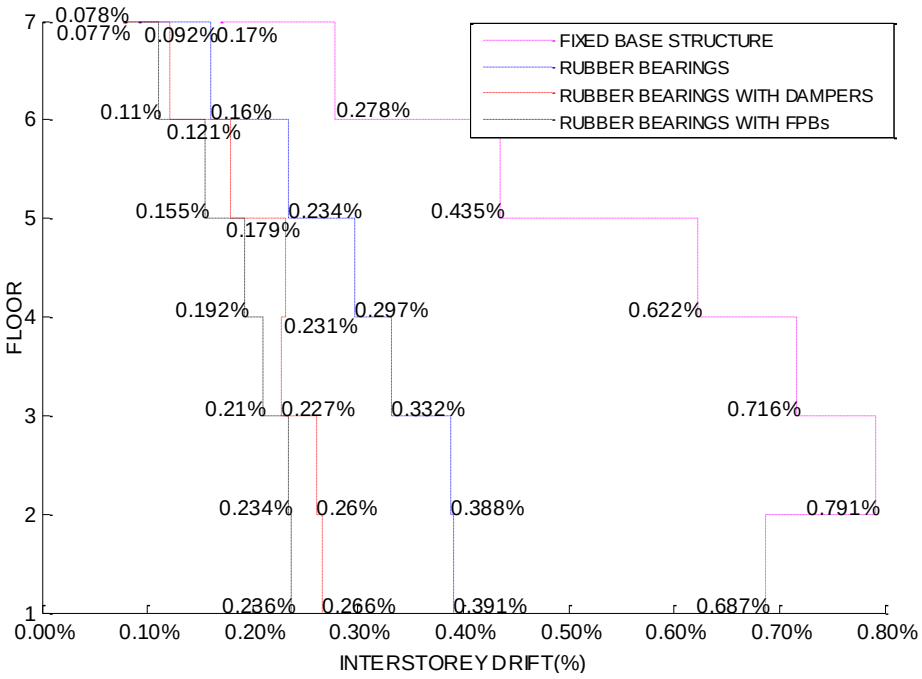

(a) Ground motion record: La11-005#1

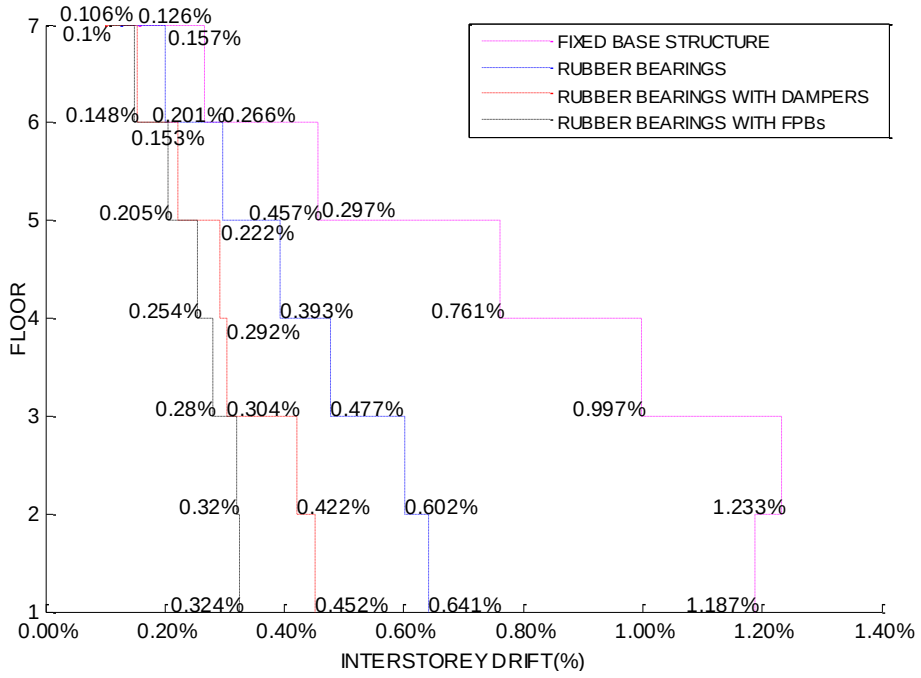

(b) Ground motion record: La11-005#2

Figure 4.24: Peak Inter-storey Drifts of Fixed-base Structures and Three Isolated Structures under Selected Earthquake Record

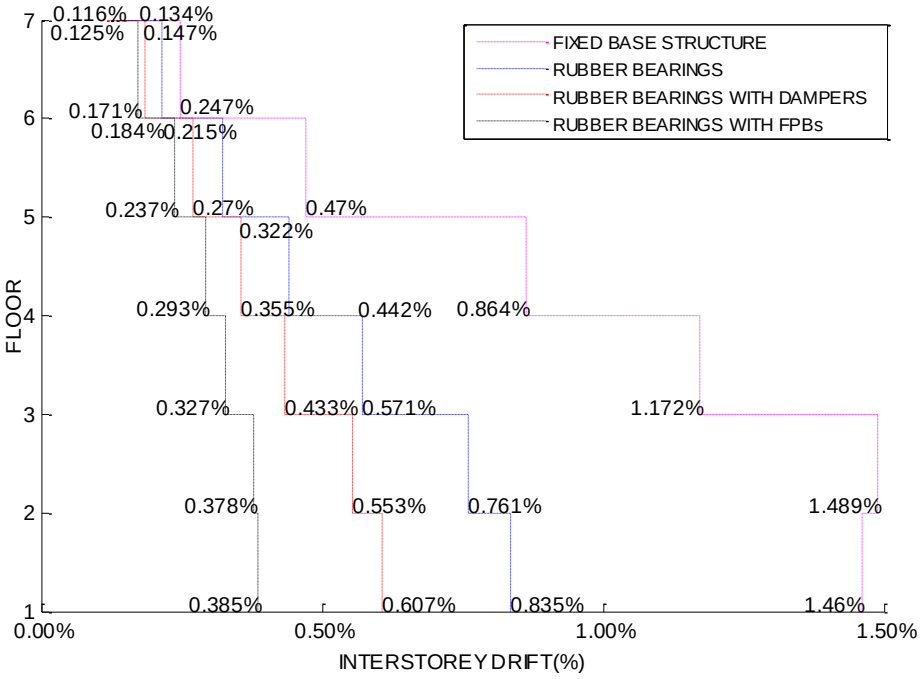

(c) Ground motion record: La11-005#3

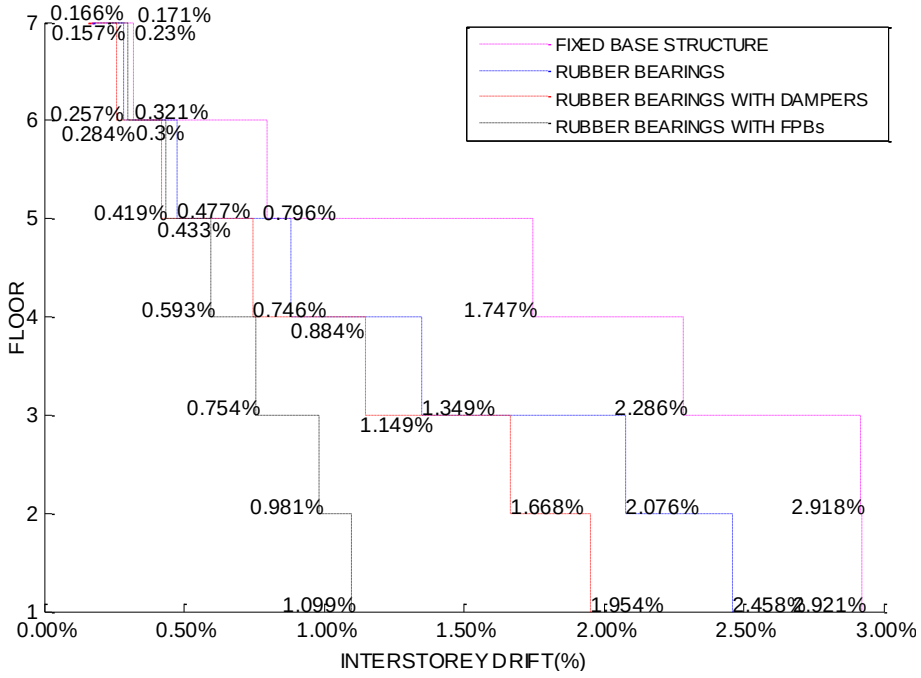

(d) Ground motion record: La11-005#4

Figure 4.24: Peak Inter-storey Drifts of Fixed-base Structures and Three Isolated Structures under Selected Earthquake Record

The results showed that the combination of fiction pendulum bearings and rubber bearings was effective in reducing floor accelerations. This hybrid isolation system produced the smallest floor accelerations, promoting superior performance of non-structural elements, as well as operational and functional components of buildings during seismic excitations. The significant control in structural accelerations was attributed to the small post-yield stiffness of the FPBs, which decreased the natural period of the rubber isolation system, thereby reducing the acceleration response spectra. Also, as can be seen in Figure 4.24, the floor accelerations of the structure with FPBs did not change along the building height, indicating that the superstructure almost rigidly moved during seismic response. This indirectly reflected the effectiveness of FPB bearings on supressing structural deformations, by isolating the superstructure from seismic effects efficiently. The hybrid isolation system also resulted in minimum structural base shear as shown in Table 4.20.

Table 4.20: Structural Base Shears (kN)

	Fixed Base Structure	Rubber bearings Solely	Rubber Bearings & Dampers	Rubber Bearings & FPBs
PGA=0.5g	31558	22147	18720	12185
PGA=0.67g	37931	28881	24352	16141
PGA=0.9g	40685	31898	26775	18158
PGA=1.2g	50977	45012	37521	28073

One of the parameters that may play an important role on the performance of FPB is axial load. The superstructure weight may influence the seismic behavior of this hybrid isolation system, because the lateral stiffness of the FPB bearings is directly proportional to the vertical loads on bearings. While the building selected was analyzed with its appropriate weight to compare the behaviours of three different types of base isolation systems, a parametric investigation was carried out to assess the significance and the sensitivity of axial load on FPB performance. This was done by keeping the building geometry and structural properties the same, but reducing floor weights. A convenient way of doing this was to reduce the density of the concrete in the analytical model. The density of concrete was reduced down to 70% and 50% of the original value, to change the weight supported by the bearings. The reduced concrete density and the corresponding building weight are tabulated in Table 4.21.

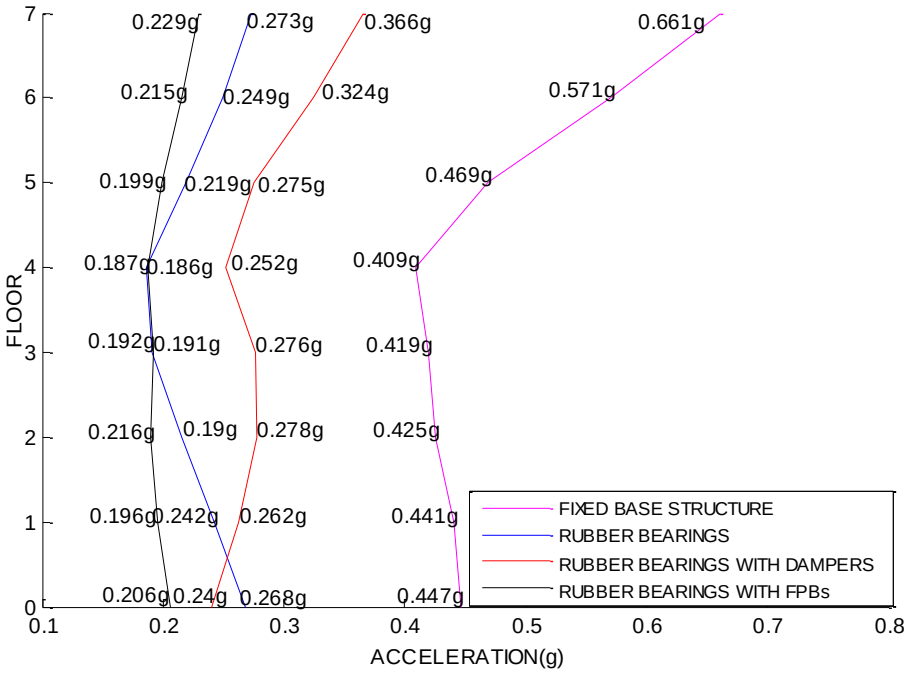

(a) Ground motion record: La11-005#1

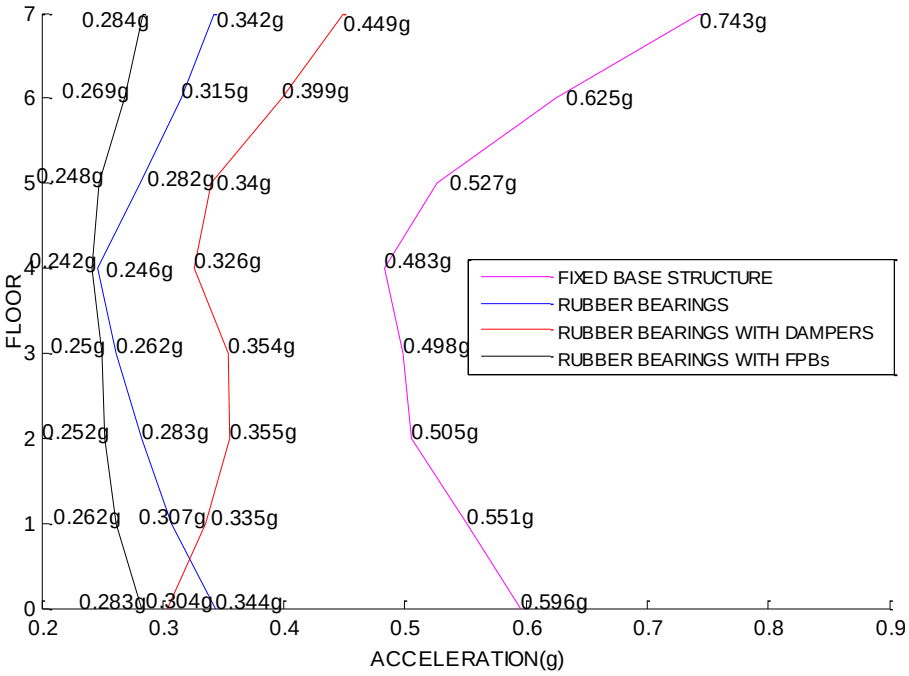

(b) Ground motion record: La11-005#2

Figure 4.25: Maximum Floor Accelerations of Fixed-base Structure and Three Isolated Structures under Selected Earthquakes Records

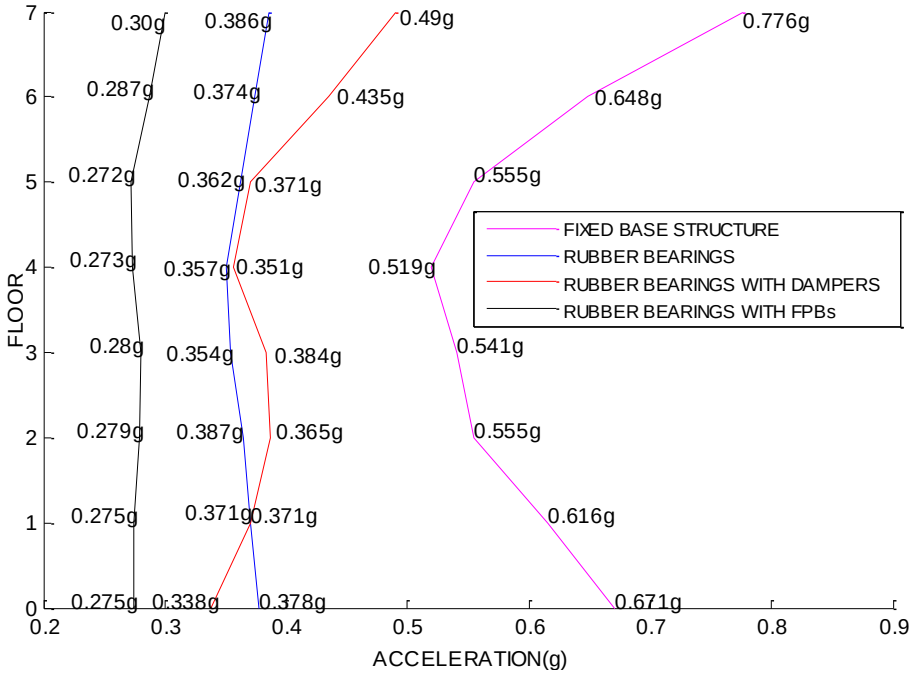

(c) Ground motion record: La11-005#3

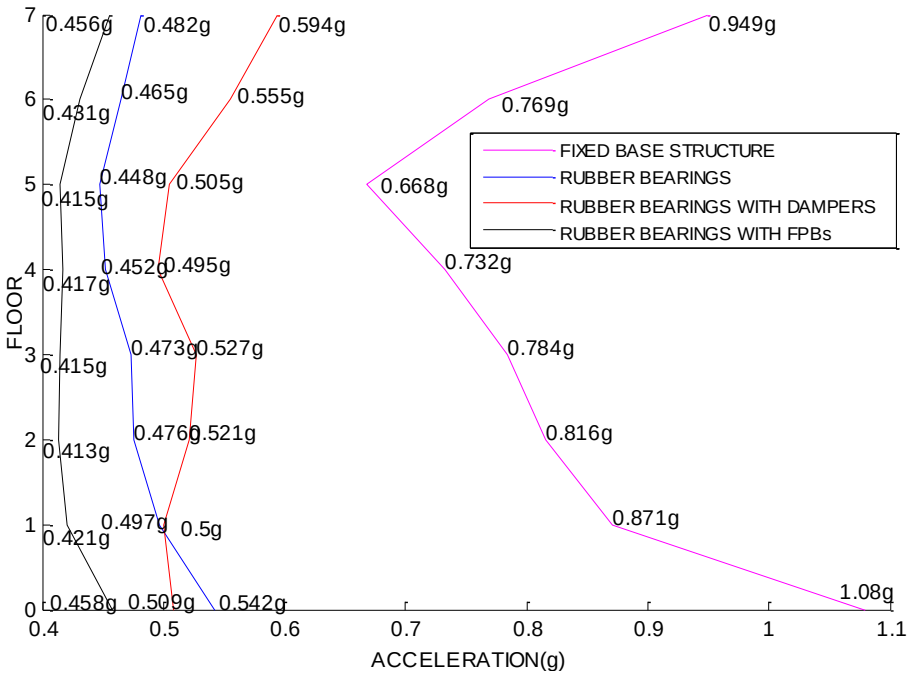

(d) Ground motion record: La11-005#4

Figure 4.25: Maximum Floor Accelerations of Fixed-base Structure and Three Isolated Structures under Selected Earthquakes Records

Table 4.21: Structural Weight in Three Analysis Cases

	100% Concrete Density	70% Concrete Density	50% Concrete Density
Density (kN/m^3)	23.56	16.49	11.78
Structural Weight(kN)	89547.56	70311.1886	57486.941

The decrease in the structural weight would influence the performance of isolated structure in multiple ways. First, the reduced weight could generate lower inertial forces at each floor of the superstructure, therefore fundamentally alleviating the structural dynamic response. Second, the reduced vertical loads could lessen the lateral stiffness of the FPBs, shifting the isolation period to a higher range and consequently resulting in lower floor acceleration response spectra. On the other hand, the reduction in lateral stiffness would reduce the area under hysteresis loops of FPBs, also reducing the isolation energy dissipation capacity.

A small superstructure weight resulted in reduced horizontal deformations. The horizontal movement of the base isolation system, as well as inter-storey drifts were reduced as the superstructure weight went down. This is shown in Table 4.22 and Figure 4.26. Surprisingly, the effect of weight reduction was an increase in floor accelerations. The maximum floor acceleration increased by 2.4%, 3.6%, 11.7% and 16.6% respectively for the four earthquake intensities considered when the building weight by reduced by 36% (50% reduction in concrete mass density). This unexpected increase may be explained by the reduction in isolation energy dissipation capacity. Further investigation is required for complete assessment of this parameter.

Variation in base shear with building weight is shown in Table 4.23, The base shear decreased with decreasing weight, as expected, because the reduced superstructure mass attracted smaller seismic forces.

Table 4.22: Maximum Horizontal Base Displacement as Affected by Building Weight (mm**)**

	100% Concrete Density	70% Concrete Density	50% Concrete Density
PGA=0.5g	146	135	128
PGA=0.67g	203	192	337
PGA=0.9g	234	220	201
PGA=1.2g	370	354	332

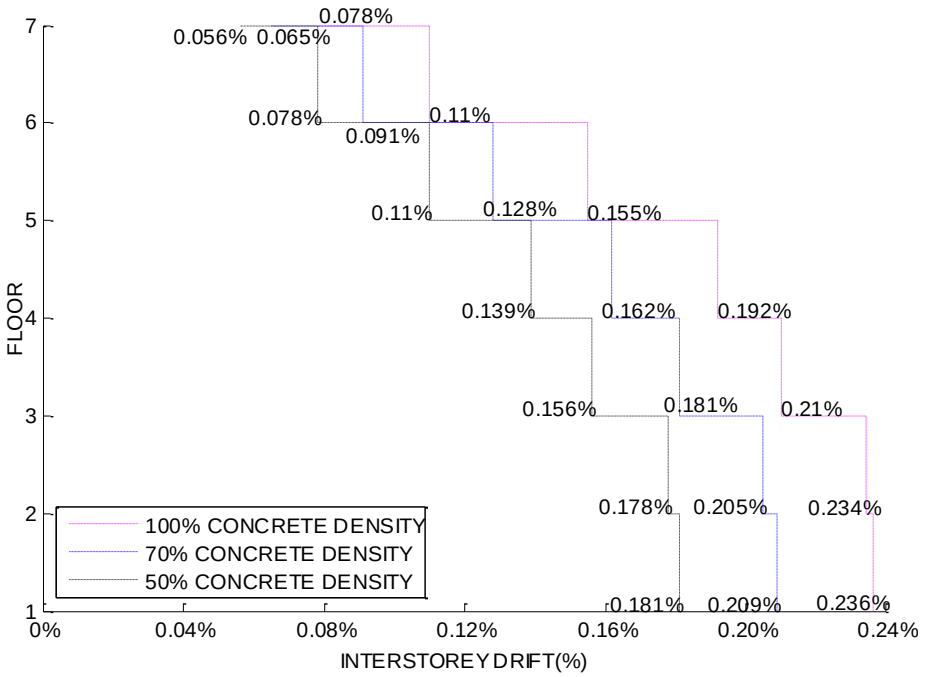

(a) Ground motion record: La11-005#1

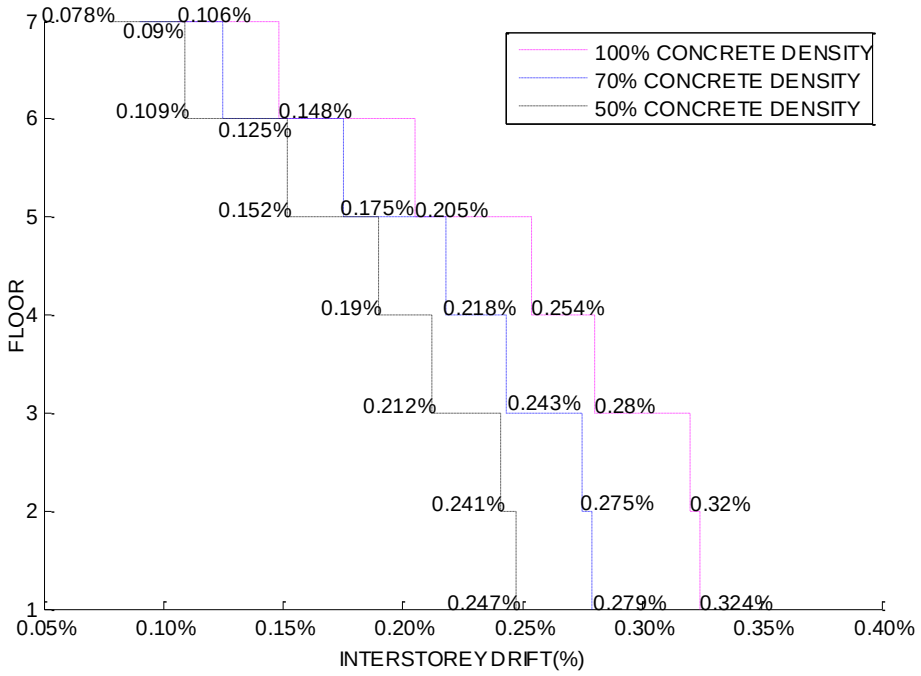

(b) Ground motion record: La11-005#2

Figure 4.26: Maximum Inter-storey Drifts as Affected by Building Weight

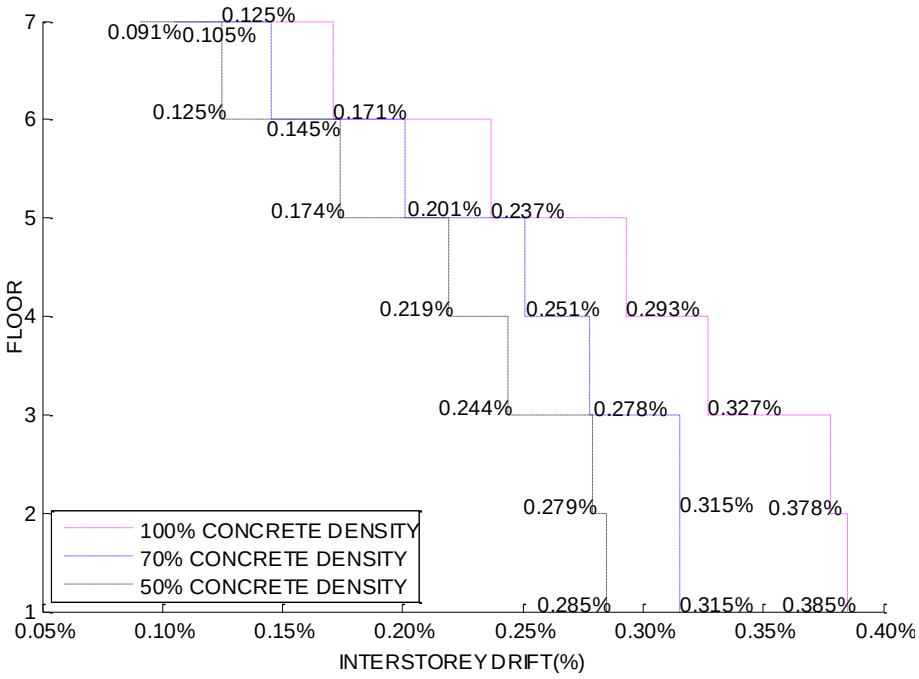

(c) Ground motion record: La11-005#3

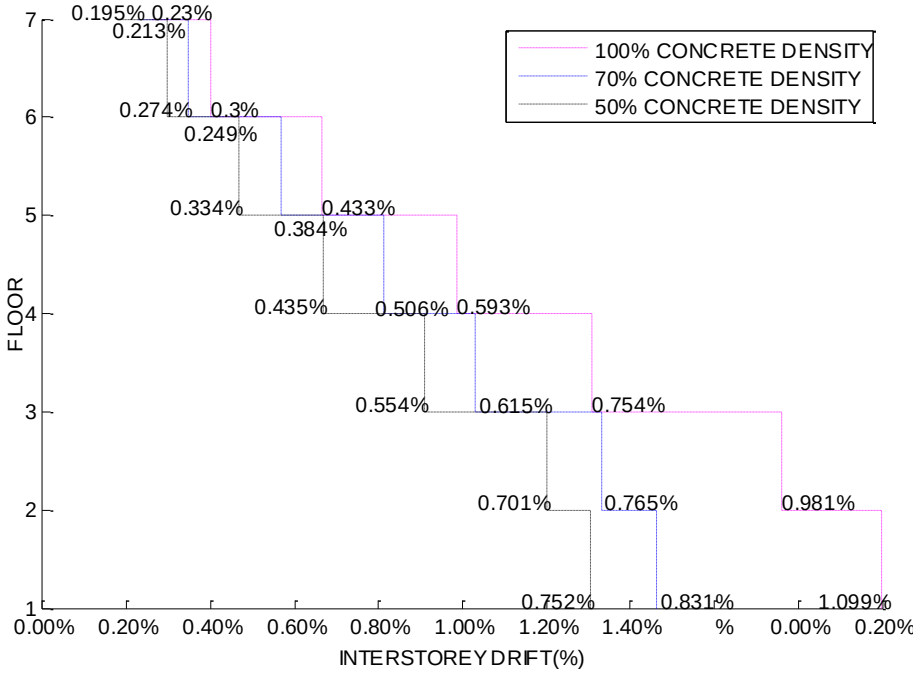

(d) Ground motion record: La11-005#4

Figure 4.26: Maximum Inter-storey Drifts as Affected by Building Weight

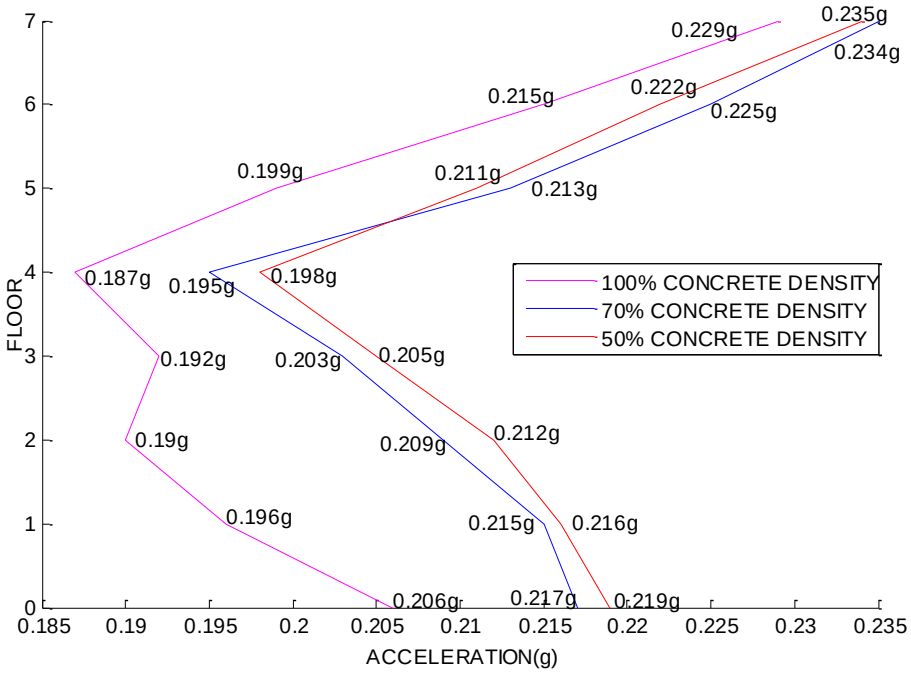

(a) Ground motion record: La11-005#1

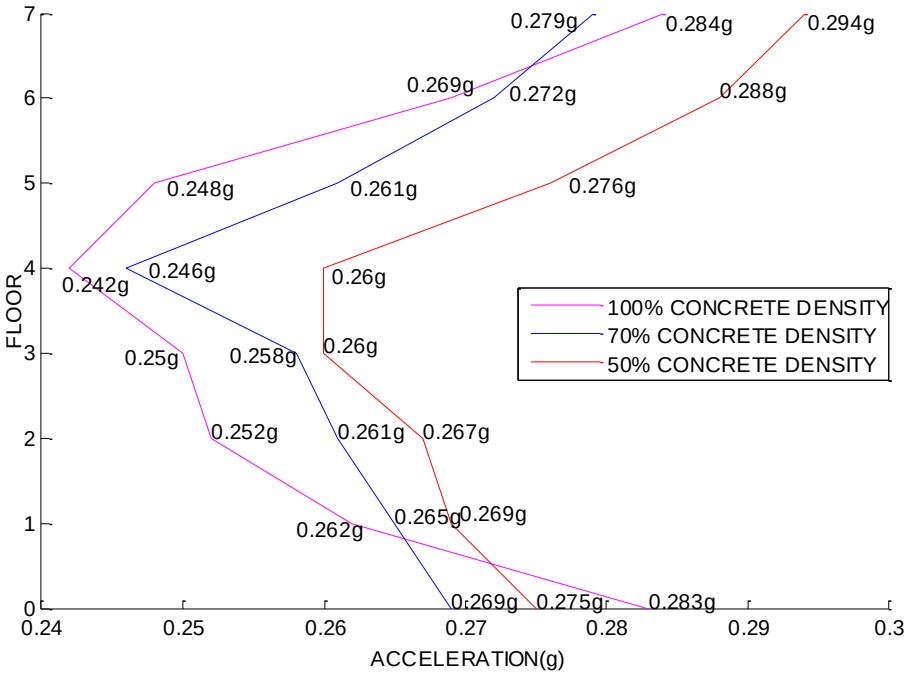

(b) Ground motion record: La11-005#2

Figure 4.27: Maximum Floor Accelerations as Affected by Building Weight

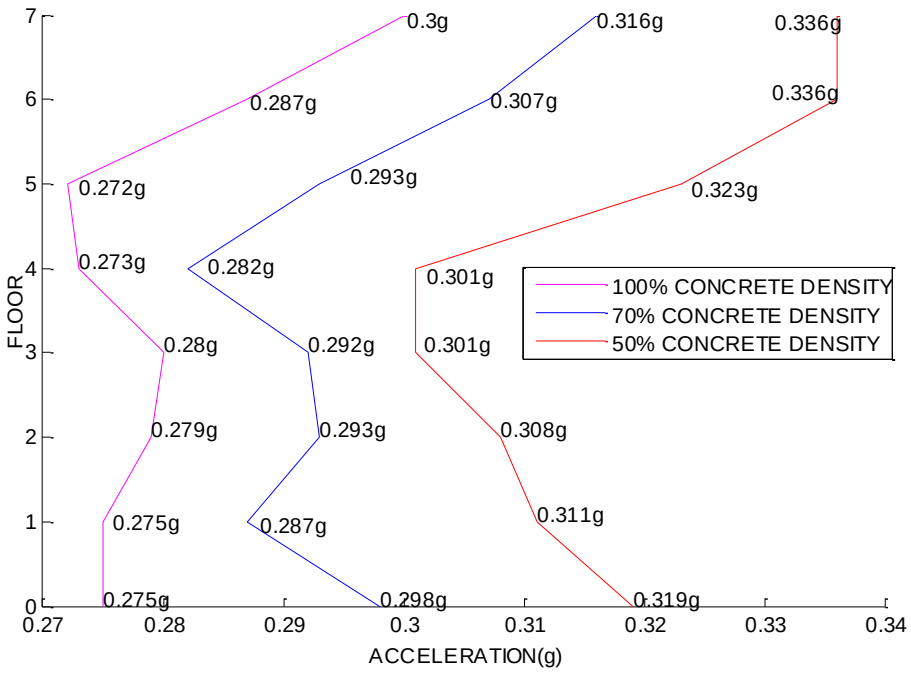

(c) Ground motion record: La11-005#3

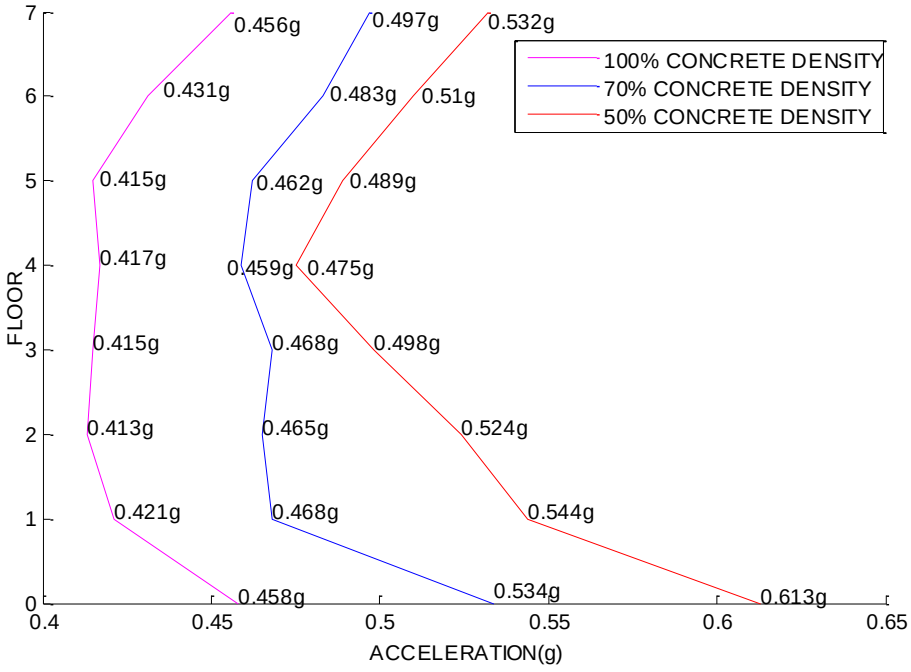

(d) Ground motion record: La11-005#4

Figure 4.27: Maximum Floor Accelerations as Affected by Building Weight

Table 4.23: Base Shear Force as Affected by Building Weights (*kN*)

	100% Concrete Density	70% Concrete Density	50% Concrete Density
PGA=0.5g	12185	10514	9305
PGA=0.67g	16141	13974	12413
PGA=0.9g	18158	15697	14023
PGA=1.2g	28073	25746	22134

In conclusion, implementing the friction pendulum bearings as part of the overall base isolation system provided the optimal approach. The hybrid isolation system, consisting of FPBs and rubber isolation systems provided effective displacement control in the superstructure with minimum horizontal movement at the isolation level. The system also resulted in low floor accelerations and base shear.

Chapter 5

Summary and Conclusion

5.1 Summary and Conclusions

Base isolation systems are widely used to improve seismic performance of reinforced concrete structures. It is based on the concept of decoupling superstructure from ground shaking, thereby limiting the transfer of seismic induced energy to the structure.

Three different types of base isolation systems were investigated in the current research project, consisting of a rubber isolation system, high damping isolation devices that are composed of rubber isolators and viscous dampers, and a hybrid isolation system consisting of rubber bearings and friction pendulum bearings. The effectiveness of these isolation systems on seismic performance of reinforced concrete frame buildings were assessed through a case study involving the outpatient building of Lushan People's Hospital in China. The building was base isolated using rubber bearings, and was subjected to the 2013 Lushan Earthquake with a Magnitude of 6.6. The building showed excellent behaviour of the superstructure, with some damage to the isolators, and higher than expected lateral movements at the base isolation level.

The prototype building was modelled as a fixed base structure first to assess its performance without the base isolation. It was subsequently analyzed with the three different base isolation systems indicated above. Structural performances were compared between the isolated and non-isolated structural buildings in terms of superstructure storey-drifts, floor accelerations, base horizontal displacements and base shears. Moreover, modeling parameters, such as the application of infill walls, isolator

characteristics, earthquake characteristics and structural weight were investigated. The following conclusions were drawn:

- The presence of masonry infill walls has significant influences on seismic response of non-isolated building. The walls provide lateral stiffness, which controls inter-storey drift ratios. However, the increased structural stiffness results in shorter period, attracting higher seismic forces and resulting in increased floor accelerations, as well as higher base shears. However, the presence of infill walls reduces inelasticity in frame members until they suffer diagonal compression failures. The overall effect of masonry infill walls on seismic response has to be assessed carefully. The walls help frame buildings until their elastic limit is exceeded. Under high-intensity earthquake loading, especially if the duration of the earthquake is long, the frames may suffer damage upon the failure of the walls.

- The application of seismic isolation can effectively improve structural performance of reinforced concrete frame buildings. It reduces dynamic forces experienced by the superstructure, controlling inter-storey drifts, floor accelerations and structural base shear. The level of improvement attained in the base isolated structure depends on the type and characteristics of the base isolation system implemented. The most optimum isolation system for a given frame building can only be determined after conducting dynamic response history analysis of the overall system with due considerations given to the interaction of the superstructure and the base isolation system.

- The rubber isolation system, consisting of LRBs and LLRBs, is effective in reducing seismic response of frame buildings under small or moderate intensity earthquakes. However, when the isolated building is subjected to strong earthquakes, the rubber isolators may experience cumulative lateral displacement, damaging bearings and causing instability in the superstructure. An increase in lead plug diameter has a positive effect on controlling and reducing lateral movements of the isolation system. However, the increase in initial stiffness and isolation damping, resulting from the use of a larger size isolator may amplify floor acceleration response. Therefore, the trade-off between reducing isolator

displacements and increasing floor accelerations should be carefully assessed for optimal use of rubber isolations systems.

- In some cases, it may be impractical to control isolator displacements by only enlarging lead plug diameters. In such cases, supplemental viscous dampers may have to be installed in combination with rubber isolators to provide additional damping. The implementation of supplemental damping reduces large isolator displacements. However, the additional damping in turn increases floor accelerations by amplifying higher mode effects. This may counteract the positive contributions towards reducing isolator displacements, and may intensify damage to non-structural systems and building contents. To ensure the effectiveness of using supplemental damping devices, the level of damping has to be carefully selected on the basis of the design hazard spectra of the region. For the building considered in the current investigation, supplemental damping of less than 30% of critical damping resulted in desired performance.

- The friction pendulum bearings (FPB) coupled with rubber isolators may produce the best base isolation system. The use of FPB provides high initial stiffness and self-centring capacity, thereby reducing lateral displacements at the isolator level without increasing dynamic response of the superstructure excessively. The latter is achieved because of adequate energy dissipation of FPBs. The hybrid isolation system, consisting of FPBs and LRBs generates an excellent structural performance in terms of minimizing inter-storey drift, floor accelerations, base shears and base displacements.

- Building weight influences the performance of isolated structure when the hybrid isolation system is used, consisting of FPBs and LRBs. This is because the inertia forces acting on the superstructure is proportional to the structure mass, but more importantly, the structure weight affects lateral stiffness of the FPBs. In general, the reduction in structural weight improves seismic performance. A small superstructure weight reduces inter-storey drifts, base displacements and base shear, although it slightly increases floor accelerations.

5.2 Recommendations for Future Research

The current research project, though covered a significant number of parameters and three different types of base isolation systems, it was limited to the performance of a single prototype buildings selected. It was also limited to the use of the same frequency content of earthquake excitation, though the earthquake intensity was varied. A more comprehensive research program is recommended in the future on different reinforced concrete frame buildings with different structural configurations, buildings height, structural mass and earthquake ground motion records. The variation of these structural and ground motion parameters will result in the generation of more extensive data, which will help expand some of the observations made at the end of the current investigation.

Furthermore, the prototype building used in current research is a moment-frame structure without shear walls. This type of building may not be an optimum choice for base isolation due to its relatively flexible behaviour, although the masonry infill walls used stiffen the superstructure. It is recommended to investigate the effectiveness of the base isolation systems considered on frame shear wall structures.

References

[1] Dolce M, Cardone D, Ponzo FC. Shaking-table tests on reinforced concrete frames with different isolation systems. *Earthquake Engineering and Structural Dynamics* 2007; **36**(5):573-596

[2] Christopoulos, C., Filiatrault A. Principles of Passive Supplemental Damping and Seismic Isolation. Pavia, Italy: IUSS Press, 2006.

[3] Matsuda A. Evaluation for mechanical properties of laminated rubber bearing using finite element analysis. *Journal of Pressure Vessel Technology* 2004; **126**(2):134-140

[4] Robinson WH. Lead-rubber hysteretic bearings suitable for protecting structures during earthquakes. *Earthquake Engineering and Structural Dynamics* 1982; **10**(4):593-604

[5] Kalpakidis IV, Constantinos MC, Whittaker AS. Modeling strength degradation in lead-rubber bearings under earthquake shaking. *Earthquake Engineering and Structural Dynamics* 2010; **39**:1533-1549

[6] Luca L, Cianluca G, Pier PD. Comparison of different models for friction pendulum isolators in structures subjected to horizontal and vertical ground motions. *Soil Dynamic and Earthquake Engineering* 2016; **81**:75-83

[7] Cardone D, Gesualdi G, Brancato P. Restoring capability of friction pendulum seismic isolation systems. *Building of Earthquake Engineering* 2015; **13**(8):2449-2480

[8] Mokha A, Constantinou MC, Reinhorn AM, Zayas VA. Experimental study of friction-pendulum isolation system. *ASCE Journal of Structural Engineering* 1991; **117**(4): 1207-1217

[9] Asher JW, Young RP, Ewing RD. Seismic isolation design of the San Bernardino Country medical center replacement project. *Structural Design of Tall Buildings* 1996; **5**:265-279

[10] Macrae GA, Morrow DV, Roeder CW. Near-fault ground motion effects on simple structures. *ASCE Journal of Structural Engineering* 2001; **127**(9): 996-1004

[11] Zhao DX, Shao AW, Chao W. Experimental and numerical study on long-span reticulate structure with multidimensional high-damping earthquake isolation devices. *Journal of sound and vibration* 2014; **333**:3044-3057

[12] Yi MW, Bijan S. Shake table testing of a base isolated model. Earthquake Engineering 2002; **24**:1203-1215
[13] Yoo B, Kim Y-H. Study on effects of damping in laminated rubber bearings on seismic response for a 1/8 scale isolated test structure. *Earthquake Engineering and Structural Dynamics* 2002; **31**:1777-1792

[14] Briseghella B, Zordan T, Liu T, Mazzarolo E. Friction pendulum system as a retrofit technique for existing reinforced concrete building. *Structural Engineering International* 2013; **23**:219-224

[15] Castaldo P, Palazzo B, Della VP. Seismic reliability of base-isolated structures with friction pendulum bearings. Engineering Structures 2015; **95**:80-93

[16] Chang S, Makris N, Whittaker E, Thompson A. Experimental and analytical studies on the performance of hybrid isolation system. *Earthquake Engineering and Structural Dynamics* 2002; **31**:421-443

[17] Providakis CP. Effect of LRB isolators and supplemental viscous dampers on seismic isolated building under near-fault excitations. *Engineering Structures* 2008; **30**:1187-1198

[18] Providakis CP. Effect of supplemental damping on LRB and FPS seismic isolators under near-fault ground motions. *Soil Dynamics and Earthquake Engineering* 2009; **29**:80-90

[19] Dolce M, Cardone D. Seismic protection of light secondary systems through different base isolation systems. *Journal of Earthquake Engineering* 2003; **7**:223-250

[20] Yu C, Goodarz A. Wind effects on base-isolated structures. *ASCE Journal of Engineering Mechanics* 1992; **118**(8): 1708-1727

[21] Elisabeth K, Ana MC, Bastien A. The impact of the 12 May 2008 Wenchuan Earthquake on industrial facilities. *Journal of Loss Prevention in the Process Industries* 2010; **23**:242-248

[22] Marshall L. Observations from the April 20, 2013 Lushan county, Ya'an city, Sichuan province, China earthquake. *SMIP13 Seminar on Utilization of Strong-Motion Data* 2013; **25** - 44.

[23] Mainstone RJ. Supplementary notes on the stiffness and strength of infilled frames. *Current Paper CP 13/74, Building Research Station, Garston Watford, U.K.* 1974

[24] Mainstone RJ, Weeks GA. The influence of bounding frame on the racking stiffness and strength of brick walls. *Proceedings of the 2nd International Brick Masonry Conference, Building Research Establishment, Watford, England* 1974; 165-171